The Oxidative Activation

of *n*-Octane

over

Titania Supported Cobalt Catalysts

by

Narainamah Gounden

School of Chemistry and Physics

University of KwaZulu-Natal

Westville

Durban

4000

Submitted in fulfilment of the academic

requirements, for the degree of

Master of Science in the

School of Chemistry and Physics

University of KwaZulu-Natal

July 2013

Abstract

This research effort explored routes to valorise alkanes via heterogeneous catalysis. Dehydrogenation and oxidative dehydrogenation are the two routes that were probed in this research effort to activate *n*-octane by means of titania supported cobalt catalysts. No literature existed on the oxidative activation of higher linear alkanes over titania supported cobalt catalysts, despite the catalyst not being novel, that prompted probing this system in this application.

Five titania supported cobalt catalysts with cobalt loadings between 5-25 wt% were synthesised via the wet impregnation technique. These catalysts were characterised to assess their structural morphology as well as their chemical and physical properties. Several techniques were used in the characterisation studies, including microscopic, spectroscopic, diffraction and surface techniques including XRD, XPS, BET, SEM-EDX, TEM, ICP, TGA, Raman and TPR analysis. The results from these studies provided insight into the structure-reactivity correlation.

The catalysts were found to comprise of spherical shaped, high surface area mesoporous material that was thermally stable at high temperatures with minimal decomposition and mass loss. The support was confirmed to be the anatase phase of titania. The surface was found to be enriched in Co_3O_4 species that were well dispersed on the surface, but with some aggregation when higher cobalt loadings were used. The catalysts were more reducible at lower temperatures for higher cobalt loadings, with the onset of reduction occurring at 350 °C.

Catalytic testing was carried out in a fixed bed reactor with air as the oxidant and nitrogen as the diluent, spanning the temperature range 350-550 °C. GHSV's of 4000 and 6000 h^{-1} were used, while the *n*-octane to oxygen ratios were varied between 1 and 2. The catalyst bed volume was held at 1 cm^3, with pellet sizes of between 500-1000 μm being used. The role of the support and the effect of cobalt content and varying *n*-octane to oxygen ratios were investigated, to establish the impact on *n*-octane conversion and the product profile.

The product distribution was qualitatively and quantitatively monitored by GC and GC-MS analysis. The dominant products were found to be the octenes, aromatics and carbon oxides, obtained in varying amounts with a variation in temperature. Comparative studies based on the different metal loadings and varied *n*-octane to oxygen ratios indicated that higher cobalt content enhanced the selectivities to octenes while oxidatively richer environments enhanced conversions as well as aromatics formation. The ideal reaction conditions were oxidatively richer environments (8C:4O) and higher cobalt contents in the catalysts, in order to obtain high yields of octenes and aromatics, which were the value added products in this study. COx formation was found to decrease significantly with an increase in temperature.

This research effort showed that higher linear alkanes can and do dehydrogenate, maintaining the chain length without cracking, to undergo dehydrocyclisation to form aromatics. This

titania supported cobalt catalyst system, together with the reaction parameters employed, successfully activates *n*-octane oxidatively to yield valorised octenes and C8 aromatics products.

Declaration

I hereby declare that the work conducted in this research effort and presented in this thesis, is my own work conducted from February 2012 to June 2013, at the Catalysis Research Group (CRG), at the University of KwaZulu-Natal, Westville, Durban, under the supervision of Prof Holger B. Friedrich. This work has not been submitted for any degree at this or any other university or tertiary institution. Where the work of others have been used, due recognition has been provided in the text.

_____

N. Gounden

As the candidate's supervisor I have approved this thesis for submission:

_____

Supervisor: Prof H.B. Friedrich

_____ day of July 2013

Acknowledgements

Dedication

To my brother Clive Gounden: you have made all this possible by your commitment to help, your love and support throughout the years. I will remain indebted and forever grateful for your input towards my education and this new chapter in my life.

To my angels, my late siblings Kami and Jay, I know I am always guided by you and I will always love you.

To my parents Kes and Marie Gounden, I am truly blessed to have you in my life for countless reasons, to share this new chapter of my life.

Conference contribution

Part of the work reflected in this thesis was presented at the following conferences:

CATSA conference, Langebaan, 2012, Poster presentation, *Oxidation of n-octane over titania supported cobalt catalysts: Catalyst characterisation studies.*

EUROPACAT conference, Lyon, France, 2013, Poster presentation, *The Oxidative Activation of n-octane over Co/TiO$_2$ catalysts.*

SACI Postgraduate Colloquium, UKZN Westville, 2013, Poster presentation, *The Oxidative Activation of n-octane over Co/TiO$_2$ catalysts.*

List of Abbreviations

%	percent
°C	degrees Celsius
Å	angstrom
AA	Atomic absorption spectroscopy
BET	Brunauer Emmett Teller
cm	centimeter
COx	carbon mono- and dioxide
CPO	catalytic partial oxidation
EDX	energy dispersive X-ray spectroscopy
EM	electron microscopy
eV	electron volt
FID	flame ionization detector
FT	Fischer Tropsch
g	gram
GC	gas chromatography
GHSV	gas hourly space velocity
h	hour
ICP-OES	inductively coupled plasma – optical emission spectroscopy
FT-IR	Fourier Transform Infrared
JCPDS	joint committee on powder diffraction standards
m^2/g	square meter per gram
mg/g	milligram per gram
ml	milliliter
ml/min	milliliter per min
mmol	millimole

ODH	oxidative dehydrogenation
ppm	parts per million
PXRD	powder X-Ray Diffraction
s	second
SEM	scanning electron microscopy
SGE	Scientific Glass Engineering
TCD	thermal conductivity detector
TEM	transmission electron microscopy
TGA	thermogravimetric analysis
Tmax	maximum temperature
TPD	temperature programmed desorption
TPR	temperature programmed reduction
μmol	micromole
μm	micrometer
VAP	value added products
viz.	namely
VPO	vanadium pentoxide
wt	weight
XPS	X-Ray Photoelectron Spectroscopy
XRD	X-Ray diffraction

Contents

Chapter One: Introduction

Chapter Two: A review of alkane oxidation chemistry

Chapter Three: Experimental

Chapter Four: Results and discussion

List of Figures

List of Tables

Chapter One

Introduction

1.1. The role of catalysis in industry

Catalysis and particularly heterogeneous catalysis is a widely researched field and is well documented. Catalysis plays an unequivocally significant role in the global industry. The majority [1] of industrial scale processes (> 85 %) and more than 90 % of new processes [2] incorporate catalysis. The global catalyst market was forecast to exceed $16 billion during 2012, of which 33 % is allocated to environmental applications [2]. The majority of the chemical giants globally (e.g. Dow, Monsanto, DuPont, BASF, GE, ICI) have facilities dedicated entirely to research and development. Catalytic cracking of crude oil uses zeolite catalysts, hydrotreating crude oil utilises Co-Mo, Ni-Mo and Ni-W catalysts, polymerisation of ethylene and propylene uses Cr and $TiClx/MgCl_2$, while Pt, Pd, Rh and vanadium oxide are used in the automotive industry, to name a few. A comprehensive breakdown of the largest processes based on heterogeneous catalysis, as well as production statistics for organic and inorganic chemicals in the World's Top 50 chemical producers, was compiled by Chorkendorf and Niemandsverdriet [1].

Catalytic processes have traditionally been widely used for bulk commodity chemical production, but now have made inroads to the fine and speciality chemical domain of pharmaceuticals, pesticides and fertilisers, water treatment, dyes and pigments, as well as the fibres and fabrics market. Among the better known processes are catalytic cracking in the gas-to-liquid and coal-to-liquid beneficiation technologies in the petrochemical industries, hydrodesulphurisation of fuels, catalytic converters in cars, pollution abatement involving amongst others NOx reduction to N_2, as well as plastics and polymers. This is also evident on the domestic front within Africa e.g. Algeria and Nigeria having four and two oil refineries respectively. In the South African industrial context, in a continuously technologically advancing environment, we clearly see a similar trend, with petroleum/chemical giants Sasol, PetroSA, Caltex/Chevron and Engen, amongst others, increasingly adopting catalytic processes, such as reforming, hydroprocessing and cracking of petroleum, with ever increasing production outputs to meet market demand. The major catalytic industrial processes include ammonia synthesis, ethylene oxidation, alkylation, propylene ammoxidation, hydrogenation, hydroformylation and carbonylation [3]. New technologies currently embracing catalysis are, amongst others, alternate energy and fuels, fuel cells, electrocatalysis, emission control and photocatalysis.

Catalysis allows for process efficiency and chemical conversions on an industrial scale to be taken to unprecedented new heights. How is this possible? In simple terms, catalysis allows for the rate at which reactions usually occur to be increased (to proceed faster than usual) or more correctly – significantly accelerated – and allows for the catalyst to be reused many times over. In more formal terms, the catalyst allows for the reaction to proceed through an

alternate lower energy reaction pathway without itself being consumed in the overall process. Catalysis allows reaction rates to be accelerated by orders of magnitude, at significantly lower temperatures and pressures. Combined with optimization of reaction conditions and good plant design, an overall more efficient and cheaper process is possible via the catalytic route.

For scientists and engineers alike, catalysis is a highly challenging multidisciplinary field. The elusive ideal is tailoring systems that have both high conversions and high selectivities to the desired products. This remains the fundamental challenge to researchers. To date very few systems deliver in this regard, to warrant economic viability, despite extensive research globally. Often systems that deliver high conversions result in poor selectivity, which is consistent with the reactivity-selectivity principle, whereby high reactivity is accompanied by low selectivity. The dehydrogenation of alkanes to olefins is a well established industrial process, especially that of propane and butane, that attain conversions of 30-60 %, while the C_{10}-C_{14} alkanes attain conversions of 10-20 % [4]. However, the oxidative alternative has yet to be commercialised and remains an active and dynamic area of research. The only system to have been commercialised that utilises an alkane as the feedstock is that of the oxidation of *n*-butane to maleic anhydride over the VPO catalyst with a 75-80 % conversion and 67-72 % selectivity to maleic anhydride [3].

1.2. Green chemistry

We have entered an age of increasingly limited fossil fuel based energy and ever dwindling natural resources, coupled with heightened awareness of our commitment to taking care of the planet. The USA and Europe initiated the concept of green chemistry in the 1990's and it has since been widely adopted by the chemical industry at large. The primary objective is the design and utilisation of processes and products that use and generate fewer or no hazardous substances with a lower environmental impact, together with a 'prevention rather than cure' approach being used, since prevention is preferred over waste remediation.

The fundamental aims of Green chemistry were summarised by Rothenberg [5] as follows:

- Prevention of waste instead of treatment
- Choice of synthetic routes using non-toxic alternatives where possible
- Design of atom efficient synthetic methods
- Design of new products that preserve functionality while reducing toxicity
- Minimal use of auxiliary reagents and solvents
- Design of processes with minimal energy requirements
- Preferable use of renewable raw materials
- Replacement of stoichiometric reagents with catalytic cycles
- Design of new products with biodegradable capabilities
- Development of real-time online process analysis and monitoring methods
- Choice of feedstock and design processes that minimise probability of accidents

Clearly catalytic routes meet most of these criteria. The major goals of green chemistry to develop and use more environmentally friendly routes in the production of valuable organic/inorganic products have been adopted in the use of catalysis as part of the process. With stricter environmental legislation and global awareness to greener and more environmentally friendly alternatives, a dire need exists to explore these routes more extensively. The shift towards a global commitment to reducing the carbon footprint makes catalytic processes far more favourable, as outlined above. On-going research in a concerted effort to reduce greenhouse gas emissions has led to more efficient production processes being sought, designed and implemented.

The advantages of catalysis are that milder reaction conditions are feasible, with decreased energy consumption, and environmentally benign processes are possible. Increased reaction rates and increased selectivities are more viable through the catalytic route. Catalysts can be tailored and tweaked to enhance selectivities to desired products. In broader terms, these factors imply that less waste is generated, which is highly desirable, resulting in a lower E factor (the mass ratio of waste and by-products to desired products) and less energy is consumed with higher yields. The review by Cavani [6] indicates the extent to which the cleaner alternatives have been adopted and the extent to which current research trends lean towards and integrate the greener options. Locally, from their sustainability reports, Sasol has committed to a target of 10 % per ton product reduction in greenhouse gas emissions by 2015.

1.3. Concepts in Catalysis

A brief explanation of key concepts relating to the field of catalysis will be given, to shed light on this interesting field in science and chemistry.

1.3.1. Catalysis Basics

Catalysis typically involves the diffusion of a reactant molecule from the bulk, followed by adsorption on an active site, surface reaction, desorption from the active site and diffusion of the product from the catalyst surface to the bulk. When a reactant molecule adsorbs onto a surface and interacts with an active site, the interaction involves either bond weakening, bond breaking and/or bond formation. As a result, transformation of the reactant to the product ensues. The active site is one that renders the reactant more reactive but itself remains unchanged, thereby promoting the transformation from reactant to product. The desorption of the product follows and upon desorption, the active site becomes free and available for reaction cycles once again. This is the basic feature – the regeneration of the active site – that distinguishes catalytic reactions from stoichiometric ones and makes catalysis so distinctly favourable. The surface of the catalyst is a dynamic one, with multiple adsorption/desorption reactions occurring simultaneously. Critical in this regard is the strength of the interaction in the adsorption/desorption stage: an intermediate strength is required, since too strong an interaction renders the site poisoned, unavailable for further reaction, and too weak an interaction will not be conducive for transformation of the reactant [1,3].

1.3.2. Heterogeneous and homogeneous catalysis

The two main branches of catalysis in an industrial context are homogeneous and heterogeneous catalysis. Homogeneous catalysis involves the reactant and the catalyst both being in the same phase viz. both in the gas phase or more commonly both in the liquid phase. Homogeneous systems generally operate at milder reaction conditions and work at greater heat transfer efficiency. These systems have widespread application in fine chemical production, predominantly relating to the complex nature and limited thermal stability of these products. The main drawback is the effort and cost of separation steps as well as recovery of the catalyst for reuse. Furthermore, corrosive liquid waste treatment may further complicate engineering and design.

In contrast, heterogeneous catalysis involves two different phases, typically a solid catalyst with a liquid or gas phase reactant. The research effort outlined in this thesis belongs to the latter, with gas phase *n*-octane being the reactant interacting with a titania supported cobalt catalyst in the solid phase. Temperature control in highly exothermic reactions may pose problems. Mass transfer limitations, interphase and intraphase, of both reactants and products may exist. Catalysts need to have thermal and mechanical stability and durability, accompanied by erosion resistance for use in heterogeneous systems. Heterogeneous catalysis is generally favoured, especially on an industrial scale, as a result of the ease of separation of the catalysts and products, which poses a major challenge on the homogeneous side. In industry, economics relating to an additional stage of separation and purification can determine the viability of the entire process [3].

1.4. Catalysts at the core of the process

Catalysts can be broadly classified by the key properties responsible for catalytic behaviour [7] :

- Redox catalysts are widely used for oxidation, hydrogenation, dehydrogenation and halogenation. Bulk and supported catalysts are the two major classes of these catalysts and primarily use transition metals. The high valent metal oxides are widely used in catalyst materials. Their use relates directly to their reducibility and/or ability to change oxidation states. V_2O_5 [8-15] and MoO_3 [16-27] catalysts are most frequently used as redox catalysts in alkane oxidation
- Acid–base catalysts are used in alkylation, dehydration, hydration, oligomerisation, cracking, isomerisation and H-transfer, with the key feature being the acidity and basicity
- Polyfunctional catalysts are used for reforming, oligomerisation and aromatisation of alkanes. These catalysts are a mixture of redox and acid-base catalysts
- CO transformation catalysts. As a result of the unique reactivity of CO, catalysts for its transformation can easily be classified separately. Catalysts

commonly used are e.g. Cu/Zn/Al/O based for MeOH synthesis and Fe catalysts for long chain paraffin synthesis from CO and H_2.

Heterogeneous catalysts are very often composite materials that are characterised by their surface areas, pore size distributions, relative ratios of the individual components, shape and size. The active species may be individual or multiple components, each with unique functional properties or with synergetic effects at the interface of interacting components.

Supports allow for the dispersion of the active phase over typically high surface area materials, but can play multiple roles. The most common supports are alumina, silica, titania and of recent and increasingly used: carbon nanotubes and porous material like SBA-15. Supports allow for the bulk of the catalysts to be made up of relatively cheaper material. The significantly more expensive active phase constitutes a minor fraction of the catalyst material. Supports give optimal surface and pore size distribution for the active species.

Chemical and physical promoters are used to tailor catalytic activity of the material. Chemical promoters are used to modify or adjust the activity and selectivity of the active species, while physical promoters help stabilize the surface area or improve mechanical resistance. Promoters are generally added in very small amounts. Noble metals like gold are among the most widely used for this application.

The classical redox catalysts performance is based on the oxidation of the hydrocarbon by the surface lattice oxygen, resulting in the reduction of the catalyst and re-oxidation via the gas-phase oxygen. Catalysis increases the rate of thermodynamically favourable reactions, but cannot transcend thermodynamic barriers. Redox properties, as well as acid-base properties of a catalyst, contribute to the effectiveness in the oxidation of reactants [3].

Zeolites belong to a class of solid acid alumina-silica based catalysts that have unique properties that promote shape selectivity. They comprise of porous crystalline metal oxides primarily made up of silicon, aluminium and oxygen. Substitution of cations into the zeolite structure allow for tailoring of the catalyst to acquire Lewis and/or Brønsted acid sites. Zeolites have widespread application and are frequently used in industry for increasing petroleum octane numbers. With these types of materials, the reactions do not occur on the catalyst surface, but rather within the pore structure

The design of catalysts is aimed at stability, activity and ideally low manufacturing costs. For industrial application they should be readily available and easy to synthesise, fully characterisable (preferably *in situ)* and they should promote clean technology with minimal production of greenhouse gases. Many research projects strive to design and develop new catalyst systems, tailoring them specifically with the desired outcome in mind. However, in equal measure, just as much research effort probes known systems to acquire a deeper understanding of the specifics that make them function the way they do. The entire field of catalyst design and materials research is an active one, with new developments occurring on an ongoing basis [1,3,7].

1.5. The chemistry behind alkanes

An outline of the properties of alkanes and their prevalence in an industrial context that validates research into their activation is briefly provided.

1.5.1. The role of alkanes in the chemical pool

Alkanes are saturated hydrocarbons of the general formula C_nH_{2n+2}, containing strong sigma bonds. The electronegativity of the carbon and hydrogen atom is almost equivalent and as a result electrons in these C-H bonds are equally shared by the bonding atoms. No net charge exists in the atoms making up the alkane and consequently neither electrophiles nor nucleophiles are attracted to them. The combination of strong sigma bonds and absence of a partial charge, render them highly inert [28]. This particular property of alkanes poses challenges to researchers delving into their activation. The need arises for severe reaction conditions to initiate their activation e.g. very high temperatures. However, within the homologous series, the longer chain alkanes are more reactive than their shorter chain counterparts. Therefore *n*-octane is more reactive than *n*-hexane and *n*-butane and will require lower temperatures to activate. Alkanes that form a continuous chain with no branching are referred to as linear alkanes and are named according to the number of carbons atoms that link to form the chain. The linear alkane of interest in this research is *n*-octane, the 8 carbon alkane. Linear alkanes comprise of primary and secondary carbons viz. a carbon atom bonded to only one other carbon atom and a carbon atom bonded to two carbon atoms respectively. C-H bond cleavage on the primary carbon is more difficult than those of the methylene bonds in the secondary carbon.

Alkanes and particularly linear alkanes are highly abundant hydrocarbon resources in the petrochemical industries. Linear alkanes have low octane numbers and make poor fuels since they cause knocking in engines. Branched alkanes have higher octane numbers and form an integral component of the fuel pool. Alkenes and aromatics have traditionally been the building blocks in the chemical industry, but alkanes provide a cheaper alternate feedstock. Hence, a need exists globally to transform and beneficiate these low value, underutilised resources to valorised products.

Dehydrogenation of alkanes results primarily in alkenes. Alkenes are unsaturated hydrocarbons of the general formula C_nH_{2n} and are more reactive than the alkanes as a result of the presence of pi or double bonds. These electron-rich double bonds are the centres of reactivity in alkenes. Linear alkenes have applications in industry in the manufacture of biodegradable detergents. The UOP Pacol process is a dehydrogenation process for production of linear alkenes on an industrial scale [4].

Oxo-functionalisation of organic molecules leads to the formation of numerous valorised products that serve as feedstock to industries. Alcohols, ketones, esters, aldehydes, carboxylic acids and lactones are the products resulting from this branch of oxidative chemistry. Acrolien, maleic anhydride and acrylonitrile are some of these valorised products that have numerous applications in industry and are of great commercial interest e.g. for use in detergents, polymers, plastics, as well as paints and solvents production, amongst others.

1.5.2. Dehydrogenation and oxidative dehydrogenation of alkanes to alkenes

The catalytic dehydrogenation of alkanes proceeds anaerobically via the following reaction:

$$C_nH_{2n+2} \rightleftharpoons C_nH_{2n} + H_2$$
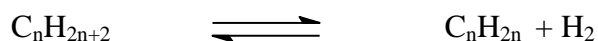
These reactions proceed endothermically and are limited by thermodynamically constraints. Side reactions like cracking are highly probable, resulting from the high temperature requirements. Furthermore, coke formation over the surface of the catalyst deactivates the catalyst and shortens its lifespan, necessitating frequent regeneration. These processes have been in existence on an industrial scale from the 1930s [4]. The early years of catalytic chemistry had butane dehydrogenated over chromia-alumina catalysts for butene production, which was further dimerised for the production of octene, which upon hydrogenation was used as high octane aviation fuel. Currently these processes represent a mature well established segment with widespread application in industry, but are both energy and capital intensive.

The aerobic dehydrogenation of alkanes proceeds via the following reaction:

$$C_nH_{2n+2} + 5/2\ O_2 \longrightarrow C_nH_{2n} + H_2O$$

Oxidative dehydrogenation reactions are, by contrast, exothermic in nature, and require lower temperature operation conditions. This, by itself, makes it an attractive option for use in industry. Coking is negligible and this also eliminates the additional step in an industrial application, making this alternative highly desirable. Challenges facing these applications are the potentially dangerous fuel/oxidant mixtures that have to be managed. The carbon oxides are the thermodynamically stable products from this chemistry. The product alkenes are far more reactive than the reactant alkanes. Stopping the reaction at the intermediate stage and preventing further reaction to the carbon oxides is an elusive goal, the solution to which has yet to be found. This oxidative dehydrogenation alternative is currently in its infancy, but has the potential to be a significant role player in industry, given its substantial thermodynamic advantages.

Oxidative dehydrogenation utilises oxygen to oxidise the coproduct H_2 from the dehydrogenation reaction. H_2O is a harmless by-product that is often recycled into the cooling systems industrially. However, hydrogen is a more valuable by-product that can be harnessed and utilised by itself. Industrial scale applications of oxydehydrogenation exist in the ethylbenzene to styrene UOP Styro-Plus and UOP Smart processes [4].

The status of catalytic selective oxidation in the context of global research is outlined by the review by Cavani [6]. This clearly outlines the present scenario (commercialisation, research, pilot plant) and relevant systems relating to selective oxidation of alkanes to petro-chemicals. The key challenge is the higher reactivity of the product compared to the reactant and stopping the reaction at the intermediate stage.

1.6. Oxidants and Oxygen species

This research effort employs air as an oxidant. Various oxidants are available to dehydrogenate and oxo-functionalise organic molecules, such as alkanes. Traditional oxidants have been peroxides, ozone, chromates and permanganates, amongst others. The hazardous nature of the peroxide chemicals, the expense and complication of the generation of ozone and the excessive use of toxic metals and the inevitable large scale toxic metal waste generation, which necessitates disposal, render these options less favourable. The quest for alternatives that increase selectivity to desired products in higher yields with minimal waste makes air an attractive oxidant. On the basis of economics, availability and environmental implications, molecular oxygen or air are clearly more desirable. This research effort employs air as the oxidant in the oxidative activation of *n*-octane to valorised products.

Oxygen plays a role in regenerating the surface oxygen sites, following the reduction of the surface, catalyses the C-H activation step, provides direct oxo-functionalisation and minimises catalyst degradation by coke build-up as is evident in anaerobic dehydrogenation studies. Several different oxygen species exist in the oxidative catalyst system, among them terminally bonded M=O, bridging M-O-M oxygen species, intermediate radical species - molecular O_2^- and atomic O^-. As outlined below, gas phase oxygen can accept electrons sequentially until it transforms into the fully reduced form, thereby re-oxidising the catalyst with migration through the lattice.

$$O_2 \quad \rightarrow \quad (O_2)_s \quad \rightarrow \quad (O_2^-)_s \quad \rightarrow \quad (O_2^{2-})_s \rightarrow \quad (O^-)_s \quad \rightarrow \quad O^{2-}(latt)$$

$$(O)_s$$
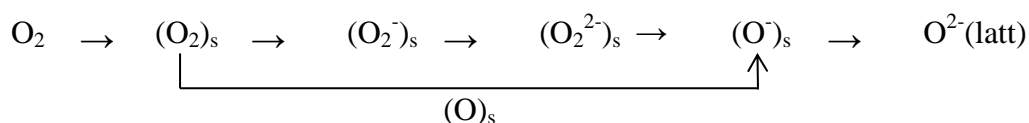
Some speculation exists as to the contribution of each of the species to the chemistry and which one specifically is the active oxidant. The questions are addressed in numerous research studies often incorporating isotopic labelling. In the absence of gas phase oxygen e.g. in anaerobic testing, the selective oxidation catalysts serve as the source of the active oxidation species for some time before their lattice is stripped of them. The generally accepted theory is that selective oxidation occurs via strongly bonded nucleophillic lattice oxygen e.g. M=O contributes to the C-H bond cleavage that results in dehydrogenation, while complete oxidation occurs via weakly bonded electrophilic species of oxygen i.e. insertion comes from the bridging oxygen [29].

Numerous research projects have employed carbon dioxide as a mild oxidant. The reviews on catalytic conversion of alkanes to olefins by carbon dioxide dehydrogenation by Wang and Zhu [30] and ethane transformation to ethene [4] clearly focus on this alternative. Catalyst systems that were found to be successful in this application are, amongst others, gallium oxide, vanadium pentoxide and titania. This option seems more favourable than the current steam cracking application being utilised, since significantly lower temperatures can be used. Furthermore, coking is a lessor problem in this regard. Utilisation of this greenhouse gas is a highly attractive option and needs probing on a large scale e.g. in the dehydrogenation of

ethylbenzene to styrene. Furthermore, this would eliminate the potentially dangerous oxygen-alkane mixtures and the safety aspects associated with it.

1.7. Reactors

Heterogeneously catalysed reactions are mainly carried out in three types of reactors: fixed bed; fluidised bed and stirred tank reactors. Stirred tank reactors are primarily used in homogeneous catalysis and offer excellent contact between catalyst and reactant, while offering applicability in both batch and continuous mode. When run under comparable conditions, lower conversions are obtained in comparison with fixed bed reactors.

1.7.1. Fluidised bed reactors

Fluidised bed reactors involve fine catalyst particles suspended in the reactant gas, enabling good mixing and contact between reactant and catalyst accompanied by good temperature control. Upward gaseous flow enables the fluidised state within the reactor. However, the engineering is complex and expensive to design and certainly not conducive to laboratory scale investigations. Industrial applications typically using fluidised beds are fluid catalytic cracking processes, with the oxidation of butane to maleic anhydride being another example. This reactor type easily handles operation with rich hydrocarbon-oxygen mixtures, which otherwise could be explosive.

1.7.2. Fixed bed reactors

Work for this thesis employed a single tube fixed bed reactor system, with relatively simple engineering, which is more practical for laboratory scale investigations and outlined in Chapter three. The gas phase reactant is fed downwards to come into intimate contact with the solid catalyst bed, passes through the voids, leaving transformed at the bottom of a closed system. Temperature control relating to exothermic reactions and pressure drops are common problems encountered in this reactor type. Application in industry often utilises multi-tubular fixed bed reactors e.g. 30 000 - 60 000 individual tubes, up to 6 m in length and 25 mm in diameter utilising 100 m^3 of catalyst [31].

1.7.3. Monolith reactors

A monolith consists of a single block of material containing separated or interconnected channels. These channels may be straight, wavy or crimped resulting in a square, circular or triangular cross section. Monolith reactors make use of monoliths constructed from porous catalyst material or the catalyst material is deposited or washcoated into the channels of the inert material. The two main types in industry and research are the metallic and ceramic monoliths. Traditionally they have been used in the automotive industry in pollution abatement. Monoliths used in reactors offer several advantages over conventional catalysts used for gas phase chemistry:

- Ease of scale up
- Higher specific catalyst surface area for mass transfer reactions
- Lower pressure drop especially under high fluid throughput

- Reduced fouling and blockage (which extends the catalyst lifetime)
- Reduced diffusion limitations especially when thinner walled monoliths are used.

References

[1]   I. Chorkendorff, J.W. Niemantsverdriet, Wiley-VCH, Weinheim, 2007, p. 22.

[2]   J.N. Armor, Catalysis Today. 163 (2011) 3-9.

[3]   B. Gates, Catalytic Chemistry, Wiley, New York, 1992.

[4]   B.B. Bhasin, J.H. McCain, B.V. Vora, T. Imai, P.R. Pujado, Applied Catalysis A: General. 221 (2001) 397-419.

[5]   G. Rothenberg, Catalysis Concepts and Green Applications, Wiley-VCH, Weinheim, 2008.

[6]   F. Cavani, Catalysis Today. 157 (2010) 8-15.

[7]   F. Cavani, F. Trifiro, Catalysis Today. 34 (1997) 269-279.

[8]   A.I. Anastasov, Chemical Engineering and Processing 42 (2003) 449-460.

[9]   D.I. Enache, E. Bordes, A. Ensuque, F. Bozon-Verdura, Applied Catalysis A: General. 278 (2004) 103-110.

[10]   M.P. Gimeno, J. Gascon, C. Tellez, J. Herguido, M. Menendez, Chemical Engineering and Processing. 47 (2008) 1844-1852.

[11]   M.P. Gimeno, J. Gascon, C. Tellez, J. Herguido, M. Menendez, Chemical Engineering and Processing. 47 (2008) 1844-1852.

[12]   B. Grzybowska-Swierkosz, Applied Catalysis A: General. 157 (1997) 409-420.

[13]   V.D.B.C. Dasireddy, S. Singh, H.B. Friedrich, Applied Catalysis A: General. 421-422 (2012) 58-69.

[14]   J. Haber, Catalysis Today. 142 (2000) 100-113.

[15]   M. Ruitenbeek, A.J. Van Dillen, D.C. Koningsberger, J.W. Geus, in: B. Delmon (Ed.), Effects of Silica and Titania Supports on the Catalytic Performance of Vanadium Phosphorous Oxide Catalysts, 1998.

[16]   K.Y.S. Ng, E. Gulari, Journal of Catalysis. 92 (1985) 340-354.

[17]   G.D. Panagiotou, T. Petsi, K. Bourikas, A.G. Kalampounias, S. Boghosian, C. Kordulis, A. Lycourghiotis, Journal of Physical Chemistry C. 114 (2010) 11868-11879.

[18]   S.K. Maity, M.S. Rana, S.K. Bej, J. Ancheyta-Juarez, G.M. Dhar, P.T.S.R. Rao, Applied Catalysis A: General. 205 (2001) 215-225.

[19]   H. Matralis, S. Theret, P. Bastians, M. Ruwet, P. Grange, Applied Catalysis A: Environmental. 1995 (1995) 271-281.

[20]   E. Heracleous, M. Machli, A.A. Lemonidou, I.A. Vasalos, Journal of Molecular Catalysis A: Chemical 232 (2005) 29-39.

[21]   K.V.R. Chary, T. Bhaskar, K.K. Seela, K.S. Lakshmi, K.R. Reddy, Applied Catalysis A: General. 208 (2001) 291-305.

[22]   K.V.R. Chary, K.R. Reddy, C.P. Kumar, Catalysis Communications. 2 (2001) 277-284.

[23]   T.J. Hall, J.S.J. Hargreaves, G.J. Hutchings, R.W. Joyner, S.H. Taylor, Fuel Processing Technology. 42 (1995) 151-178.

[24]   D.L. Stern, R.K. Grasselli, in: R.K. Grasselli, S.T. Oyama, J.E. Lyon (Eds.), 3rd World Congress on Oxidation Catalysis, 1997.

[25]   R.K. Grasselli, J.D. Burrington, J.D. Buttrey, P. DeSanto, C.G. Lugmair, F.A. Volpe, T. Weingand, Topics in Catalysis. 23 (2003) 5-22.

[26]   R.K. Grasselli, J.D. Burrington, J.D. Buttrey, C.G. Lugmair, P. DeSanto, F.A. Volpe, T. Weingand, Catalysis Today. 91-92 (2004) 251-258.

[27]   J. Barrault, C. Batiot, L. Magaud, M. Ganne, in: R.K. Grasselli, S.T. Oyama, J.E. Lyon (Eds.), 3rd World Congress on Oxidation Catalysis, 1997.

[28]   P.Y. Bruice, Organic Chemistry, 4th ed., Pearson Prentice Hall, 2004.

[29]   G.I. Panov, K.A. Dubkov, E.V. Starokon, Catalysis Today. 117 (2006) 148-155.

[30]   S. Wang, Z.H. Zhu, Energy and Fuels. 18 (2004) 1126-1139.

[31]   B.K. Hodnett, Heterogeneous Catalytic Oxidation, Wiley, New Jersey, 2000.

Chapter Two

A review of alkane oxidation chemistry over heterogeneous catalysts

2.1 A survey of alkane oxidation within the Catalysis Research Group (CRG)

In-house research into paraffin activation at the CRG at the University of KwaZulu-Natal began over a decade ago. Several interesting projects were undertaken spanning varied catalyst systems with greater emphasis on the higher linear alkane, n-octane. A breakdown of the various research initiatives in heterogeneous catalysis is outlined in Table 1.

Table 1: Research initiatives delving into paraffin oxidative activation at the CRG

	Student Name	Year	Feed	Catalyst
1	Govender Nishlan	2002	n-butane	Co promoted VPO
2	Ramdeen Manuja	2003	n-butane	Ru promoted VPO
3	Mahomed Abdul	2005	n-octane	Hydrotalcite-like compounds incorporating divalent (Mg, Ni, Zn, Co, Cu) ions and trivalent (V, Al, Cr, Fe) ions
4	Chetty Jonathan	2007	n-hexane, n-octane	VMgO
5	Govender Nishlan	2007	n-butane, n-hexane, n-octane	VPO and VMgO
6	Masilo Neoentle	2009	n-butane	Fe and Ru promoted VPO
7	Pillay Bavani	2009	n-hexane	NiMoO$_4$
8	Naicker Thirusha	2010	n-hexane	V-ZSM-5 zeolites
9	Elkhalifa Elwathig	2010	n-octane	VMgO
10	Bux Mayashree	2010	n-octane	Vanadium based hydrotalcite
11	Sewsunker Shantal	2011	n-octane	Carbon nanotube supported NiMoO$_4$
12	Makatini Thobekile	2012	n-octane	MoVTeNbO
13	Dasireddy Venkata	2012	n-octane	Hydroxyapatite supported V$_2$O$_5$

Maleic anhydride is one of the major bulk chemicals produced for use in the polymer industry. n-Butane transformation to maleic anhydride is the only heterogeneous oxidative process using an n-alkane as the feedstock, to have been commercialised to date. The pioneering research initiatives at the CRG in oxidative alkane activation began with n-butane as the feed to produce maleic anhydride. Govender's initial project [1] delved into the use of Co promoted and unpromoted VPO catalysts for the activation of n-butane. Three parameters were varied: GHSV, Co loadings and temperature, in order to find the optimum reaction conditions that favoured the enhanced selectivity to maleic anhydride. An online GC system allowed for up to 200 hours monitoring of catalytic activity. The best results obtained were

from the cobalt promoted catalyst system that yielded 45 % maleic anhydride at 275 °C and using a 2878 h^{-1} GHSV, achieved with a 73 % conversion of *n*-butane. This outcome surpassed all reported results for maleic anhydride yields at that temperature [2]. This set the momentum for further research within the context of alkane activation.

Govender [3] then proceeded to investigate the higher linear alkanes as a feed. The comparative study of mixed metal oxides in C4, C6 and C8 linear alkane activation was an intensive investigation delving into non-catalytic and catalytic influences on the oxidative chemistry. Phase composition, morphology and crystallinity of the catalyst material, type of catalytically active species and the average oxidation state of the active metal were studied and shown to be the critical factors that ultimately influenced the product distribution and the selectivities to the desired products. Govender's study clearly showed that under similar reaction conditions, the VPO catalyst system favoured increased selectivity to COx compared to the VMgO system. Furthermore, the orthovanadate phase in VMgO was more active and selective than the pyrovanadate in the C6 and C8 linear alkane activation. In the selective oxidation of *n*-butane to maleic anhydride, the best performing VPO catalyst had a platelet morphology which resulted directly from the incorporation of cobalt into the catalyst. In contrast, this system in *n*-hexane and *n*-octane activation, showed high tendency to deep oxidation and greater selectivity to cracked products and to a lesser extent cyclic and linear oxygenates. The effects of voids and dilution were further investigated under a constant 3000 h^{-1} GHSV, and the *n*-hexane oxidation was found to be influenced by the location of the voids and non-catalytic influences, but enhanced by packing the reactor tube completely with inert material [4].

Ruthenium as the promoter in the VPO catalysts system was the choice made by Ramdeen [5] in further research delving into that catalyst system. This research effort probed the effect of different Ru loadings (0.2, 0.6 and 1 % Ru) on catalytic activity and selectivity to maleic anhydride. The optimal performance of the VPO catalyst was achieved by doping using 0.6 % Ru. Conversions were enhanced with increasing temperature up to 450 °C at a GHSV of 1960-2170 h^{-1}, but catalyst degradation resulted with further temperature ramping. The influence and sensitivity to promoter loadings was evident from results obtained on the 1 % Ru doped VPO catalyst, showing lower maleic anhydride yields.

Masilo [6] in her research effort, continued investigations into *n*-butane oxidation using the VPO system, but chose iron and ruthenium as the promoters in an attempt to enhance activity of the catalyst and increase selectivity to maleic anhydride. Three different loadings of the dopant were used viz. 0.1 %, 0.3 % and 1.0 %. Furthermore, the catalysts were pelletised and sieved to uniform sizes by screening through 300-600 μm sieves. Uniformity of the catalyst particle size is a critical factor since uneven pellet sized particles can cause plugging of the void spaces by smaller particles, which would inhibit the passage of gases through the catalyst bed. This may contribute to back pressure build up within the reactor tube and significantly compromise testing. These catalysts were tested under varied feed to oxidant ratios, temperatures and GHSV's to find the optimum reaction parameters. Promotion by the 0.1 % Fe of the VPO catalyst did enhance the selectivity to maleic anhydride by ca. 10 %. The yields obtained at 400 °C and at GHSV of 2573 and 1450 h^{-1} were 46 and 55 %

respectively. This research effort clearly indicates the importance of the choice of promoter as well as the loadings, since dopants seem to be effective in small amounts, typically under 1 %.

The research effort of Chetty [7] probed both *n*-hexane and *n*-octane activation over VMgO catalytsts. Catalysts with different loadings of vanadium were prepared and fully characterised, revealing the presence of two phases, that of magnesium oxide and magnesium orthovanadate $Mg_3(VO_4)_2$. Catalytic testing of these materials comprised of varying oxidative environments, temperatures and GHSV's. The optimum loading was found to be 19 % V_2O_5 and this catalyst was extensively studied for promotion effects. The promoters that were investigated were the oxides of molybdenum, cesium, antimony, niobium, tellurium and bismuth. Initial testing of the promoted catalysts involved the *n*-hexane feed and those indicating enhanced activity were further tested with the *n*-octane feed. Tellurium and molybdenum promoted catalysts displayed enhanced performance. The reactor system was adapted to incorporate parallel fixed beds for catalytic testing of the promoted catalysts.

Zeolite catalysts broke new ground in alkane activation chemistry within the CRG. The research initiative by Naicker on *n*-hexane activation [8] probed the aerobic and anaerobic effects over H-ZSM-5 with different SiO_2/Al_2O_3 ratios (100 and 320) as well as Na-ZSM-5 at a SiO_2/Al_2O_3 ratios of 100. A major finding in this research effort was the cracking ability being enhanced over H-ZSM-5 when the aluminium content decreased (higher ratio SiO_2/Al_2O_3) under oxidative conditions. The selectivity to cracked products increased from 8 % to 32 % upon comparison of the 100 and 320 SiO_2/Al_2O_3 ratios respectively. The sodium form of the zeolite completely eliminated acid cracking. The study was extended to preparation and catalytic testing of vanadium exchanged zeolites. The Na-V-ZSM-5 catalyst was found to be more active for aromatic and cyclic compound formation than the other catalysts and also gave a yield of 8 % towards primary C6 products.

Nickel molybdate catalysts were chosen in the investigations probing *n*-hexane oxidative dehydrogenation by Pillay *et al*. [9, 10] following the effectiveness of the system in ethane, propane and butane ODH. Based on outcomes of previous in-house research into beta phase nickel molybdate, this research initiative aimed to enhance already promising activity, particularly to the alpha olefin and hexenes in general. Terminal functionalization of the linear alkane in a general way poses a challenge, owing to the lower reactivity of primary carbons in alkanes. Results obtained from this project show a 55 % selectivity to hexenes, of which 27 % was to the alpha olefin 1-hexene. Reaction parameters were closely monitored and sequentially varied to drive the selectivity towards hexenes in order to find the optimum conditions for catalytic testing. Nitrogen dilution, contact time and feed to oxidant ratios bordering flammability limits were thoroughly investigated to establish the precise impact on hexenes selectivity.

One of the early research efforts at the CRG using higher linear alkanes was undertaken by Mahomed [11, 12], in the partial oxidation of *n*-octane. Hydrotalcites that incorporated several metal ions, viz. Mg, Ni, Zn, Co, Cr, Fe, Al and V in varying ratios, were the catalysts under investigation. Different combinations of divalent and trivalent ions were used to

investigate which family of compounds yielded the best results. The catalytic system incorporating aluminium was found to yield the best selectivity to olefins, while the bimetallic systems with Zn-Cr and Co-Cr produced a significant amount of oxo-functionalised products like ketones and cyclic ethers. The catalyst systems incorporating Mg and V produced mainly dehydrogenation products: olefins, dienes, trienes and aromatics, predominantly styrene, together with COx products.

Further research into paraffin activation using hydrotalcites was carried out by Bux [13]. Results from this project indicate that the Mg-V hydrotalcite catalyst produced the best results at 500 °C with an aromatic selectivity of 19 % (predominantly styrene) and octenes selectivity of 22 % with 1-octene of ca. 7 %. With a contact time of 0.5s and a 15 % octane in air ratio, the lowest levels of deep oxidation products were recorded at this temperature accompanied by 41 % octenes and aromatics selectivity. This catalytic system was further investigated for promotion effects by using boron, cesium and barium. The Cs and B dopants were shown to marginally enhance the selectivity to C8 alkenes.

In more recent research by Elkhalifa [14, 15] on *n*-octane activation, VMgO catalysts were chosen, given their good performance in short chain linear alkane activation. This research effort explored the influence of dopants, the strength of the oxidative environment and the effect of varied vanadium loadings. Upon comparison of the results from the comprehensive study of the 5-25 wt% V_2O_5 loadings, it was found that the 15 wt% catalyst had the best selectivity to the targeted products, octenes and C8 aromatics. This catalyst was then tested further to evaluate the influence of the oxidative environment on the catalytic activity. The oxygen richer environment was found to enhance conversions at the expense of selectivity to octenes, in contrast to the oxygen leaner environments, that showed lower conversions and enhanced selectivity to the oxidative dehydrogenation products. An additional aspect that was investigated was the effect of acidic (boron) and basic (barium) dopants on the activity of the catalyst. Overall, the barium doped catalyst showed enhanced activity and selectivity to ODH products. These catalyst systems also were shown to provide, to a very limited degree only, the oxygen species that lead to insertion into the organic reactant to form oxofunctionalised products like ketones and alcohols.

Recent research explored by Makatini [16] probed the activity of MoVTeNbO mixed metal oxide catalysts. The work follows on that of Lopez-Nieto *et al*. [17, 18] who studied the ODH of ethane using these catalysts. The focal point of the study was the effect of the metal atomic ratio on the catalytic activity in the oxidation of *n*-octane. Vanadium contents were varied with ratios of 2:3:4 for the three catalysts. Testing was conducted with a constant GHSV of 4000 h^{-1} and temperature was restricted to 350 °C and 400 °C. The three catalysts that were tested showed the same 12 % selectivity to the dominant product, methanol. At an isoconversion of 10 % at 350 °C, the catalysts showed selectivities to oxygenated products of 20.3 %, 18.9 % and 19.2 %, in order of increasing vanadium content. The catalyst with the highest vanadium content was further tested, and at 400 °C and 2000 h^{-1} GHSV, the selectivity to oxygenated products was 56.8 %. Furthermore, the selectivity to COx products was less than 1%. Post reaction studies of the used catalysts were also carried out to evaluate

the changes, viz. chemical, physical and textural, that occurred during reaction under those specific conditions.

Carbon nanotubes (CNT) have unique structure and surface properties accompanied by high thermal stability. Rresearch had reflected that carbon nanotubes had significant catalytic activity in paraffin activation and had been used in the oxidative dehydrogenation of ethylbenzene to styrene and propane to propene. Sewsunker's research [19] delved into the activity of carbon nanotube supported nickel molybdate catalysts. Other research clearly showed that the alpha and beta phases of nickel molybdate had also been extensively used in short- to medium chain paraffin activation. Individual catalytic testing of the CNT, alpha nickel molybdate, beta nickel molybdate and the CNT supported nickel molybdate showed that all were catalytically active in the ODH of n-octane. From the results obtained for the 10 % isoconversion at 300 °C, it was evident that CNTs showed increased selectivity to oxygenates and C8 alkenes, and simultaneously lower the selectivity to COx and cracked products compared to the alpha phase. Likewise the alpha phase, once supported on the CNT, yielded higher selectivity to C8 alkenes, with decreased selectivity to COx. Clearly, supporting the alpha molybdate proved advantageous. The *in situ* generated beta phase proved to be more active and selective than the alpha phase, with a 16 % selectivity to oxygenates and 12 % selectivity to C8 alkenes compared to the 13 and 7 %, respectively, for the alpha phase.

The ODH of n-octane over vanadium pentoxide supported hydroxyapatite catalysts was the the research initiative of Dasireddy [20]. The literature clearly showed the success of V_2O_5 and hydroxyapatite in the ODH of lower linear alkanes to valorised products, and hence the study was extended to the higher C8 linear alkane. At isothermal (450 °C) isoconversion of 36 %, the 2.5 wt% catalyst achieved a maximum selectivity of 56 % to octenes, while the 15 wt% catalyst achieved a 10 % maximum selectivity to aromatics. These results significantly clarify the impact of the vanadium loadings on the product distribution and selectivity to the desired products. Further *in situ* XRD investigations in this research effort revealed the presence of two different phases. At lower vanadium loadings (<10 %) vanadium was found only in the vanadium pentoxide phase, while for loadings > 10 % an additional pyrovanadate phase was detected. The different phases directly influenced catalytic activity. The vanadium pentoxide phase favoured octenes selectivity over aromatics. The pyrovanadate phase drove the selectivities towards the aromatics, despite the dominance of the octenes. The synergistic effect from the co-existance of the two phases is the probable reason for the enhanced selectivity to octenes. Both conversion and selectivity to C8 alkenes was enhanced by increasing temperatures, since this further influenced the phase composition. In terms of carbon oxides, all the catalysts displayed moderate to high selectivities to CO and CO_2.

The CRG continues to run parallel research projects in n-octane activation with the view to extending the research into n-decane activation. The molybdates (Fe, Ga, Ni, Co), SBA-15 supported catalysts and ceria based catalysts are currently being investigated. A greater understanding of alkane activation has evolved from exposure to the various systems currently under investigation, as well as from those systems investigated in the past.

2.2. Overview of alkane oxidation

Globally, alkane activation remains an active and dynamic field of research, particularly in relation to the oxidative route. Research motivation is driven primarily in the quest for systems that deliver high activity: high conversions and high selectivity to targeted products that are economically favourable and have the potential for commercialisation. As a research community, better understanding of catalytic systems and their functioning on a microscopic level steers much effort into sophisticated characterisation techniques, as the researchers' toolbox has evolved tremendously over time. When scanning the literature, numerous studies globally by industry and academia encompassing both characterisation and catalytic testing, serve to educate newcomers and the experienced alike, to this branch of chemistry.

2.2.1. A lifetime of passion and dedication to science and catalysis

Some authors have dedicated a lifetime and their careers to this specialised field of science and their passion for catalysis. Among the better known names in the research field are those of Hutchings, Corma, Lopez-Nieto, Grasselli, Trifiro and Cavani.

Through numerous independent studies, as well as collaborative efforts, Hutchings has made a very significant contribution to catalysis and alkane activation in particular [21-42]. The research work of Hutchings has incorporated and integrated gold in a major way, showing the enhanced activity of the nanosized particles [21, 22, 25, 34], but gold as a redox catalyst has only recently been discovered and has the potential to grow significantly. This paves the way for extensive research into this new branch of 'golden' chemistry. CO and alcohol oxidation [21] are but two of the areas that have achieved success in the application of gold as a redox catalyst. The gold loading, as well as the particle size were found to be critical factors that affected the activity of these gold catalysts. In Temporal Analysis of Products (TAP) reactor studies, incorporating cobalt oxide as a support to gold, good activity in the deep oxidation of propane was reported. Cobalt oxide by itself was found to be highly active and gold had a promoting effect, but gold supported on titania catalysts were previously investigated and showed poor activity to propane combustion. A novel supercritical CO_2 (SAS) preparation of titania [37] as a support for gold was investigated, following the use of this method in the preparation of other supports for gold catalysts, where the novel technique contributed to superior performance of the catalyst system.

n-Butane oxidation to maleic anhydride [28, 29] was one of many projects of focus by Hutching's research initiatives into alkane activation [24, 26, 31, 34-36, 39, 41] using a multitude of catalyst systems, primarily investigating shorter chains but progressing in recent years, increasingly, to the higher linear alkanes [43, 44]. Cobalt as a promoter, improved specific activity but molybdenum was found to enhance both specific activity and the selectivity to maleic anhydride at conversions in excess of 90 % [28]. A ball milling technique was used to pulverise the catalysts precursors [29], and was found to decrease the crystallite size significantly to yield high surface area catalysts that enhanced maleic anhydride selectivties, from n-butane oxidation. The higher linear alkane *n*-decane, was investigated under mild conditions [44], by means of aerobic oxidation, to produce

oxygenates via ceria based catalysts, which were found to enhance selectivities to alcohols. Further work on *n*-decane [43] using various mixed metal-oxide catalysts, showed that iron molybdate catalysts were particularly effective in forming oxygenated aromatics at 350 °C. At higher temperatures the product profile was dominated by alkenes and aromatics, consistent with the redox mechanism at higher temperatures.

The field of interest for Corma [45-51], in relation to selective oxidation, has been meso- and microporous materials and zeolite catalysts in particular. Solid acid catalysts and materials like molecular sieves [45, 48], present shape selectivity that is unique to these classes of materials. Corma's work delved into addressing some of the challenges within this field, tailoring and designing material with ultra large pores so that reaction with bulkier reactants became possible [45]. His research made it possible to oxidise benzene to phenol with yields of 70 – 80 % over ZSM-5 zeolites with N_2O as the oxidant. Other research [48] focused on attempting the epoxidation of propylene using transition metal zeolites with iron doping, which was unsuccessful. Corma further designed mesoporous-microporous hybrid materials to develop unique shape selectivity effects. Corma's research has explored the strength and nature of acid sites in these materials and their contribution to the chemistry. Selectivities to desired products can be tailored by manipulation of properties of these materials e.g. acidity, pore and channel sizes [47]. Other contributing factors are the high surface areas and adsorption capacity of these materials, as well as the nature and intricacy of their channels. Fouling of pores and pore blockage are the major challenges facing these scientists and places a limitation to the application of these otherwise versatile catalysts [51], hence catalyst design became the focal point, to overcome the current challenges mentioned.

2.2.2. Vanadium based catalysts for alkane oxidation

Vanadium based catalysts are by far the most intensively studied catalyst system: particularly following its successful application in *n*-butane to maleic anhydride oxidation on industrial scale. The literature covers many such systems and several different aspects have been investigated by many researchers. Synthesis of numerous catalysts and the catalyst characterisation studies cover a large portion of literature available, while their applications in various oxidation reactions under varying testing conditions covers the majority of the research initiatives. The influence of supporting catalysts, catalytic activity of bulk versus supported catalysts, investigations into different supports, electronic factors, the different phases that vanadium exists in and individual phase influences, mixed vanadia based catalysts and their application, as well as catalyst deactivation, are just a few of the many aspects explored by researchers.

Lopez-Nieto also has made a significant impact on research in the field of oxidation catalysis. A significant research effort has gone into investigation of vanadium based catalysts, including the VPO systems. One of the aspects relating to catalysis, covered by this established researcher [18, 52-62] is the oxidation of light alkanes. His research [52] on C2-C4 linear alkanes, highlighted the importance of the choice of the metal oxide support and its associated acid/base character in influencing the chemistry, e.g. the dispersion of

vanadium and well as the vanadium species. He found the tetrahedral V^{5+} species to be particularly active and selective in the oxidation of short chain alkanes.

From work carried out on VMgO catalysts [52, 55], the size of the reactant and the dispersion of the active sites were found to directly influence selectivities in ODH reactions. Larger molecules were found to be able to react simultaneously with adjacent active sites that were in close proximity to each other, resulting in deeper oxidation, than when smaller molecules were used, or when reacting with isolated active sites. The preparation technique [57] used for catalyst synthesis was further identified as one of the significant factors that ultimately influenced the catalytic activity. Catalyst re-oxidation was found to be the rate limiting step in propane oxidation over VMgO catalysts [60], while higher reaction temperatures were found to accelerate redox exchanges and enhance catalytic activity in reactions of *n*-butane. Hence, the rate at which redox processes occurred was identified as being directly influential in catalytic performance.

Considerable effort has also gone into the mixed metal oxide [18, 53, 59] $MoVTeNbO_x$ catalysts, tailoring them using different synthesis techniques as well as doping for enhancement of their activity. Phase co-operation, relative ratios of the constituents and synergistic influences are some of the factors that were found to impact on the activity of these catalysts. The activity was found to be critically influenced by small variations of molybdenum, the dominant metal in these catalysts, and less so by constituents like tellurium. Lopez-Nieto focussed to a lesser extent on *n*-pentane oxidation [54], but found that phthalic anhydride formed via a parallel reaction pathway with maleic anhydride during the oxidation of *n*-pentane. The $(VO)_2P_2O_7$ catalyst was the most effective in this application to activate *n*-pentane oxidatively.

Haber [63] has by far the longest (50 year) track record with vanadium oxide catalyst research. He found several important factors that made the vanadium oxides particularly interesting and challenging to research. Vanadium oxides and vanadium oxide based catalysts have partially filled d-orbitals that contribute to their unique interrelated electronic, magnetic and catalytic properties, together with the wide variation in oxidation state from two to five. His research showed that the ease of formation of oxygen vacancies in these catalysts made them good selective oxidation catalysts.

Maurya *et al*. [64] reviewed supported vanadium complexes in oxidation and functionalisation of alkanes and alkenes. Their research focussed on immobilisation of the active phase on mesoporous materials, amongst others, via encapsulation, entrapment and adsorption. These catalysts showed a key finding: preference for oxidation of smaller alkane substrates over longer chains in competitive oxidative environments.

Herrmann [65] covered the electronic factors and related redox processes with respect to the vanadyl pyrophosphate case study. This research effort focussed on the semiconductor properties of oxides in their pure, supported, mixed or doped forms, that allow them to function as redox catalysts. Electrical conductivity measurements taken *in situ* on titania during catalytic oxidation of CO, showed the O^- species to be the oxidising agent.

Guliants [66] closely investigated structure-reactivity relationships in supported vanadium catalysts in *n*-butane activation. The choice of support was critical, with titania forming a well dispersed VPO phase. Silica on the other hand, did not have a strong interaction with the VPO precursor and hence resulted in unsupported bulk VPO material while alumina had too strong an affinity for phosphate and resulted in a supported phosphate depleted VPO phase.

Enache *et al*. [67] probed vanadium oxide supported on titania and zirconia for application into selective oxidation of ethane to ethylene and acetic acid. The zirconia supported catalyst was found to perform better than the titania equivalent, with ethylene yields of 16 % and 75 % selectivity to ethylene.

In application to the oxidation of o-xylene and other hydrocarbons, Gimeno *et al* [68] delved into the kinetics of catalytic testing in fluidised bed reactors, using the V_2O_5/TiO_2 system for the oxidation of o-xylene to phthalic anhydride. Mass and heat transfer limitations were found to significantly influence the results of catalytic testing.

Luciani *et al*. [69] studied anatase phase supported vanadium catalysts and found that the support could catalyse formation of heavy compounds. Furthermore, the effect of water on the reactivity and physico-chemical properties of the catalysts was studied, and steam was found to enhance activity. Grzybowska-Swierkosz [70, 71] also investigated vanadia-titania catalysts, studied the active centres and their role in the oxidation of o-xylene to phthalic anhydride, amongst others. Vanadia based catalysts were found to follow a mechanism of parallel-consecutive reactions. Carbon oxides formed in a parallel route, directly from the substrate or intermediate products or via the consecutive route from deep oxidation of the oxygenated products.

Ruitenbeek *et al.* [72, 73] investigated bulk as well as silica and titania supported VPO catalysts and found the catalytic activity remarkably different. The differences in catalytic activity was attributed to the different phases present even when comparable yields to maleic anhydride were obtained on the bulk and silica supported VPO catalysts.

Anastasov [74] looked into the deactivation of industrial V_2O_5/TiO_2 catalysts. The deactivation profile along the catalyst bed was monitored as a function of time, clearly indicating the significant influence of 'hotspots', in relation to both sintering and long term deactivation. These catalysts based on the anatase phase titania were found to have a lifetime of five years, in industrial applications.

2.2.3. Research into titania based catalysts

The use of cobalt titania catalysts in higher linear alkane oxidative activation, to the best of my knowledge, does not exist and this niche in research prompted the investigation of this topic in this thesis. The catalyst, however, is not novel and a few investigations exist in its application as an oxidation catalyst. Titania has numerous applications as a photocatalyst and one such study by Deng and Gao [75] focusses on the gas phase reaction of hexane to the combustion products. Nanosized titania particles with varying surface areas, particle sizes

and crystalline phases were compared in this study. Surface area was found to be the dominant factor in determining activity and smaller titania particles were found to have a detrimental effect on activity.

Brik *et al*. have used boron [76] and phosphorus [77] as dopants in their comparative study with titania supported cobalt promoted and unpromoted catalysts for the ODH of ethane. Low loadings of cobalt led to the surface being covered in Co^{2+} species but at loadings higher than 3.7 wt%, Co_3O_4 spinel species formed. The 7.6 wt % cobalt unpromoted catalyst performed the best in ethane ODH, with conversions of 33 % at 550 °C being reported. Phosphorous doping was unsuccessful in enhancing the catalyst performance but boron loadings lower than 0.25 wt %, did enhance conversions and selectivity to ethylene by 6 % and 7 % respectively.

Yung *et al*. [78] have utilised cobalt supported on both titania and zirconia in an oxidative application, transforming nitric oxide to nitrogen dioxide. The zirconia supported cobalt catalyst with a 10 wt% loading gave the best performance. This catalyst prepared via wet impregnation was better than the equivalent prepared using the sol-gel technique.

Cobalt oxide nanoparticles, in their application to transform cyclohexane - the model for jetfuel - oxidatively, have been researched by Tyo *et al*. [79]. The 6 nm particles were found to yield benzene at high temperatures, while the 12 nm particles transformed cyclohexane to cyclohexene at low temperatures. These findings demonstrated that larger particle size and higher temperatures, promoted significantly greater dehydrogenation activity.

The focus of the study by Xiao *et al*. [80] investigated cobalt impregnation on various supports and their corresponding catalytic activity in methane combustion. This showed that the zirconia supported cobalt catalysts displayed better activity than the titania supported catalysts. The catalytic activity was a strong function of the zirconia but the overall activity was reported to be due to the synergetic effect of the cobalt oxide and zirconia. The 1 wt% cobalt catalyst was the best performing one. Titania was reported to have a higher oxygen mobility and lower acidity than zirconia, which may be key factors relating to its poorer catalytic performance in this application.

Tiernan *et al*. [81] have concentrated on linear heating thermo-analytical techniques to monitor this catalyst system in methane combustion and found that the reduction behaviour closely correlated with the catalyst performance. The supported cobalt catalysts were reported to have enhanced catalytic performances compared to bulk cobalt oxide catalysts.

Cobalt titania catalysts have been characterised using a multitude of sophisticated techniques available to researchers. Backman [82], Hamadanian *et al*. [83], Riva *et al*. [84] and Vob *et al*. [85] have characterised catalysts with cobalt supported on silica, alumina and titania. Cobalt dispersion on titania with anatase and rutile phases was probed by Jongsomjit *et al*. [86]. These researchers' characterisation studies have collectively provided insight into the most frequently used surface, spectroscopic, diffraction and thermo-analytical techniques that were common to the research initiative reported in this thesis.

Titania supported cobalt catalysts have been extensively studied in their applications in Fischer-Tropsch (FT) reactions and have been widely researched and documented by the global research community. Bartholomew *et al*. [87] delved into the kinetic aspects, finding that no information existed explicitly on cobalt/titania, whereas those for alumina and silica were available in the literature. This research found that mass transfer and diffusion limitations, together with surface area, impacted significantly on kinetics. Coville and Li [88] probed the effects of boron doping, finding that doping inhibited the reduction of the catalysts while simultaneously decreased the Co_3O_4 crystallite sizes. Doping with < 0.1 % boron enhanced the alkene/alkane ratio, while higher loadings enhanced carbon oxide formation. Hutchings *et al*. [89] used gold doping and found that it enhanced methane and light products selectivities, with the optimum loading of 1 %. Atashi *et al*. [90] considered kinetic aspects on manganese doped catalysts, finding the best system to be based on a 1Co: 3Mn ratio on a 30 wt% titania. This system was suitable for the hydrogenation of CO to light olefins.

Khodakov [91] investigated the structure-activity relationship in FT catalysts, particularly particle size and phase composition, textural effects and effects of noble metal dopants. This research found that significant modifications of the catalysts occur during startup and during the course of the reaction. The key factors that contribute to the modification were identified to be the exothermicity of the reactions, temperature control, impurities in the feed and cobalt sintering. Furthermore, the presence of water, CO, heavy hydrocarbons and organic compounds in the product stream, also had an impact.

Hydrogen is the conventional reducing gas used in catalysis. Jalama *et al*. [92] recently activated FT catalysts using syngas as opposed to the conventional hydrogen and found that this led to greater catalyst stability and overall enhanced activity of the catalyst. A 2: 1 H_2: CO ratio was used and this was found to improve the catalyst reduction. Feyzi *et al*. [93] probed the use of Co/TiO_2 catalysts in the FT application in light olefin production, but focused on the effect of preparation and operation parameters. A 40 % Co/TiO_2 catalyst promoted with 6 % zinc, prepared using the precipitation method, produced the highest yields of light olefins. De Sousa *et al*. [94] investigated cobalt content on olefin and paraffin selectivity, finding that increasing temperature was the driving force behind enhanced olefin formation with simultaneous high selectivity to methane. Niemantsverdriet *et al*. [95], in collaboration with Sasol Technology, have investigated deactivation by oxidation, following the discrepancies in the literature, on this aspect of catalysis. The oxidation of cobalt to cobalt oxide had been postulated to be the major deactivation mechanism, but Niemantsverdriet's study ruled that out as the key cause of deactivation in their study on Co/Al_2O_3. The optimum reaction conditions that prevented oxidation of cobalt, were found in the process of this investigation.

A review of deactivation of cobalt FT catalysts was compiled by Tsakoumis *et al*. [96], finding that localised heating, together with exothermicity of reactions, contributed in a major way to degradation and eventual deactivation of the catalysts.

2.2.4. Activation of short and medium chain linear alkanes

Short chain alkane activation typically involves methane, ethane, propane and butane. Extensive research already exists in this area, as related in the literature. A fair amount of research exists in the activation of medium linear chains: *n*-pentane and *n*-hexane.

Cavani and Trifiro [97] have studied the selective oxidation of all the linear alkanes (from methane to *n*-pentane) and focused particularly on the gas phase interaction with the catalyst surface on different classes of catalytic materials, carefully considering redox properties of mixed metal oxide systems, as well as tailoring catalysts to control oxidising properties. They found that structural defects improved the mobility of ionic species through the bulk, thereby enhancing catalyst performance. Co-operative effects of different phases, the metal to oxygen bond strength as well as reducibility and re-oxidisability of the active sites were further identified as critical factors

Mamedov and Cortes-Corberan [98] reviewed short chain linear alkane activation over vanadium based catalysts. One of the key findings pertaining to titania supported vanadia catalysts, is that they showed lower activity than alumina and silica supported systems, even when the same phases were identified on each of these supports.

Enache *et al*. [67] have delved into the selective oxidation of ethane to acetic acid and ethylene over anatase phase of the titania and zirconia supported vanadium oxide catalysts. Several different methods were employed in the synthesis of the catalysts, each uniquely affecting the outcome of catalytic testing. The best catalytic system was found to be the VOx/zirconia prepared by a colloidal deposition technique, yielding 16 mol % ethylene with a 75 mol % selectivity. The acetic acid selectivity was better on titania supported catalysts, rather than the equivalent supported on zirconia, showing the greater basicity of zirconia. It was found that due to the basicity of the catalyst surface, acetic acid would have a stronger interaction and longer contact time with the catalyst surface, hence leading to cracking and further oxidation to carbon oxides, thereby lowering selectivities to acetic acid on this support.

2.2.5. Activation of higher linear alkanes

The higher linear alkanes like *n*-octane and *n*- decane have not been studied extensively and limited information exists in this field.

Hutchings *et al*. [43, 44] have explored the oxidative activation of *n*-decane. An important development arose from this study, where non-lattice oxygen has been reported to be responsible for selective oxidation [43]. Conventionally, lattice oxygen has been accepted as the species that dictates selective oxidation, while the gas phase oxygen is responsible for the re-oxidation of the catalysts surface as well as non-selective oxidation to the carbon oxides [97].

The review by Busto *et al*. [99] probed the isomerisation and cracking of long chain paraffins using *n*-decane as the feed and the Pt-Pd-WO$_3$ zirconia supported catalyst system. This double promotion approach to manipulate the acid strength of the catalysts proved fruitful in

improving the octane rating of fuel. Acid sites were furthermore identified as the sites at which coking proceeded, which provided insight into the mechanism behind coke formation. Activity and selectivity were manipulated by varying the acid properties of the catalyst system to find optimal ratios.

Valuable insight into the aromatisation mechanism of *n*-octane on Pt doped zeolitic catalysts was obtained from the investigation by Jongpatiwut *et al*. [100]. The zeolitic material formed more <C8 aromatics viz. benzene and toluene, which was found to form from hydrogenolysis of ethylbenzene and o-xylene. Their comparative study on Pd/SiO$_2$ however, showed the opposite trend, with C8 aromatics as the dominant products.

Heavy hydrocarbons and their structure–reactivity link was the focal point of the investigation into C6-C20 chains by Diehl *et al*. [101]. The hydrocarbon reactivity was found to be highly dependent on the nature of the carbon atom in the molecule. The trend observed related to the enhanced ability to oxidise of C2 and C3 atoms on the alkane chain, compared to C1 and C4 atoms on the alkane chain. The other finding related to the oxidisability of the short chain alkylbenzenes, like toluene and ethylbenzene, which were more resistant to oxidising than benzene. Mixtures mimicking both petrol and diesel fuels came under investigation by Subramanian *et al.* [102] in which *n*-octane, *i*-octane, *n*-decane, *n*-hexadecane and naphthalene were used in varying proportions. Air was used as the oxidant over a rhodium coated monolith for reaction catalytic testing and the reactivities and selectivities were the focal point. This investigation clearly showed that in mixtures where differences in reactivities of the individual components existed, competition for the oxygen at the active site prevailed. Hence, the most reactive species consumed the bulk of the oxygen, leading to pyrolysis of the less reactive components.

Lintz and Reitzmann [103] have provided a wealth of information on technical factors, having studied the influence of reaction engineering aspects like reactor configuration and operations, together with suitable alternatives with respect to partial oxidations on oxidic catalysts. They found improvements or new innovative ways compared to the traditional manner in which testing was conducted. One excellent alternative that was proposed was using different catalysts with multiple catalysts beds, in tandem, as a means to achieve improved catalytic activity. This approach is one that is highly appealing for long term research plans.

References

[1]   N. Govender, MSc Thesis, University of KwaZulu-Natal, 2002.

[2]   N. Govender, H.B. Friedrich, M. Janse Van Vuuren, Catalysis Today. 97 (2004) 315-324.

[3]   N. Govender, PhD Thesis, University of KwaZulu-Natal, 2007.

[4]   N. Govender, H.B. Friedrich, M.R. Mathebula, Applied Catalysis A: General. 297 (2006) 81-89.

[5]   M. Ramdeen, MSc Thesis, University of KwaZulu-Natal, 2003.

[6]   N. Masilo, MSc Thesis, University of KwaZulu-Natal, 2009.

[7]   J. Chetty, PhD Thesis, University of KwaZulu-Natal, 2006.

[8]   T. Naicker, PhD Thesis, University of KwaZulu-Natal, 2010.

[9]   B. Pillay, M.R. Mathebula, H.B. Friedrich, Applied Catalysis A: General. 361 (2009) 57-64.

[10]   B. Pillay, M.R. Mathebula, H.B. Friedrich, Catalysis Letters. 141 (2011) 1297-1304.

[11]   A.S. Mahomed, PhD Thesis, University of KwaZulu-Natal, 2005.

[12]   A.S. Mahomed, H.B. Friedrich, Applied Catalysis A: General. 347 (2008) 11-22.

[13]   M. Bux, PhD Thesis, University of KwaZulu-Natal, 2010.

[14]   E.A. Elkhalifa, PhD Thesis, University of KwaZulu-Natal, 2010.

[15]   E. Elkhalifa, H.B. Friedrich, Catalysis Letters. 141 (2011) 554-564.

[16]   T.C. Makatini, MSc Thesis, University of KwaZulu-Natal, 2012.

[17]   P. Botella, J.M. Lopez Nieto, A. Dejoz, M.I. Vazquez, Catalysis Today. 78 (2003) 507-512.

[18]   J.M. Lopez Nieto, P. Botella, P. Concepcion, A. Dejoz, M.I. Vazquez, Catalysis Today. 91-92 (2004) 241-245.

[19]   S. Sewsunker, H.B. Friedrich, 2012 (unpublished work).

[20]   V.D.B.C. Dasireddy, S. Singh, H.B. Friedrich, Applied Catalysis A:General. 421-422 (2012) 58-69.

[21]   G.J. Hutchings, Catalysis Today. 100 (2005) 55-61.

[22]   G.J. Hutchings, Catalysis Today. 122 (2007) 196-200.

[23]   G.J. Hutchings, J.K. Bartley, C.K. Goh, Y.H. Taufiq-Yap, N. Dummer, Catalysis Today. 131 (2008) 408-412.

[24]   G.J. Hutchings, J.K. Bartley, Y.H. Taufiq-Yap, S.N. Asrina, N. Dummer, Journal of Natural Gas Chemistry. 20 (2011) 635-638.

[25]   G.J. Hutchings, E. Cao, M. Sankar, S. Firth, K.F. Lam, D. Bethell, D.K. Knight, P.F. McMillan, A. Gavrilidis, Chemical Engineering Journal. 167 (2011) 734-743.

[26]   G.J. Hutchings, T.J. Hall, J.S.J. Hargreaves, R.W. Joyner, S.H. Taylor, Fuel Processing Technology. 42 (1995) 151-178.

[27]   G.J. Hutchings, J.S.J. Hargreaves, R.W. Joyner, S.H. Taylor, Studies in Surface Science and Catalysis. 107 (1997) 41-46.

[28]   G.J. Hutchings, R. Higgins, Journal of Catalysis. 162 (1996) 153-168.

[29]   G.J. Hutchings, R. Higgins, Applied Catalysis A: General. 154 (1997) 103-115.

[30]   G.J. Hutchings, S. Holmes, L. Sartoni, A. Burrows, V. Martin, J.C. Volta, C.J. Kiely, V. Martin, Studies in Surface Science and Catalysis. 130 (2000) 170-175.

[31]   G.J. Hutchings, G. Jin, W. Weng, Z. Lin, N.F. Drummer, S.H. Taylor, Journal of Catalysis. 296 (2012) 55-64.

[32]   G.J. Hutchings, C.J. Kiely, M.T. Sananes-Schulz, A. Burrows, J.C. Volta, Catalysis Today. 40 (1998) 273-286.

[33]   G.J. Hutchings, M.T. Sananes-Schulz, S. Sajip, C.J. Kiely, A. Burrows, I.J. Ellison, J.C. Volta, Catalysis Today. 33 (1997) 161-171.

[34]   G.J. Hutchings, B. Solsona, T. Garcia, C. Jones, S.H. Taylor, A.F. Carley, Applied Catalysis A: General. 312 (2006) 67-76.
[35]   G.J. Hutchings, B. Solsona, T. Garcia, S.H. Taylor, M. Makkee, Applied Catalysis A: General. 365 (2009) 222-230.
[36]   G.J. Hutchings, S.H. Taylor, Catalysis Today. 49 (1999) 105-113.
[37]   G.J. Hutchings, S.H. Taylor, J.K. Bartley, Z.R. Tang, in: E.M. Gaigneaux (Ed.), Scientific Bases for the Preparation of Heterogeneous Catalysts, 2006.
[38]   G.J. Hutchings, S.H. Taylor, J.S.J. Hargreaves, R.W. Joyner, Applied Catalysis A: General. 126 (1995) 287-296.
[39]   G.J. Hutchings, S.H. Taylor, J.S.J. Hargreaves, R.W. Joyner, C.W. Lembacher, Catalysis Today. 42 (1998) 217-224.
[40]   G.J. Hutchings, S.H. Taylor, I.D. Hudson, Science and Technology in Catalysis, 1998.
[41]   G.J. Hutchings, S.H. Taylor, M.L. Palacois, D.F. Lee, Catalysis Today. 81 (2003) 171-178.
[42]   G.J. Hutchings, S.H. Taylor, D.J. Willock, C.A. Cooper, C.R. Hammond, K. Tabata, in: J.J. Spivey, E. Iglesia, T.H. Fleisch (Eds.), The Role of Gallium Oxide in Methane Partial Oxidation Catalysts, 2001.
[43]   S. Pradhan, J.K. Bartley, D. Bethell, A.F. Carley, M. Conte, S. Golunski, M.P. House, R.L. Jenkins, R. Lloyd, G.J. Hutchings, Nature Chemistry. 4 (2012) 134-139.
[44]   R. Lloyd, R.L. Jenkins, M. Piccinini, Q. He, C.J. Kiely, A.F. Carley, S.E. Golunski, D. Bethell, J.K. Bartley, G.J. Hutchings, Journal of Catalysis. 283 (2011) 161-167.
[45]   A. Corma, Journal of Catalysis. 216 (2003) 298-312.
[46]   A. Corma, M. Boronat, Catalysis Today. 169 (2011) 52-59.
[47]   A. Corma, H. Garcia, Catalysis Today. 38 (1997) 257-308.
[48]   A. Corma, D. Kumar, Studies in Surface Science and Catalysis. 117 (1998) 201-222.
[49]   A. Corma, C. Martinez, F.V. Melo, L. Sauvanaud, J.Y. Carriat, Applied Catalysis A: General. 232 (2002) 247-263.
[50]   A. Corma, J. Moscoso, L. Nemeth, N. Erdman, A. Oroskar, S.R. Bare, S.D. Kelly, S. Valencia, M. Renz, Studies in Surface Science and Catalysis. 154 (2004) 2626-2631.
[51]   A. Corma, V. Perez, M.L. Ruiz- Gonzalez, J.M. Gonzalez-Calbel, P. Concepcion, M. Boronat, Catalysis Today. 180 (2012) 59-67.
[52]   J.M. Lopez Nieto, T. Blasco, Applied Catalysis A: General. 157 (1997) 117-142.
[53]   J.M. Lopez Nieto, P. Botella, E. Garcia-Gonzalez, J.M. Gonzalez, Solid State Sciences. 7 (2005) 207-519.
[54]   J.M. Lopez Nieto, G. Centi, D. Pinelli, F. Trifiro, F. Ungarelli, in: G. Centi, F. Trifiro (Eds.), New Developments in Selective Oxidation, 1990.
[55]   J.M. Lopez Nieto, A. Corma, N. Paredes, A. Dejoz, M.I. Vazquez, in: V. Cortes Corberan, S.V. Bellon (Eds.), New Developments in Selective Oxidation, 1994, pp. 113-123.
[56]   J.M. Lopez Nieto, A. Corma, N. Paredes, M. Perez, Y. Shen, H. Cao, S.L. Suib, Studies in Surface Science and Catalysis. 72 (1992) 213-220.
[57]   J.M. Lopez Nieto, A. Dejoz, F. Marquez, M.I. Vazquez, Applied Catalysis A: General. 180 (1999) 83-94.
[58]   J.M. Lopez Nieto, A. Dejoz, M.I. Vazquez, W. O'Leary, J. Cunningham, Catalysis Today. 40 (1998) 215-228.
[59]   J.M. Lopez Nieto, I. Ramli, P. Botella, F. Ivars, W.P. Meng, H.A. Ahangar, Journal of Molecular Catalysis. 342-343 (2011) 50-57.
[60]   J.M. Lopez Nieto, J. Soler, J. Herguido, M. Menendez, P. Concepcion, J. Santamaria, Journal of Catalysis. 185 (1999) 324-332.

[61] J.M. Lopez Nieto, B. Solsona, A. Dejoz, P. Concepcion, M.I. Vazquez, M.T. Navarro, Catalysis Today. 117 (2006) 228-233.

[62] J.M. Lopez Nieto, B. Solsona, V.A. Zazhigalov, I.V. Bacherikova, Studies in Surface Science and Catalysis. 130 (2000) 1853-1858.

[63] J. Haber, Catalysis Today. 142 (2000) 100-113.

[64] M.R. Maurya, A. Kumar, J.C. Pessoa, Coordination Chemistry Reviews. 255 (2011) 2315-2344.

[65] J.M. Herrmann, Catalysis Today. 112 (2006) 73-77.

[66] V.V. Guliants, Catalysis Today. 51 (1999) 255-268.

[67] D.I. Enache, E. Bordes, A. Ensuque, F. Bozon-Verdura, Applied Catalysis A: General. 278 (2004) 103-110.

[68] M.P. Gimeno, J. Gascon, C. Tellez, J. Herguido, M. Menendez, Chemical Engineering and Processing. 47 (2008) 1844-1852.

[69] L. Luciani, N. Ballarini, F. Cavani, C. Cortelli, Catalysis Today. 142 (2000) 132-137.

[70] B. Grzybowska-Swierkosz, Applied Catalysis A : General. 157 (1997) 409-420.

[71] B. Grzybowska-Swierkosz, Applied Catalysis A: General. 157 (1997) 263-310.

[72] M. Ruitenbeek, A.J. Van Dillen, A. Barbon, E.E. Van Faassen, D.C. Koningsberger, J.W. Geus, Catalysis Letters. 55 (1998) 133-139.

[73] M. Ruitenbeek, A.J. Van Dillen, D.C. Koningsberger, J.W. Geus, in: B. Delmon (Ed.), Effects of Silica and Titania Supports on the Performance of Vanadium Phosphorous -Oxide Catalysts, 1998.

[74] A.I. Anastasov, Chemical Engineering and Processing 42 (2003) 449-460.

[75] X. Deng, Y. Yue, Z. Gao, Applied Catalysis B: Environmental. 39 (2002) 135-147.

[76] Y. Brik, M. Kacimi, F. Bozon-Verdura, M. Ziyad, Journal of Catalysis. 211 (2002) 470-481.

[77] Y. Brik, M. Kacimi, M. Ziyad, F. Bozon-Verdura, Journal of Catalysis. 202 (2001) 118-128.

[78] M.M. Yung, E.M. Holmgreen, U.S. Ozkan, Journal of Catalysis. 247 (2007) 356-367.

[79] E.C. Tyo, C. Yin, M.D. Vece, Q. Qian, ACS Catalysis. 2 (2012) 2409-2423.

[80] T. Xiao, S. Ji, H. Wang, K.S. Coleman, M.L.H. Green, Journal of Molecular Catalysis A: Chemical. 175 (2001) 111-123.

[81] M.J. Tiernan, E.A. Fesenko, P.A. Barnes, M. Ronane, G.M.B. Parkes, Thermochimica Acta. 379 (2001) 163-175.

[82] L. Backman, PhD Thesis, Helsinki University of Technology, 2009.

[83] M. Hamadanian, A. Reisis-Vanani, A. Majedi, Journal of the Iranian Chemical Society. 7 (2010) 52-58.

[84] R. Riva, H. Miessner, R. Vitali, G. Del Piero, Applied Catalysis A: General. 196 (2000) 111-123.

[85] M. Vob, D. Borgmann, G. Wedler, Journal of Catalysis. 212 (2002) 10-21.

[86] B. Jongsomjit, C. Sakdamnuson, J.G. Goodwin, P. Praserthdam, Catalysis Letters. 94 (2004) 209-215.

[87] R. Zennaro, M. Tagliabue, C.H. Bartholomew, Catalysis Today. 58 (2000) 309-319.

[88] J. Li, N.J. Coville, Applied Catalysis A: General. 181 (1999) 201-208.

[89] K. Jalama, N.J. Coville, D. Hildebrandt, D. Glasser, L.L. Jewell, J.A. Anderson, S. Taylor, D.I. Enache, G.J. Hutchings, Topics in Catalysis. 44 (2007) 129.

[90] H. Atashi, F. Siami, A.A. Mirzaei, M. Sarkari, Journal of Industrial and Engineering Chemistry. 16 (2010) 952-961.

[91] A.Y. Khodakov, Catalysis Today. 144 (2009) 251-257.

[92] K. Jalama, J. Kabuba, H. Xiong, L.L. Jewell, Catalysis Communications. 17 (2012) 154-159.

[93] M. Feyzi, M.M. Khodaei, J. Shahmoradi, Fuel Processing Technology. 98 (2012) 90-98.

[94] B.V. De Sousa, M.G.F. Rodrigues, L.A. Cano, M.V. Cagnoli, J.F. Bengoa, S.G. Marchetti, G. Pecchi, Catalysis Today. 172 (2011) 152-157.

[95] J.V.D. Loosdrecht, B. Balzhinimaev, J.A. Dalmon, J.W. Niemantsverdriet, S.V. Tsybulya, A.M. Saib, P.J. Van Berge, J.L. Visagie, Catalysis Today. 123 (2007) 293-302.

[96] N.E. Tsakoumis, M. Ronning, O. Borg, E. Rytter, A. Holmen, Catalysis Today. 154 (2010) 162-182.

[97] F. Cavani, F. Trifiro, Catalysis Today. 51 (1999) 561-580.

[98] E.A. Mamedov, V. Cortes Corberan, Applied Catalysis A: General. 127 (1995) 1-40.

[99] M. Busto, V.M. Benitez, C.R. Vera, J.M. Grau, J.C. Yori, Applied Catalysis A: General. 347 (2008) 117-125.

[100] S. Jongpatiwut, P. Sackamduang, T. Rirksomboon, S. Osuwan, D. Resasco, Journal of Catalysis. 218 (2003) 1-11.

[101] F. Diehl, J. Barbier, D. Duprez, I. Guibard, G. Mabilon, Applied Catalysis B: Environmental. 95 (2010) 217-227.

[102] R. Subramanian, G.P. Panuccio, K.K. Krummenacher, I.C. Lee, L.D. Schmidt, Chemical Engineering Science. 59 (2004) 5501-5507.

[103] H.G. Lintz, A. Reitzmann, Catalysis Reviews. 49 (2007) 1-32.

Chapter Three

Experimental

3.1. Catalyst synthesis

3.1.1. Introduction

The literature was surveyed to find a suitable synthesis method for the catalyst preparation. Various techniques exist but the most commonly used techniques are:

- wet impregnation
- incipient wetness
- precipitation-deposition/deposition/co-precipitation
- sol-gel method
- ion exchange
- solution combustion

The wet impregnation technique was chosen for its simplicity, ease of scale up and applicability to an industrial context. The cobalt nitrate precursor was chosen because of availability and cost, and the chloride precursors were excluded as it was known from previous research to introduce impurities and poisoning into the catalysts.

3.1.2. Catalyst preparation: Reagents

- Titanium(IV) oxide (TiO_2), Alfa Aesar , min 98%
- Cobalt nitrate ($Co(NO_3)_6 \cdot 6H_2O$), ACE platinum line (AR), min 99%
- Sulphuric acid (H_2SO_4), Merck, 98%
- ICP Cobalt standard 1000 mgL^{-1}, DLD suppliers

3.1.3. Preparation of titania supported cobalt catalysts

Commercial TiO_2 support was crushed to a fine powder in a mortar and pestle and calcined under flowing air at 500 °C for 8 hours. The catalysts were prepared using a wet impregnation method [1-5]. A series of Co/TiO_2 catalysts were synthesised by a single impregnation of the support with an aqueous solution of the metal nitrate salt. A pre-calculated mass of the nitrate precursor, $Co(NO_3)_6 \cdot 6H_2O$, was dissolved in hot deionised water (ca. 10 ml/g) and heated to ca. 80 °C. An appropriate mass of TiO_2 was added and with continuous heating and stirring, left to form a thick pink paste. The paste was left in the oven at 110 °C for 20 hours, to dry at constant heating and to ensure complete removal of water prior to calcination.

The resulting grey solid was crushed in a mortar and pestle to a fine powder and then calcined for 8 hours under flowing air at 500 °C (ramped at a rate of 1.5 °C/min). This resulted in the cobalt oxide formation under thermal decomposition of the nitrates. This method was employed to yield 10 g of each catalyst of ca. 5, 10, 15, 20 and 25 wt% Co/TiO_2. The colour of the catalysts varied from grey (lower cobalt loadings) to black (higher cobalt loadings) and white for the titania support. The catalysts were stored in pill vials and kept in desiccators until required.

For use in catalytic testing, the powdered catalysts was pressed into a tablet in a KBr pellet die for ca. 15 minutes under pressure, then crushed before being screened through 600-1000 μm sieves to obtain uniform-sized pellets. A single reaction was carried out with smaller pellets screened through 500-600 μm sieves.

3.2. Catalyst Characterisation

All characterisation, except for XPS analyses, was carried out at UKZN. The SEM/TEM analyses were carried out at the UKZN microscopy unit. The majority of the analyses were carried out in-house at the Catalysis Research Group, while the remaining analyses were undertaken at the UKZN instrumental laboratories.

The state and appearance of the catalyst surface was investigated and examined by spectroscopic, microscopic and diffraction techniques, amongst others. In order to evaluate the physical, textural and chemical properties of the synthesized catalysts, several characterization techniques have been employed as outlined below:

3.2.1. Inductively Coupled Plasma-Optical Emission Spectroscopy (ICP-OES)

The cobalt loading on each catalyst was verified by ICP-OES analysis using a Perkin Elmer Optima 5300 DV spectrometer. Approximately 50 mg of catalyst was digested in 10 ml of concentrated H_2SO_4 and transferred to a 100 ml volumetric flask and made up to volume in deionised water. The calibration was done using 20, 40, 60, 80 and 100 mg/L standards. The catalysts were found to consist of 4, 9, 14, 19 and 22 wt% Co.

3.2.2. Brunauer-Emmet-Teller (BET) Surface Area and Pore Volume

The BET surface areas measurements were obtained by nitrogen physisorption isotherms at 77 K using the standard multipoint method on a Micromeritics Gemini instrument. Samples were degassed in a stream of nitrogen at 200 °C for 24 hours, prior to the analysis. Sample size used was between 100-200 mg. Samples were reweighed after degassing. The pore volumes of the catalysts were simultaneously measured during surface area analysis. Analyses were carried out on fresh catalysts.

Adsorption/desorption experiments were carried out using the Micromeritics Tristar instrument. Sample pretreatment and size was the same as for the Gemini instrument above. The Tristar was used to obtain surface area, pore width and pore volume measurements for the spent catalysts

3.2.3. Powder X-Ray Diffraction (PXRD)

Powder X-Ray diffraction patterns were recorded on a Bruker D8 Advance diffractometer equipped with a graphite monochromator and operated at 40 kV and 40 mA. The source of radiation was the λ= 1.5406 Å Cu Kα radiation. The range covered was between 15° and 90° 2θ. Employing the diffraction peaks at 2θ 25 ° and 50 °, the crystallite size for the titania and supported cobalt catalysts was calculated using the Scherrer equation. This technique was employed for fresh and spent catalyst characterisation.

3.2.4. X-Ray Photoelectron Spectroscopy (XPS)

XPS spectra were recorded on a ThermoScientific Multilab 2000 spectrometer, employing Al Kα radiation and considering the C (1s) as the reference 284.5eV for all binding energies. The support, as well as the 15% Co/TiO_2 catalyst, was subjected to XPS analysis to evaluate the surface composition and dispersion of cobalt on the support surface respectively. All XPS analyses were conducted at the Solid State and Structural Chemistry Unit at the Indian Institute for Science in Bangalore, India.

3.2.5. Laser Raman Spectroscopy

Raman spectra were recorded on a DeltaNu Advantage 532 instrument using a 532 nm laser source. Laser strength was varied between 'low' and 'high'. Analysis began with low laser strength and was gradually increased depending on the results obtained. The best resolution was often obtained by keeping the laser at 'medium' with an integration time of 60 seconds. All analyses were carried out on powdered samples contained in quartz vials at room temperature.

3.2.6. Fourier Transform Infrared Spectroscopy (FTIR)

Analysis was carried out on a Perkin Elmer Spectrum 100 FTIR Spectrometer fitted with a Universal Attenuated Total Reflectance (ATR) sampling accessory. IR spectra were recorded at room temperature by placing a small amount of powdered catalyst onto the ATR crystal (made up of composite diamond and zinc selenide) and applying a pressure of ~ 90 gauge to achieve good contact between the catalyst material and the crystal. Spectra were obtained for the TiO_2 as well as 5, 10, 15, 20, 25 % Co/TiO_2 catalysts. The results reflect the presence of a strong vibrational band that is not well resolved, between 900 – 380 cm^{-1}, corresponding to the metal oxide band. No further information was inferred from the analysis.

3.2.7. Temperature Programmed Reduction (TPR)

TPR analysis was carried out on a Micromeritics AutoChem II Chemisorption Analyser with a sample of approximately 50 mg loaded onto quartz wool within a U-shaped tubular quartz reactor tube. The sample was initially flushed with argon as the temperature was increased to 400 °C followed by cooling to 80 °C. The gas mixture used for the reduction was 5% H_2 in argon with uniform heating at 10 °C/min up to a maximum of 950 °C.

3.2.8. Thermogravimetric Analysis (TGA)

To evaluate the thermal stability of the catalysts and support, TGA analysis was conducted on a TA SDT Q600 instrument under air flowing at 50 ml/min and at a temperature ramp rate of 10 °C /min from room temperature up to a maximum of 1000 °C. A sample size of ca. 10 mg was used in both fresh and spent catalyst characterisation.

3.2.9. Transmission Electron Microscopy (TEM)

Images were obtained on a Jeol JEM 1010 Transmission Electron Microscope operated at a voltage of 100 kV. Samples were prepared as follows: a small quantity of sample was dissolved in ethanol and sonicated for a few minutes. The holey copper grids were dipped into the solution containing the catalyst and the ethanol, and were then left aside to dry. In this manner, deposition of a small amount of the catalyst onto the grid was achieved for viewing under the microscope. Transmission electron microscopy (TEM) analysis evaluated the physical state and morphology of the support and the catalysts.

3.2.10. Scanning Electron Microscopy (SEM) and Energy Dispersive X-Ray Spectroscopy (EDX)

Analysis by means of SEM and EDX were carried out to obtain a clear evaluation of the morphology of the support and the catalysts as well as the elemental distribution of the catalyst samples. Samples were gold coated after mounting onto suitable stubs, prior to microscope viewing. SEM images and micrographs were obtained using a LEO 1450 Scanning Electron Microscope and EDX was carried out using a Jeol JSM 6100 Scanning Electron Microscope equipped with a Bruker EDX Detector.

3.3. Catalytic testing components and conditions

All testing was carried out in a continuous flow fixed bed reactor built in-house from Swagelok stainless steel fittings and tubing, as outlined in Figure 1. The design was based on previous research [6-9] but adapted to suit current testing conditions. The HPLC pump, wet-gas flowmeter, mass flow controllers and balances were serviced and/or calibrated prior to use in testing.

The fixed bed reactor system was chosen for this research effort for its relatively low cost as well as its practical applicability to laboratory scale assembly and ease of testing. Oxidative dehydrogenation reactions are exothermic and hence heat transfer within the reactor tube may prove problematic. Hence a narrow reactor tube was chosen (1/2 inch outer diameter) to provide a high surface to volume ratio, thereby minimising heat transfer differences [10]. Furthermore, a constant 1 ml catalyst bed volume was maintained for all testing.
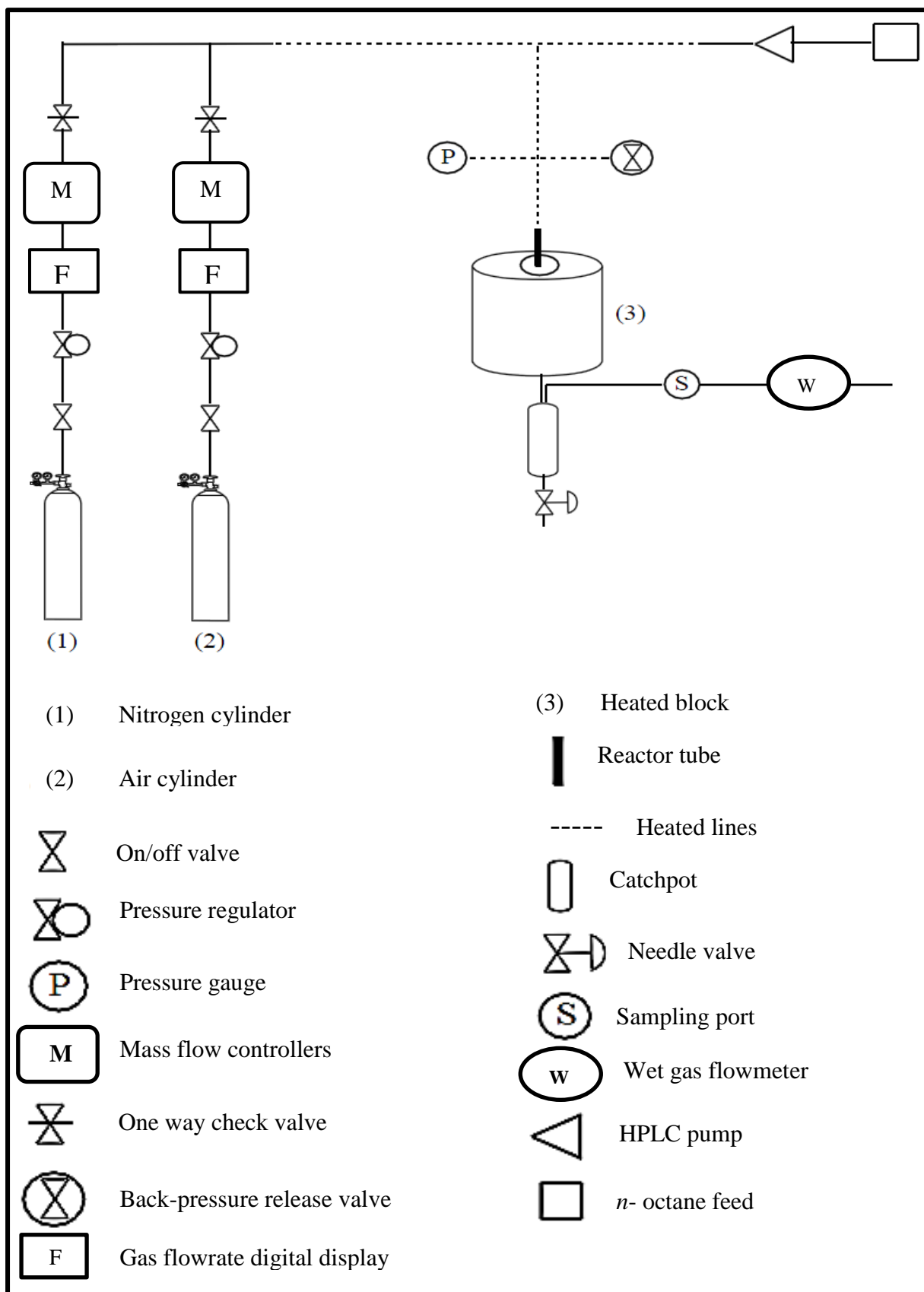
3.3.1. Reactor description

Figure 1: Reactor scheme used in catalytic testing (see Appendix pgs 84-85 for reactor setup)

3.3.2. Reactor tube

The 1/2 inch outer diameter stainless steel tubing (supplied by Swagelok) was cut to a length of 20 cm. Suitable Swagelok stainless steel fittings, including nuts and ferrules were attached to the tubing for use in the reactor. The reactor tube was packed with 1 ml of the pelletised catalyst, sandwiched between two layers of glass wool and positioned to correspond to the predetermined hotspot within the reactor heating block. The remainder of the reactor tube was packed with 24 grit carborundum and the ends were stoppered with additional layers of glass wool. This ensured that all the carborundum and catalyst material remained within the reactor tube and did not enter the feed or product stream (see Appendix pg 85).

3.3.3. System equilibration

The reactor tube was fitted within the heating block. A leak test was performed by pressurising the system under nitrogen, to ensure that no leaks were present. The thermocouple monitoring the heating block temperature was appropriately positioned at the hotspot. The thermocouple monitoring the catalyst bed temperature was fitted into the jacket attached to the reactor tube. The ¼ inch outer diameter reactor lines that carried the *n*-octane into the reactor tube were heated from room temperature and kept constantly heated at 180 °C throughout the duration of the testing. This ensured that the feed/air mixture was kept vapourised as it entered the reactor and catalyst bed. These lines were kept heated for a further 2 hours post reaction to ensure that all the feed was carried out of the system to prevent condensation of the unreacted feed and products within the reactor lines. This was a preventative measure to ensure that no fouling and blockage of the lines occurred. The heating block temperature was gradually increased from room temperature to 350 °C. Once the catalyst bed temperature exceeded the boiling point of *n*-octane (> 160 °C), the pump feeding the *n*-octane was switched on. The chiller unit that was responsible for cooling the products collected in the catchpot (see Section 3.4), was switched on. Air and nitrogen were fed through the system just prior to the feed being pumped into the system. This was maintained for two hours prior to beginning testing.

3.3.4. Gas feed system

Bronkhorst mass flow controllers (model F 201 CV500-AGD-22V) were used to control incoming gases to the reactor viz. air as the oxidant and nitrogen the diluent. For testing under a GHSVs of 4000 and 6000 h^{-1}, a summary of the flowrate data is outlined in Table 3.1. It is critical to safety to avoid explosive mixtures, to keep the alkane in air mixture above the upper flammability limit (6.5 % for *n*-octane at 25 °C). Feed in the table below refers to the alkane and air mixture, while the fuel refers to the alkane.

$$\text{GHSV (h}^{-1}) \quad = \quad \frac{\text{Total flow rate } (\frac{\text{ml}}{\text{h}})}{\text{Volume of catalyst (ml)}}$$

Table 3.1: Summary of gas flowrates and ratios used in catalytic testing

GHSV (h^{-1})	N$_2$ (ml/min)	Air (ml/min)	*n*-octane (ml/min)	Fuel (oxidant) (%)	Fuel (feed) (%)
4000	31	36	0.05	21	9
6000	57	43	0.06	21	11

3.3.5. Feed delivery

The *n*-octane feed (Merck >99%) in a reagent bottle was placed on an OHAUS balance with constant monitoring of the mass, and the feed was delivered through the system using a LabAlliance Series II HPLC pump, at a constant rate of 0.05 ml/min except for reaction 3 in Table 3.2 where the rate was increased to 0.06 ml/min to adjust the testing to achieve a 6000 h^{-1} GHSV. A homogeneous feed delivery into the system was assumed at constant pressure (atmospheric pressure) and $\pm$ 5 °C fluctuation in temperature.

3.3.6. Temperature

The temperatures investigated for the purpose of this study were 350, 400, 450, 500 and 550 °C. A 15 cm heating block was used, accommodating the 1/2 inch outer diameter reactor tube. The hotspot in the heating block was determined prior to testing. The temperature within the catalyst bed and at the hotspot of the heating block was monitored by appropriately positioned K-type thermocouples.

3.4. Products from catalytic testing

Outgoing gaseous products from the reactor system were measured by means of a Ritter drum type wet gas flowmeter. Gaseous samples for GC analysis were drawn through a septum fitted onto a T-piece on the exit lines to the flowmeter from the reactor.

All liquid products and unreacted feed were collected in a cylindrical stainless steel vessel, referred to as a catchpot, which was cooled to ca. 1 °C by means of a FHM Instruments chiller. The liquid products were collected in vials and manually weighed. The organic and aqueous layers were separated, weighed and analysed.

3.4.1. Product analysis

Analysis was conducted to separate, identify and/or quantify the components of the product mixture by means of GC and GC-MS. Gaseous products were drawn using a SGE gas tight syringe and were analysed by means of the Perkin Elmer Clarus 400 GC fitted with a 30 m Supelco Carboxen column and TCD detector (0.1 µL injection volume) for separation and quantification of the carbon oxides, while the remaining gaseous (0.2 µL injection volume) and liquid products (0.2 µL injection volume) were analysed on the Clarus 400 GC fitted with a 50 m PONA capillary column and FID detector. GC-MS analysis was carried out on the Perkin Elmer Clarus 500, equipped with a 50 m PONA column, to identify unknown products (0.2 µL injection volume).

Temperature programming on the GC-FID was as follows: the temperature was held at 40 ℃ for 15 minutes, ramped up to for 120 ℃ at 10 ℃/min and held for 2 minutes, followed by ramping up to 200 ℃ at 20 ℃/min and held for 1 minute. The temperature programming for the GC-TCD was as follows: the temperature was held at 36 ℃ for 1.5 minutes then ramped up to 65 ℃ at 25 ℃/min and held for 3 minutes

3.4.2. Catalytic testing summary

Table 3.2: The summary of the catalytic runs that were carried out in the fixed bed reactor

4000 h^{-1} GHSV	Catalyst (600-1000 μm pellets)	n-Octane to air ratio	Other
1.	5CoTiO$_2$	8C: 0O	Dehydrogenation : anaerobic testing
2.	5CoTiO$_2$	8C: 2O	
3.	5CoTiO$_2$	8C: 2O	6000 h^{-1} GHSV
4.	5CoTiO$_2$	8C: 2O	500-600 μm pellets
5.	5CoTiO$_2$	8C: 4O	
6.	10CoTiO$_2$	8C: 4O	
7.	20CoTiO$_2$	8C: 2O	
8.	Support TiO$_2$	8C: 2O	

The catalytic runs outlined in Table 3.2, were carried out in order to probe the suitability of the titania and titania supported cobalt catalyst system in activating n-octane in the dehydrogenation and oxidative dehydrogenation reactions. The different feed to oxygen ratios formed the basis of comparison of aerobic and anaerobic catalytic testing on the product profile and activity of the catalyst, establishing the influence of the strength of the oxidative environment. The testing of the 500-600 μm pellet size catalysts and higher GHSV of 6000 h^{-1} provided insight into mass transfer and diffusion limitations in this catalytic system under the n-octane oxidative dehydrogenation reaction conditions.

The duration of the runs, at each temperature of interest, was one hour long. At the beginning of the run, the catchpot was emptied, to remove the liquids accumulated during equilibration time. The wet gas flowmeter reading was recorded. The balance was tarred. A timer was set for 60 minutes. At 30 minutes into the run, a gas sample was drawn for injection into the GC-TCD and GC-FID respectively. At sixty minutes the wet gas flowmeter reading was recorded, the mass of feed delivered was recorded, the catchpot was drained and the sample collected for further separation, weighing and analysis. This procedure was repeated for each temperature from 350-550 °C at 50 °C intervals. Duplicate testing was done at each temperature of interest. The spent catalyst was removed, after cooling down to room temperature, upon completion of the run at 550 °C. Spent catalysts were characterised by BET, TGA, XRD, Laser Raman and microscopy techniques.

Quantification of the products was defined in terms of conversion, selectivity and yields. Conversion is the proportion of feed introduced that is transformed to products:

$$\text{Conversion} \quad = \quad \frac{\text{moles of n-octane reacted} \times 100}{\text{moles of n-octane in feed}}$$

Selectivity is the molar ratio of desired products formed to the total moles of products formed (based on carbon atoms).

The yield is molar fraction of the desired product to the total number of moles of *n*-octane feed introduced (based on carbon atoms).

$$\text{Yield} \quad = \quad \text{Selectivity} \quad \text{x} \quad \text{Conversion}$$

References

[1]   B. Jongsomjit, C. Sakdamnuson, J.G. Goodwin, P. Praserthdam, Catalysis Letters. 94 (2004) 209-215.

[2]   R. Riva, H. Miessner, R. Vitali, G. Del Piero, Applied Catalysis A: General. 196 (2000) 111-123.

[3]   K. Jalama, PhD Thesis, University of Witwatersrand, 2007.

[4]   K. Jalama, N.J. Coville, D. Hildebrandt, D. Glasser, L.L. Jewell, J.A. Anderson, S. Taylor, D.I. Enache, G.J. Hutchings, Topics in Catalysis. 44 (2007) 129.

[5]   K. Jalama, J. Kabuba, H. Xiong, L.L. Jewell, Catalysis Communications. 17 (2012) 154-159.

[6]   N. Govender, MSc Thesis, University of KwaZulu-Natal, 2002.

[7]   N. Govender, PhD Thesis, University of KwaZulu-Natal, 2007.

[8]   A.S. Mahomed, H.B. Friedrich, Applied Catalysis A: General. 347 (2008) 11-22.

[9]   E.A. Elkhalifa, PhD Thesis, University of KwaZulu-Natal, 2010.

[10]   A.S. Mahomed, PhD Thesis, University of KwaZulu-Natal, 2005.

Chapter Four

Results and Discussion

4.1. Catalyst characterisation

Catalyst evaluation by various techniques was carried out to ascertain the chemical, physical and textural properties. The different techniques support and complement each other and collectively render the information required to establish the properties of the catalytic material as well as those properties that influence the catalytic activity. Furthermore, characterisation of the spent catalysts revealed the changes to the catalyst induced by its use in the reaction. Every effort has been made to establish the link between the structure of the material and its associated contribution to activity/reactivity.

4.1.1. ICP

The results from ICP analysis reflect that the catalysts contained 4, 9, 14, 19 and 22 wt% cobalt for the catalysts denoted as 5, 10, 15, 20 and 25 Co/TiO_2 respectively. All values were obtained in triplicate and the samples were prepared in duplicate, with good agreement in the results obtained.

4.1.2. BET

An important property of catalytic material is the level of exposure to the gas phase. Typically, this is evaluated by means of surface area measurements mainly via nitrogen physisorption at very low temperatures. The commercial titania support was reported to have a surface area of 150 m^2/g with a pore volume of 0.38 cm^3/g. The results obtained by BET analysis confirm this. Upon calcination of the commercial support, after grinding of the extrudates to a powder, a significant decrease (34 %) in surface area and (18 %) pore volume resulted. The most probable reason is the agglomeration of particles and a partial collapse of the pore structure, upon heating during calcination.

Table 4.1: BET Surface area and pore volume results obtained on the support and catalyst

SAMPLE	SURFACE AREA (m^2g^{-1})	PORE VOLUME (cm^3g^{-1})	Decrease SA (%)	Decrease PV (%)
Support uncalcined	151	0.35	-	-
TiO_2 Support	99	0.31	34	18
5 % Co/TiO_2	68	0.23	31	26
10 % Co/TiO_2	65	0.22	34	29
15 % Co/TiO_2	62	0.20	37	35
20 % Co/TiO_2	61	0.18	38	42
25 % Co/TiO_2	54	0.16	45	48

A 31-45 % decrease in surface area was noted in the 5-25 % cobalt loaded catalysts respectively, relative to the calcined support that was used in the synthesis. Simultaneously a decrease of 26-48 % in pore volume was noted in the 5-25 % cobalt loaded catalysts respectively, relative to the support (Table 4.1). This can be attributed to sintering or blockage of the pores by the Co_3O_4 clusters dispersed on the TiO_2 support, occurring within the pores and covering a significant part of the surface.

Overall the results for the surface area and pore volume indicate a trend that is also observed in literature [1, 2]: a decrease in surface area with an increase in metal loading as is evident in Table 4.1.

Adsorption/desorption experiments carried out on the catalyst material indicate that the material is mesoporous, with pore diameters of 10-15 nm recorded for the titania support and cobalt catalysts. The commercial support was reported to have a 14 nm pore diameter. There is good agreement with the reported values and the experimental results obtained overall for the surface area, pore volume and pore diameter.

4.1.3. PXRD

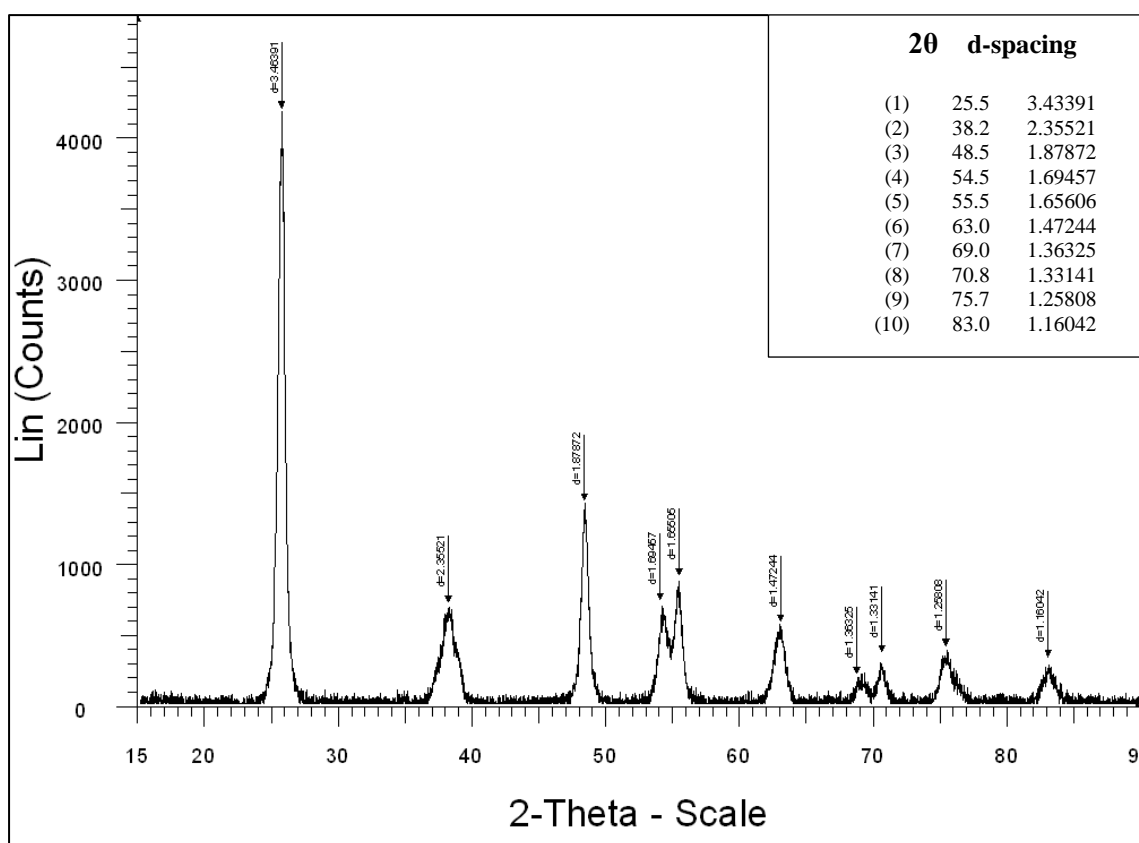|	2θ	d-spacing
(1)	25.5	3.43391
(2)	38.2	2.35521
(3)	48.5	1.87872
(4)	54.5	1.69457
(5)	55.5	1.65606
(6)	63.0	1.47244
(7)	69.0	1.36325
(8)	70.8	1.33141
(9)	75.7	1.25808
(10)	83.0	1.16042

Figure 4.1: Diffractogram of the calcined titania support indicating the presence of the anatase phase of titania, corresponding to JCPDS file no 21-1272
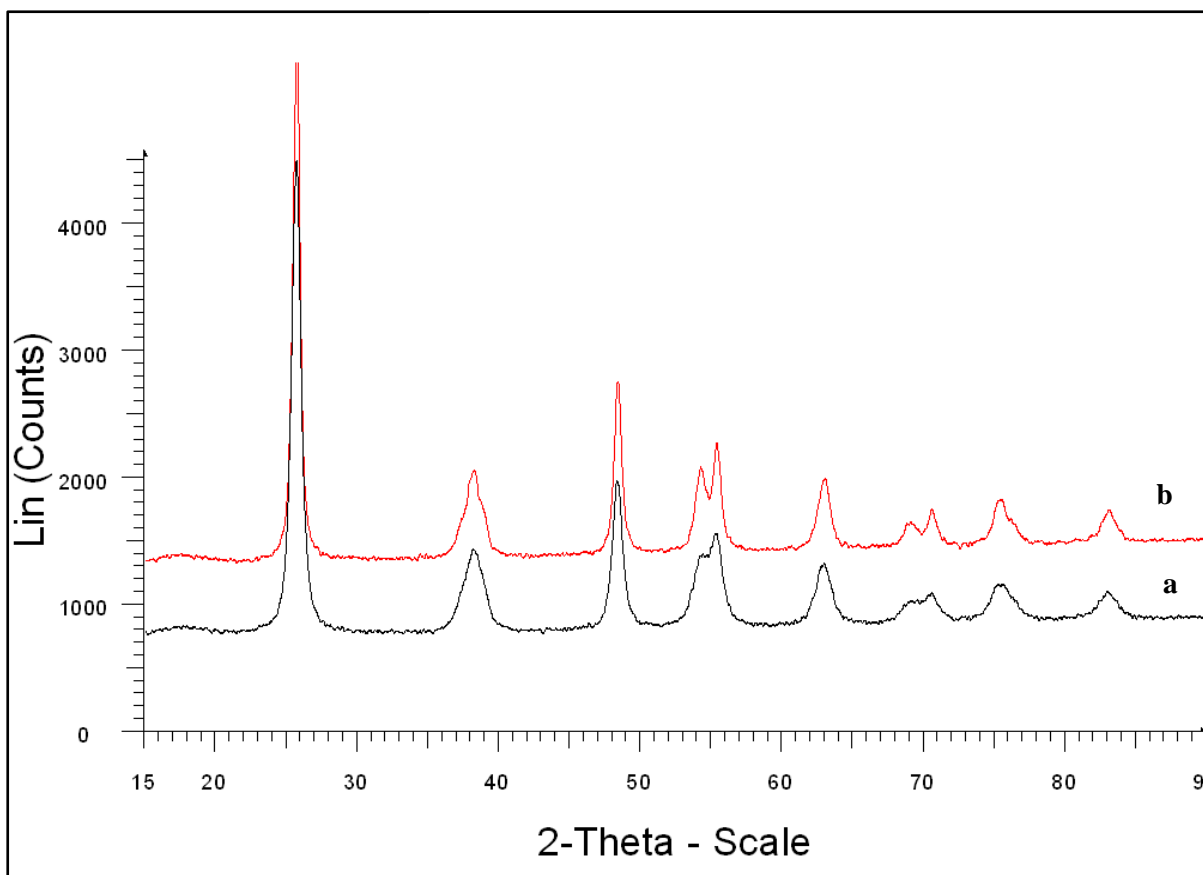
Figure 4.2: Diffractogram of (a) the uncalcined anatase and (b) the calcined anatase phase of the TiO$_2$ support showing greater crystallinity in the calcined material

The bulk crystalline phases present in Figure 4.1 were obtained from the PXRD analysis. The results obtained for the d-spacing values corresponded to the JCPDS file no. 21-1272 for the anatase phase of titania. In situ XRD studies by several researchers including Yung *et al*. [3] have indicated the presence of anatase up to 600 °C. Thereafter the transformation to rutile occurred. Diffractograms of the uncalcined and calcined TiO$_2$ in Figure 4.2 reflect more defined, sharper peaks in the calcined material, indicative of greater crystallinity. The average crystallite sizes for the titania support and titania supported catalysts were calculated using the Scherrer equation and were found to lie between 16–19 nm for the support and 16-22 nm for the catalysts, respectively.

From the analysis of the 5 and 10 % Co/TiO$_2$ catalyst, new reflections for cobalt in the catalyst were present, but not very distinct. This may relate to the instrument detection limitations or a conclusion may be drawn that the cobalt is in a poorly crystalline state. An overview of results from PXRD analysis in Fig.4.3 of the 5-25 % Co/TiO$_2$ catalysts indicate new reflections observed as a result of the oxidic cobalt phase viz. Co$_3$O$_4$ in the catalyst. Co$_3$O$_4$ or (Co$_2$O$_3$.CoO) is the mixed valence compound, made up of trivalent and divalent cobalt, with the former occupying octahedral sites and the latter occupying tetrahedral sites in the lattice. This compound adopts a spinel structure [1].

Furthermore there is a slight shift to higher d-spacing and lower 2θ values in Figure 4.3, indicative of slight distortion of the lattice framework with higher metal loadings because of

incorporation of cobalt into the titania lattice. This may be linked to the encapsulation of the cobalt species by the titania. Titania was found to encapsulate surface metal as reported by Niemantsverdriet [4] and Gates [5] .
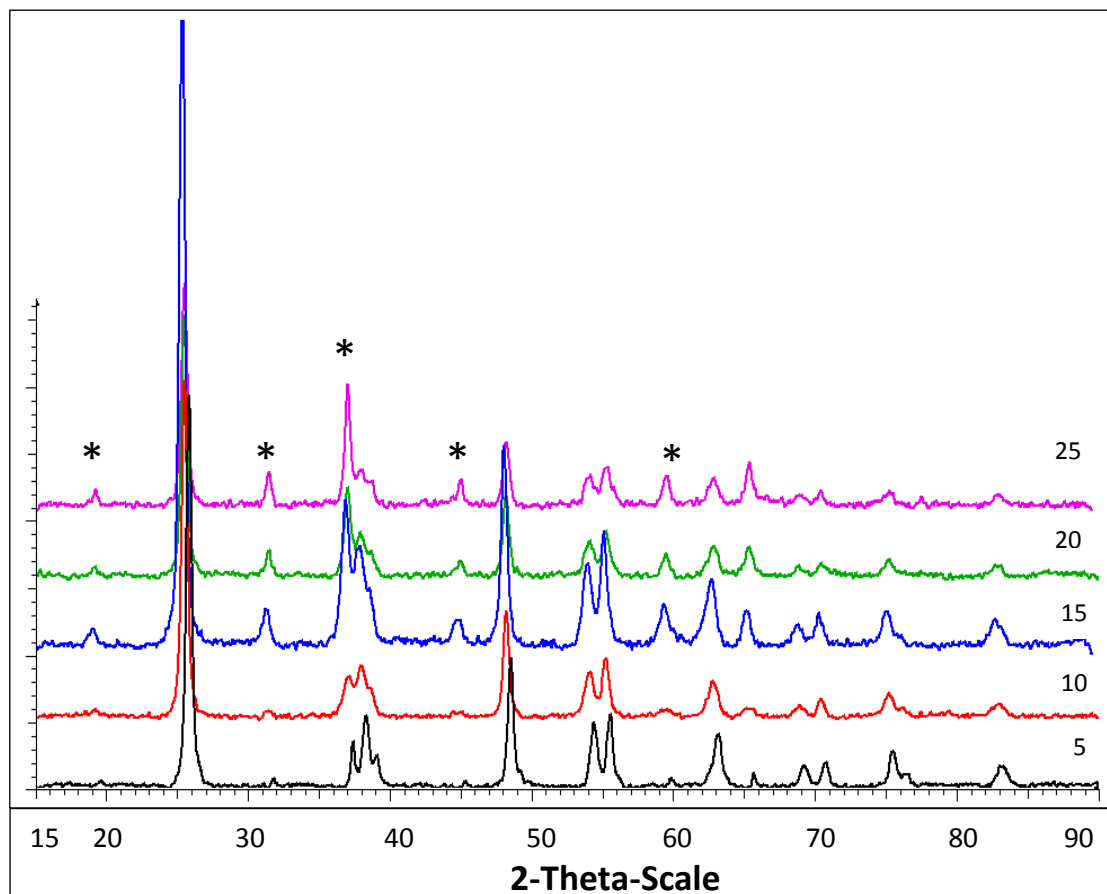

Figure 4.3: Diffractograms of the 5-25 Co/TiO$_2$ catalysts indicating the emergence of the Co$_3$O$_4$ phase, denoted by the * above the peak.

Several researchers [4, 6, 7] have made mention of strong metal-support interactions that result in the formation of cobalt titanate species. The results from this study do not reflect the presence of CoTiO$_3$ species from the analyses, even at loadings as high as 22 wt% cobalt. This works favourably in this research effort, since these cobalt species are not easily reducible species and would compromise catalytic activity. Yung *et al*. [3] found, via in situ XRD studies, that cobalt titanate species formed when preparing material using the sol-gel technique at 500 °C, but only at 700 °C when the wet impregnation technique was used. This directly supports the results from this research which used the wet impregnation technique. Factors such as detection limits of the instrument or a highly dispersed amorphous nature of the possible cobalt titanate species may limit detection, should these be present at all.

4.1.4. XPS

The 15% Co/TiO_2 catalyst was subjected to XPS analysis to evaluate the dispersion of cobalt on the support surface. The C1s binding energy of 285 eV was taken as the reference in agreement with literature [8,10]. Two characteristic peaks for Co_3O_4 are evident in Figure 4.4 (b), the Co $2p_{1/2}$ and Co $2p_{3/2}$ peaks with binding energies of 779 eV and 794 eV respectively, with the ΔE values (Co $2p_{1/2}$ – Co $2p_{3/2}$) equal to 15 eV. These results indicate that the surface layer is enriched in Co_3O_4. These peak identifications are in agreement with results for the exact assignment of the cobalt compounds on supports from pure reference materials and material synthesised by other researchers [8,10]. A satellite peak is evident from the deconvolution, on the high intensity side of $2p_{3/2}$ at ca. E_b of 781eV, which is typical of the Co(II) ion and synonymous with the high spin state of divalent cobalt. The shoulder is not very distinct, but this is consistent with a greater prevalence of Co(III) with the Co^{3+}/Co^{2+} ratio of 2:1 in Co_3O_4. Similar observations were made by Yung *et al*. [3] and Vob *et al*. [8].
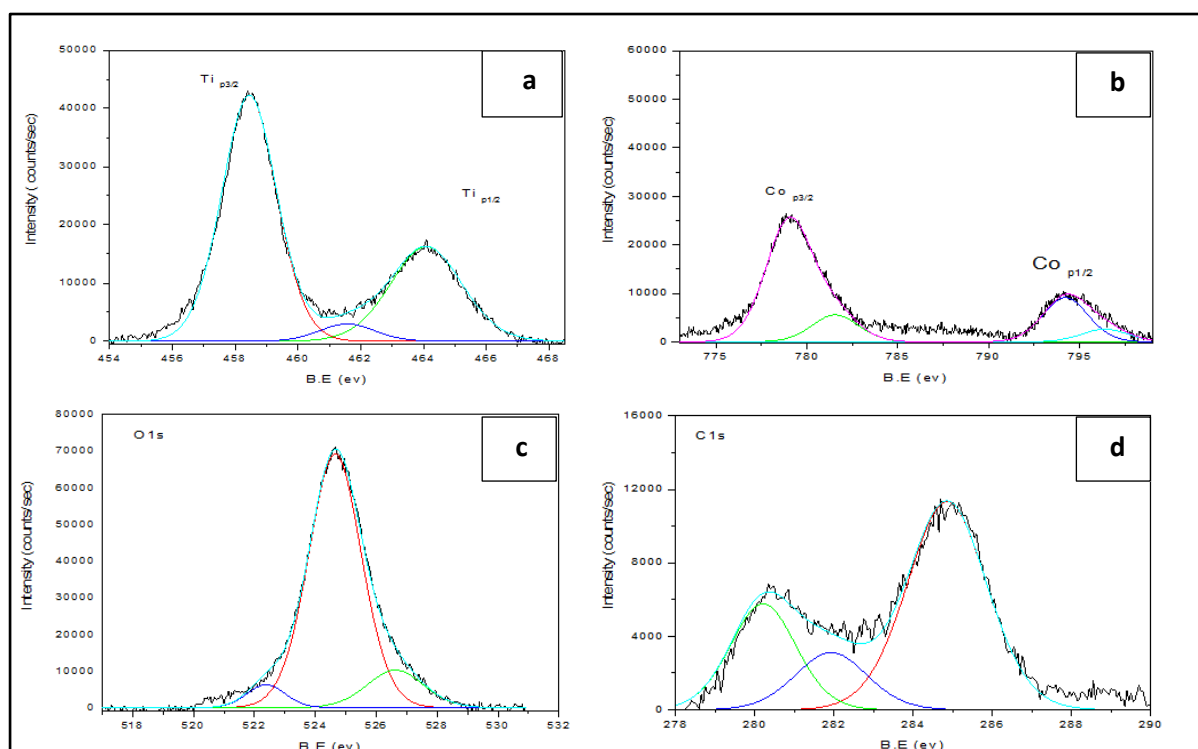

Figure 4.4: XPS spectra of the (a) titania support and (b) $15Co/TiO_2$ catalyst, as well as reference (c) C1s and (d) O1s spectra.

4.1.5. Laser Raman Spectroscopy

The results in Figure 4.5 (a) obtained from laser Raman analysis of the support clearly show three distinct strong bands at 396, 517 and 639 cm^{-1}. These bands confirm the presence of the anatase phase of titania. The spectrum in Figure 4.5 (b) for the $25Co/TiO_2$ catalyst displays a very strong band indicative of cobalt oxide at 687 cm^{-1}. These results are in good agreement with the findings of Ozkan *et al*., Xiao *et al.* and Che *et al*. [3, 7, 11] in their research involving cobalt titania catalysts.
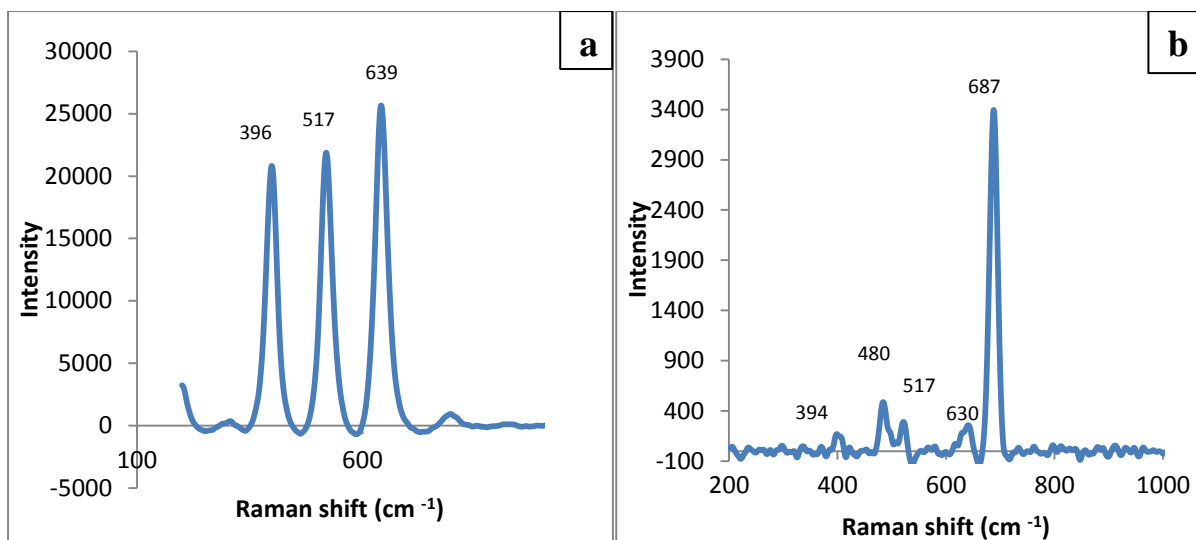
Figure 4.5: Laser Raman spectra of the (a) titania support and (b) 25Co/TiO$_2$ catalyst

4.1.6. TPR

Thermal treatment and its impact on the reducibility of a catalyst is important. Ease of reduction of a catalyst often closely correlates to the catalyst activity [3], since these catalysts function on a redox cycle. The reducibility of the catalysts was investigated by means of TPR analysis. Hydrogen consumption was measured as a function of temperature up to 950 °C.
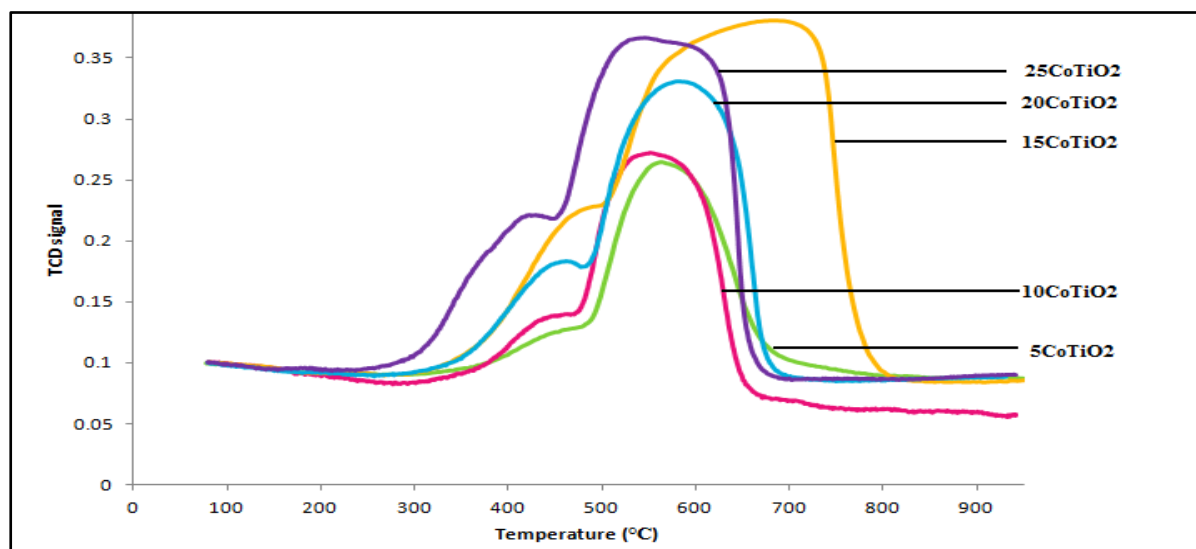
Figure 4.6: Combined TPR results for titania supported cobalt catalysts

The onset of reduction occurred at 300 °C for the 5-20 wt % cobalt loaded catalysts and at 250 °C for the 25 wt % catalyst. From the results obtained, it is evident that the reduction occurs in a stepwise manner in two stages. Looking at the hydrogen consumption and the peak shape, two distinct peaks are apparent which correspond to the reduction of Co$_3$O$_4$ species to metallic cobalt via CoO. The smaller peak, consuming less hydrogen, is indicative of the presence of Co$_3$O$_4$ and its reduction to CoO, which occurred in the lower temperature

45

range of 300 °C - 500 °C for all the catalysts, as displayed in Figure 4.6. The higher temperature reduction peak corresponds to that of CoO to Co^0. Furthermore, the reduction occurred at progressively lower temperatures as the cobalt loadings increased. Results by Yung *et al*. [3] on titania supported cobalt catalysts for the oxidation of nitric oxide showed the same trends in reduction behaviour and TPR experiments on the bare titania showed no reduction.

Overall the catalysts displayed very similar reduction behaviour as is evident in Figure 4.6. Reduction was complete by a temperature of 750 °C, but with increasing hydrogen consumption as the metal loading increased, indicative of an increasing number of reducible species with increase in metal loading. The results for the 15% Co/TiO_2 catalyst do not follow the trend observed for the other catalysts and requires further investigation.
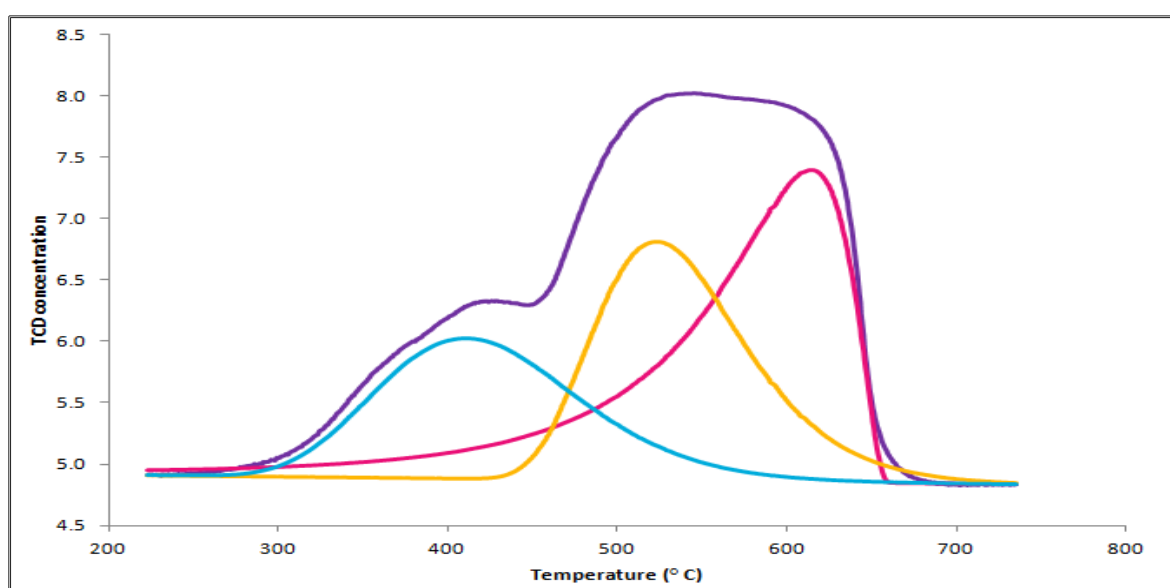

Figure 4.7: TPR profile showing deconvolution of the peaks for the 25 % Co/TiO2 catalyst with temperature maxima at 411 ° C, 524 ° C and 615 ° C.

From the TPR analysis of the 25% Co/TiO_2 catalyst, in Figure 4.7, the results reflect three consecutive merged peaks for the two-step reduction of Co_3O_4 to metallic cobalt via CoO. The first step occurs at 524 °C, while the second step occurs at 615 °C. The second step higher temperature reduction is attributed to species that have stronger degrees of interaction with the titania support e.g. cobalt titanate species or cobalt oxide species within the support pore structure. It has been reported in literature that under reducing conditions, strong support-metal interactions occur, forming less easily reduced species. Titania specifically is known to encapsulate the metal particles [4, 7], thereby hindering interaction with the gas phase. These results are consistent with work carried out on titania and other supports by Vob *et al*. [8], Backman [12] and Li *et al*. [13]. The stepwise reduction of the cobalt species also indicates that the majority of the trivalent species are completely reduced to the divalent species, before subsequent reduction to the metallic state begins, as is clearly seen from the deconvolution of the peaks.

4.1.7. TGA

Thermogravimetric analysis provides a means of assessing the thermal decomposition behaviour of materials. From TGA analysis of the uncalcined support material, inferences were made regarding suitable calcination temperatures and hence 500 °C was chosen for this research effort. From the results in Figure 4.8, it is evident that the mass loss on heating was constant and minimal (ca. 5 %) over the temperature range up to 1000 °C under air. A yield of > 95 % for all catalysts was observed after thermal treatment up to 1000 °C. A conclusion may be drawn that these catalysts are thermally stable under air in the temperature range investigated. Thermal stability is one of the most sought after criteria in catalytic material, in order to withstand rigorous reaction conditions over extended periods of time. The derivative of the TGA curve displays the maximum mass loss temperature (T_{max}) to be ± 80 °C. This mass loss is attributed to loosely bound/adsorbed water molecules. At higher temperatures, lattice expansion is known to occur, resulting in sputtering of the anatase particles and the violent release of water molecules ie waters of hydration. The mass loss evident at a higher temperature, ± 680 °C, can also possibly result from the anatase being consumed in another process e.g. in the formation of cobalt titanate ($CoTiO_3$) species during the phase transformation from anatase to the rutile stage, with some amount of the anatase not being transformed to rutile. This is in good agreement with work done by Rayner [6] on the thermal treatment and particle size evaluation of titania supported cobalt catalysts, as well as studies by Yung *et al*. [3] and Iglesia *et al*. [14] showing the relationship between cobalt titanate species and the anatase to rutile phase transformation in titania supported cobalt catalysts. They reiterate that phase transformation is accompanied by reduction in surface area as well as volume contraction. Their results reflect that cobalt titanate species form from temperatures in excess of 650 °C.
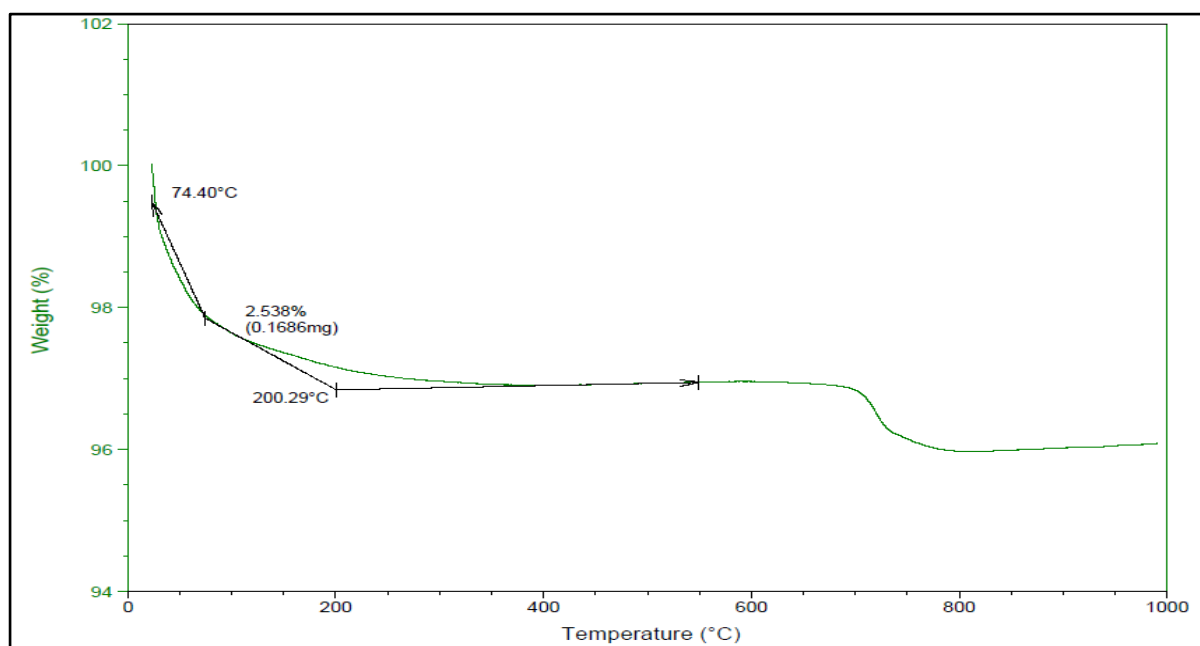

Figure 4.8: Graph depicting the weight loss profile of the 10 Co/TiO$_2$ catalyst, following thermal treatment under air

4.1.8. TEM

From the TEM micrographs in Figure 4.9 (a) and (b), the TiO_2 support and cobalt catalyst material comprise of elongated, spherical and other irregular shaped particles of varying sizes between 8-12 nm and 15-20 nm for the support and Co/TiO_2 catalysts respectively. From the micrographs it is further evident that the catalyst material is crystalline. It is difficult to distinguish between the cobalt and titania particles. This may be as a result of insignificant mass contrast owing to the small difference in mass of the two components as well as the orientation of the particles.
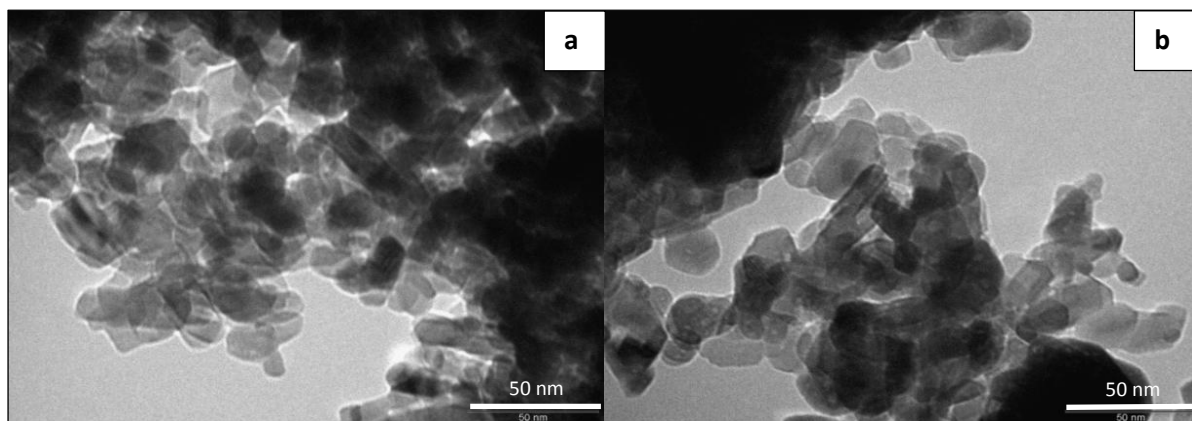
Figure 4.9: TEM micrographs of the (a) TiO_2 support and (b) 20% Co/ TiO_2 catalyst at 600K magnification.

4.1.9. SEM

The function of the support is to allow good dispersion of the catalytically active phase. In this regard medium to high surface area materials are preferred over lower surface area materials. Good dispersion of the active phase is a pre-requisite for commercial catalysts and is a challenge during synthesis. SEM micrographs show that the support and catalyst material comprise predominantly of spherically shaped particles which appear to have aggregated and clustered to form small 'florettes'.
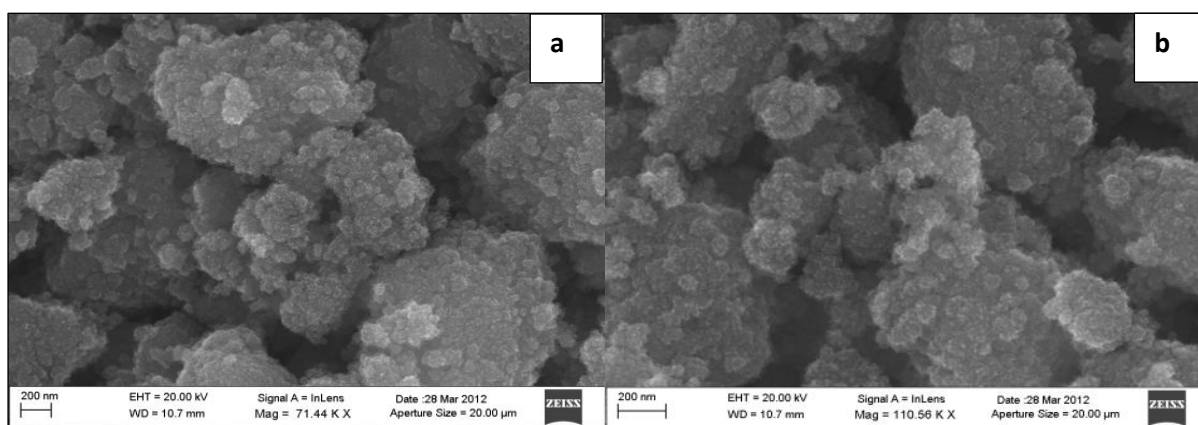
Figure 4.10: SEM images of the TiO_2 support revealing clusters of particles at (a) 71.44 K and (b) 110.56 K magnification.

Upon close perusal and comparison of the images in Figure 4.11 of the titania supported catalysts, distinct 'patches' or white spots are visible - as indicated by the circles - of the

cobalt oxide strewn on the surface of the support. This was also observed in material synthesised by Jongsomjit *et al.* [15].
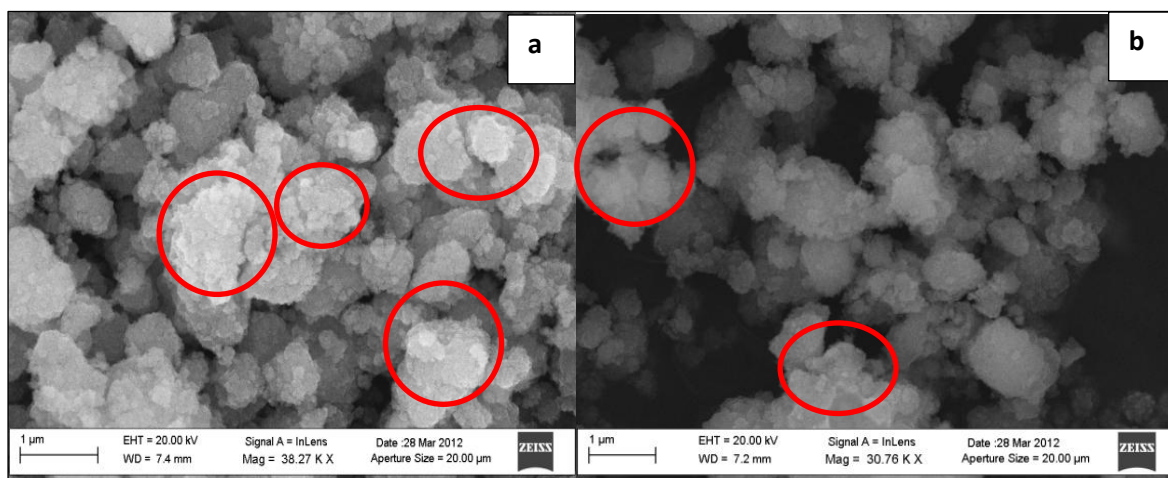
Figure 4.11: SEM images of the (a) 20% Co/ TiO_2 and (b) 25% Co/ TiO_2 catalyst at 38.27 K and 30.76 K magnification respectively, with encircled regions denoting the presence of cobalt oxide.

It is apparent from the images that the material is very coarse textured and appears to be multiple-layered, revealing stepped ridges at the edges. This is particularly noticeable in Figure 4.12
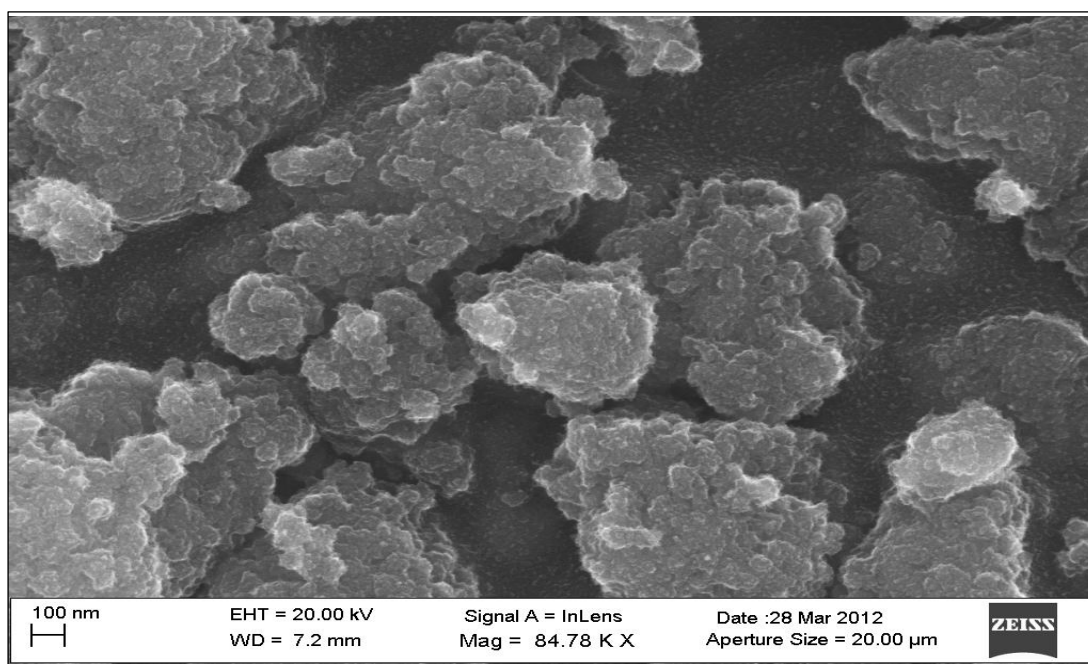
Figure 4.12: SEM image showing coarse textured layered material with patches of cobalt oxide strewn on the surface of the titania

EDX elemental mapping was able to approximate the surface composition of the catalysts, the breakdown of which appears in Table 4.2. These results correlate very closely with results obtained from ICP analysis.

Table 4.2: EDX elemental mapping of cobalt and carbon composition in catalysts

Catalyst	Nominal wt % cobalt	EDX % cobalt	
		Sample A	Sample B
1	5	4.77	4.32
2	10	10.37	10.59
3	15	14.97	14.73
4	20	18.81	18.65
5	25	22.85	24.97

From the elemental mapping, it is evident that the cobalt is well dispersed on the titania support, when lower cobalt loadings were used e.g. in the $5Co/TiO_2$ catalyst in Figure 4.13 (a) and in the $10Co/TiO_2$ catalyst.

Figure 4.13: SEM-EDX elemental mapping indicated good dispersion of cobalt (green) on titania (red) in the (a) $5Co/TiO_2$ catalyst and with aggregation in the (b) $15Co/TiO_2$, (c) $20Co/TiO_2$ and (d) $25Co/TiO_2$ catalysts

With higher cobalt loadings, some aggregation of the cobalt species exists as indicated by the encircled regions in Figure 4.13.

4.3. Spent catalyst characterisation

4.2.1. PXRD

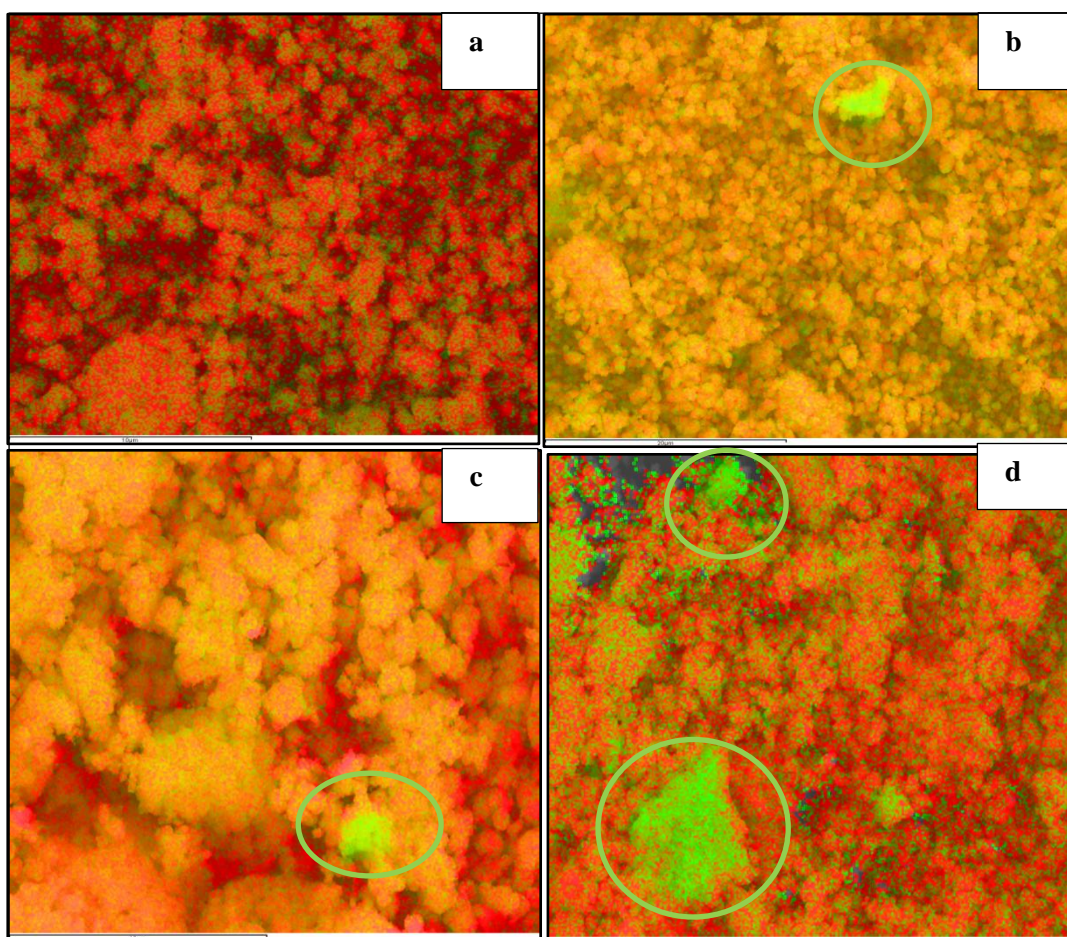The diffractograms of the spent catalysts, from the dehydrogenation reaction, in Figure 4.14, showed far less crystallinity of the material, with less sharpness and definition in the peaks. Only the major peaks from the titania support were clearly visible and those attributed to cobalt oxide were absent. An additional peak was observed at a d-spacing of 2.71 which corresponds to cobalt titanate species [16]. Overall these results show a less crystalline material than the fresh catalyst (see Figures 4.1-4.3)
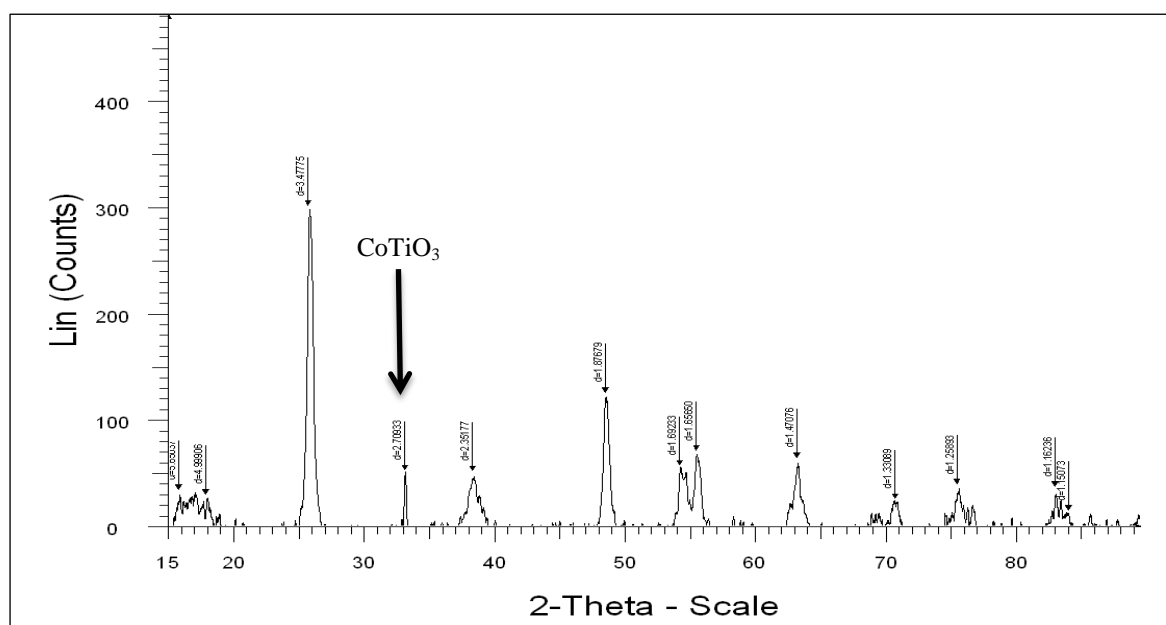
Figure 4.14: Diffractogram of the spent $5Co/TiO_2$ catalyst after the dehydrogenation reaction, with the new peak for $CoTiO_3$

In contrast to the spent catalyst after the dehydrogenation, the diffractogram of the $20Co/TiO_2$ spent catalyst after the ODH reaction, in Figure 4.15 showed the presence of the Co_3O_4 phase. This confirms that the reoxidation of the catalyst occurred, following reduction during the reaction cycle. This confirms that this catalyst, in the ODH reaction performs via an efficient redox cycle. Furthermore, a new minor reflection due to $CoTiO_3$ was present, which was not present in the fresh catalyst.
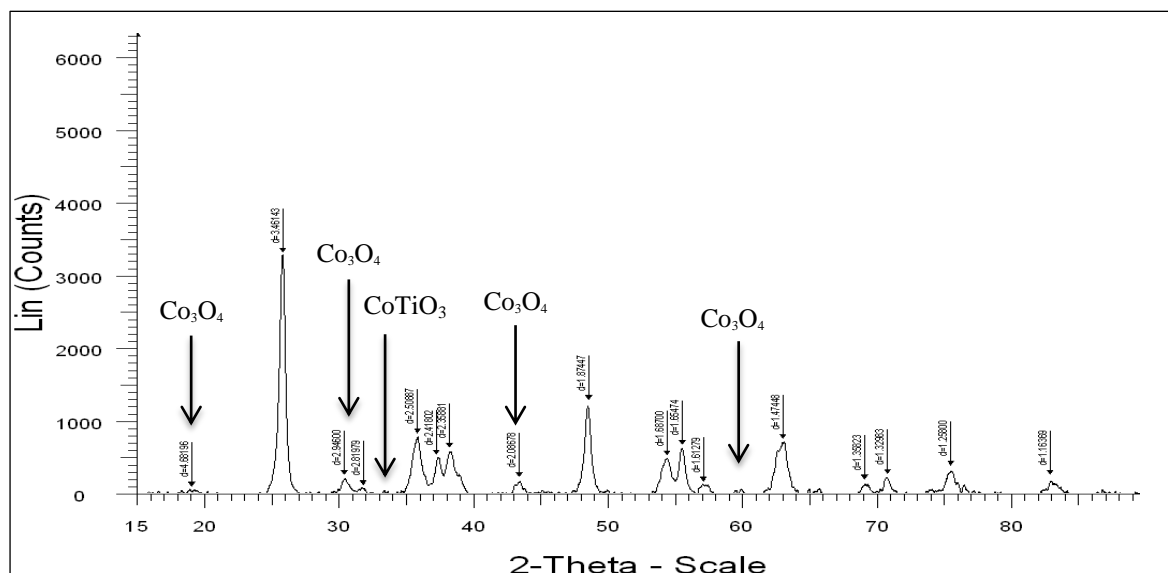
Figure 4.15: Diffractogram of the spent $20Co/TiO_2$ catalyst after the ODH reaction, showing the presence of the cobalt oxide phase and a new peak for the cobalt titanate phase

4.2.2. BET

Table 4.3: BET Surface area and pore volume results obtained on the spent catalysts

Catalyst	Fresh catalyst		Spent catalyst	
	Surface area	Pore volume	Surface area	Pore volume
TiO_2	99	0.31	42	0.16
5 $CoTiO_2$dehydrog	68	0.23	56	0.21
5 $CoTiO_2$(8C:2O)	68	0.23	50	0.19
5 $CoTiO_2$(8C:4O)	68	0.23	35	0.15
10 $CoTiO_2$(8C:4O)	65	0.22	25	0.13
20 $CoTiO_2$(8C:2O)	61	0.18	53	0.17

The most significant decrease in surface area and pore volume was observed in the titania run as a catalyst by itself, the $5Co/TiO_2$ catalyst and the $10Co/TiO_2$ catalyst, run under oxygen rich conditions. This may be as a result of the higher conversions over these catalysts and greater deformation of the surface structure from repeated reduction/oxidation cycles.

4.2.3. TGA

Different types of coke appear on the spent catalysts. Coking can exist in the form of soft coking with non-crystalline amorphous carbon or hard coking comprised of polymeric or graphitic type carbonaceous material [5]. Coking leads to blockage of active sites and causes deactivation of the catalyst, thereby compromising the catalyst lifetime.

Figure 4.16: The TGA weight loss profile of the 5Co/TiO$_2$ spent catalyst after the catalytic testing under anaerobic conditions.

The weight loss profile in Figure 4.16 of the spent catalyst from the dehydrogenation reaction, displayed a significantly higher mass loss of ca. 8 % following thermal treatment compared to the fresh catalyst. This mass loss occurred under 400 °C, indicative of soft coking on the catalyst post reaction. This spent catalyst's appearance was distinctly different from the spent catalyst run under aerobic conditions. The former was black, while the latter was green. Brik *et al*. [1] noted the same colour in their spent catalysts from ethane ODH and attributed this colour change to possible change in co-ordination and/or oxidation state of the cobalt cations. The 5Co/TiO$_2$ spent catalyst after the aerobic catalytic testing, showed a weight loss (Figure 4.17) of ca. 2 % at temperatures below 200 °C, which is due to adsorbed water. This catalyst had the same weight loss profile as the fresh catalyst with a weight loss of <3 %, thus indicating the absence of coke on the catalyst.
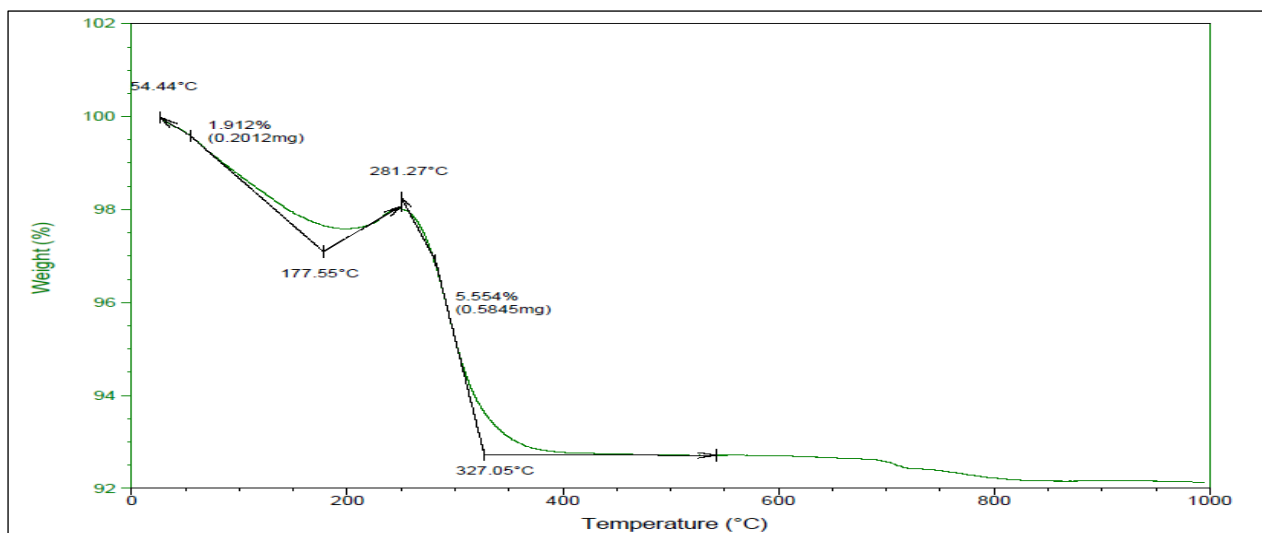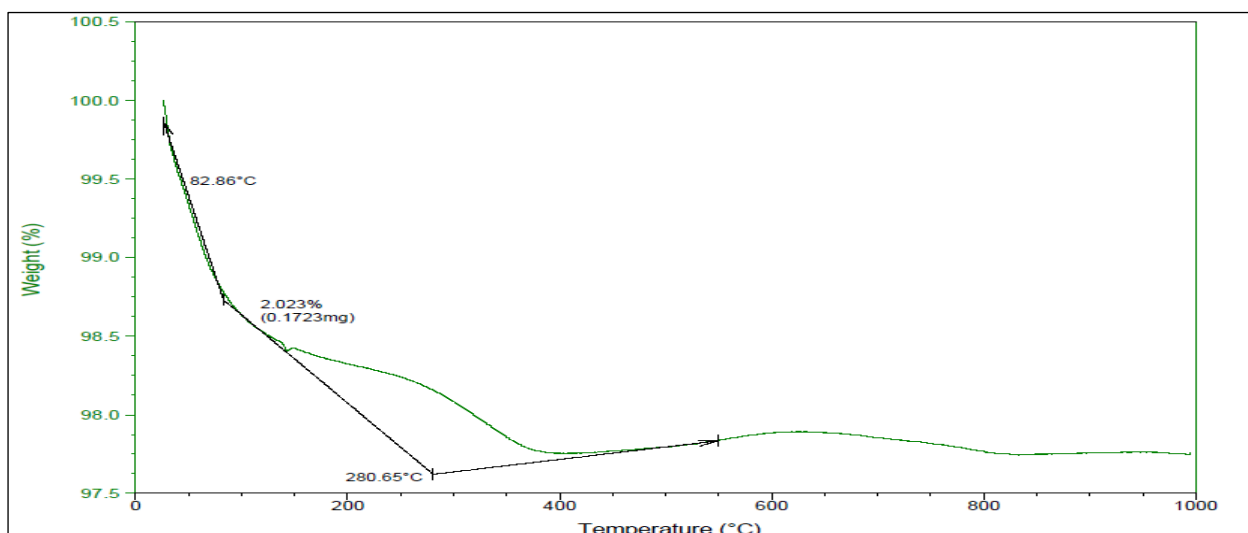

Figure 4.17: The TGA weight loss profile of the 5Co/TiO$_2$ spent catalyst after the catalytic testing under aerobic conditions with an 8C:4O ratio.

4.2.4. Laser Raman spectroscopy

Upon comparison of the laser Raman spectra for the $5Co/TiO_2$ fresh catalyst in Figure 4.18 (a) and the catalysts run under oxygen richer (8C:4O) conditions in Figure 4.18 (b) the latter only showed the bands due to anatase with the absence of any bands representing carbonaceous species. Generally the distinct bands at 1582 cm^{-1} and 2700 cm^{-1} in laser Raman spectra (when using a 514.5 nm laser source) are indicative of the G and G´ band which represents polyaromatic hydrocarbons (PAH's) or graphitic material with sp^2 carbons.

This supports the argument that the oxidising environment for the oxidative dehydrogenation reaction suppresses coke formation and inhibits catalyst deactivation. Most of the carbon forms carbon oxides as opposed to forming a layer over the catalyst surface, which is typical of ODH catalysts. The green colour of the catalyst post reaction also provided a visual indication of the absence of coke.
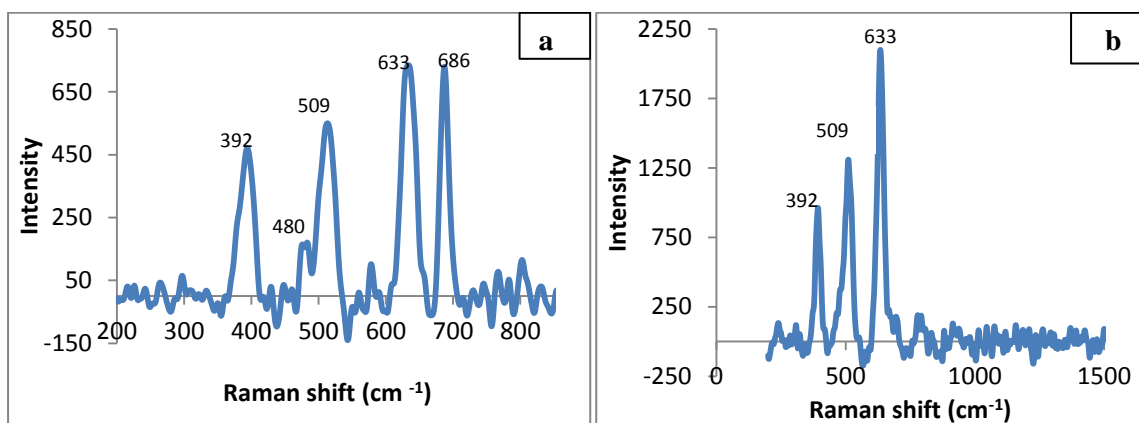
Figure 4.18: Laser Raman spectra of the $5Co/TiO_2$ (a) fresh catalyst and (b) spent catalyst after the catalytic testing under aerobic conditions with an 8C:4O ratio.

Upon comparison of the laser Raman spectra from the fresh $5Co/TiO_2$ catalysts in Figure 4.18 (a), and the spent $5Co/TiO_2$ catalysts in Figure 4.18 (b) and Figure 4.19 (a), it is clear that the catalyst run under anaerobic conditions has additional bands at 788, 1552 and 2330 cm^{-1}. These bands at 1552 and 2330 cm^{-1} are possibly indicative of sp^2 carbon species. This is consistent with deposition or accumulation on the catalyst surface of aromatics like benzene, ethylbenzene and styrene, which were the product profile from the catalytic testing. The spent catalyst's black appearance also provided a visual indication of coke.

The bands at 788 and 798 cm^{-1} in Figure 4.19 may be as a result of the formation of other cobalt species, as observed by Brik *et al*. [1] on the spent cobalt titania catalysts in ethane ODH. The strong band observed at 483 and the weaker band at 687 cm^{-1} in Figure 4.18 (b), is indicative of Co_3O_4 [3] species in the spent $20Co/TiO_2$ catalyst, thereby showing that following reduction, the cobalt was reoxidised. This spent catalyst, showed the absence of any carbonaceous species, from the Raman analysis.
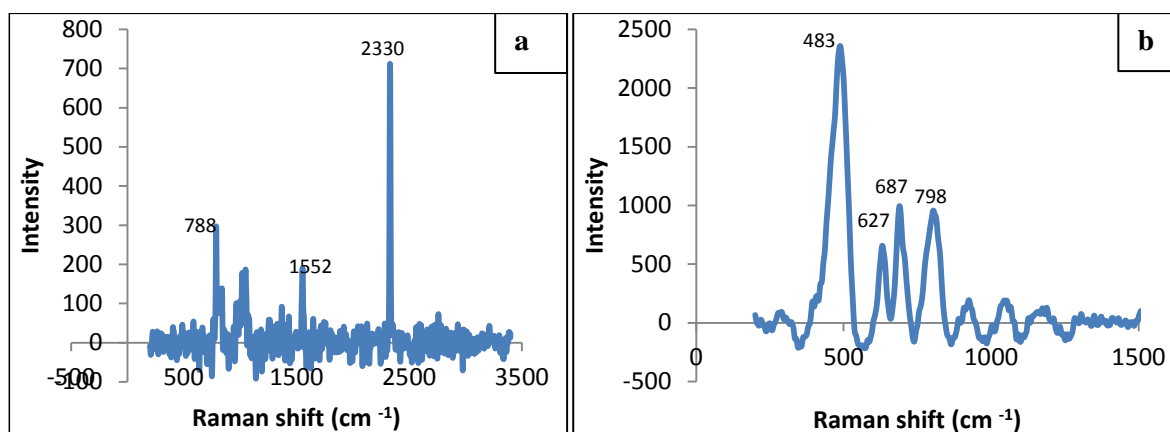
Figure 4.19: Laser Raman spectra of the (a) 5Co/TiO$_2$ spent catalyst after the catalytic testing under anaerobic conditions and (b) 20 Co/ TiO$_2$ after aerobic (8C: 2O) catalytic testing

Titania amongst the other oxide supports is reported to be excellent in inhibiting or suppressing carbon deposition according to research by Takanabe *et al*. [16]. Evidence of this was obtained by the absence of carbon species deposited on the catalysts during the ODH reactions, as was found for the spent catalysts characterised by the above techniques.

4.2.5. TEM

The TEM micrographs in Figure 4.20 (a) reveal that the spent titania support maintained crystalline structure post reaction, while the 10 Co/TiO$_2$ catalyst shows deformation of the original shape as observed in Figure 4.20 (b) and a fused appearance of the catalyst particles, which may be attributed to sintering and agglomerating of individual particles.
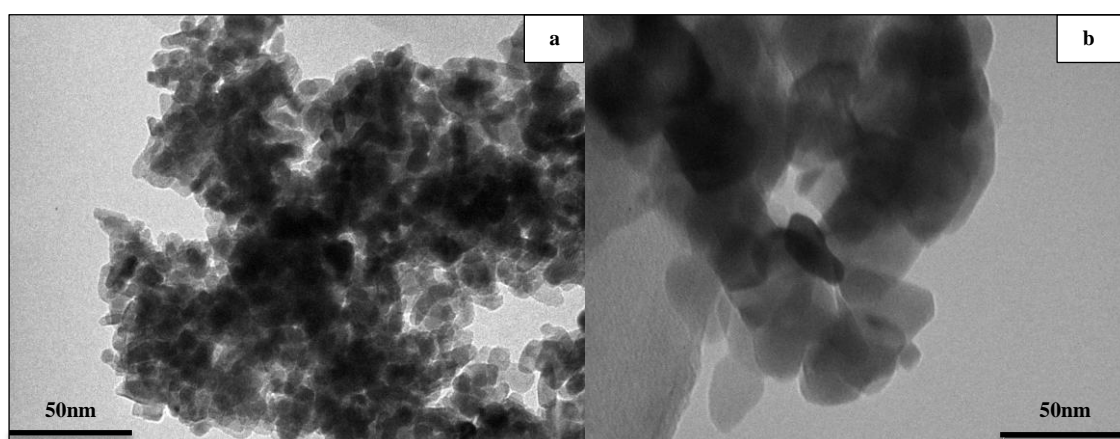
Figure 4.20: TEM micrographs of the spent catalysts: (a) Titania support (b) 10Co/TiO$_2$ catalyst after the (8C: 4O) ODH reaction

The spent catalyst from the dehydrogenation reaction in Figure 4.21 clearly reveals the presence of metallic cobalt particles, (the larger of which is encircled and measures ca. 40 nm) as a result of the reduction of the Co$_3$O$_4$, with *n*-octane acting as the reductant, as well as the presence of the hydrogen generated in the dehydrogenation reaction.
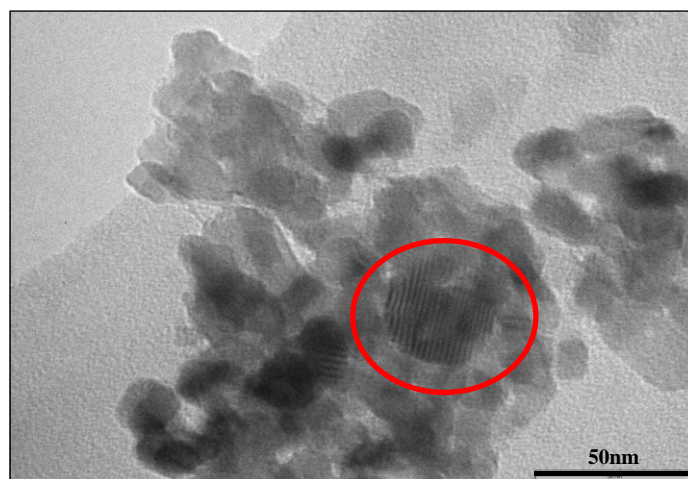
Figure 4.21: TEM micrographs of the spent 5 Co/TiO$_2$ catalysts after the dehydrogenation reaction with the encircled region showing the presence of the metallic cobalt particle

4.2.6. SEM

SEM images in Figure 4.22 reflect a significant change in the morphology of the catalyst, upon comparison of the fresh and spent catalysts. These images show the complete transformation of the surface structure with fragmentation and disintegration clearly visible, after cooling down back to room temperature, post reaction.
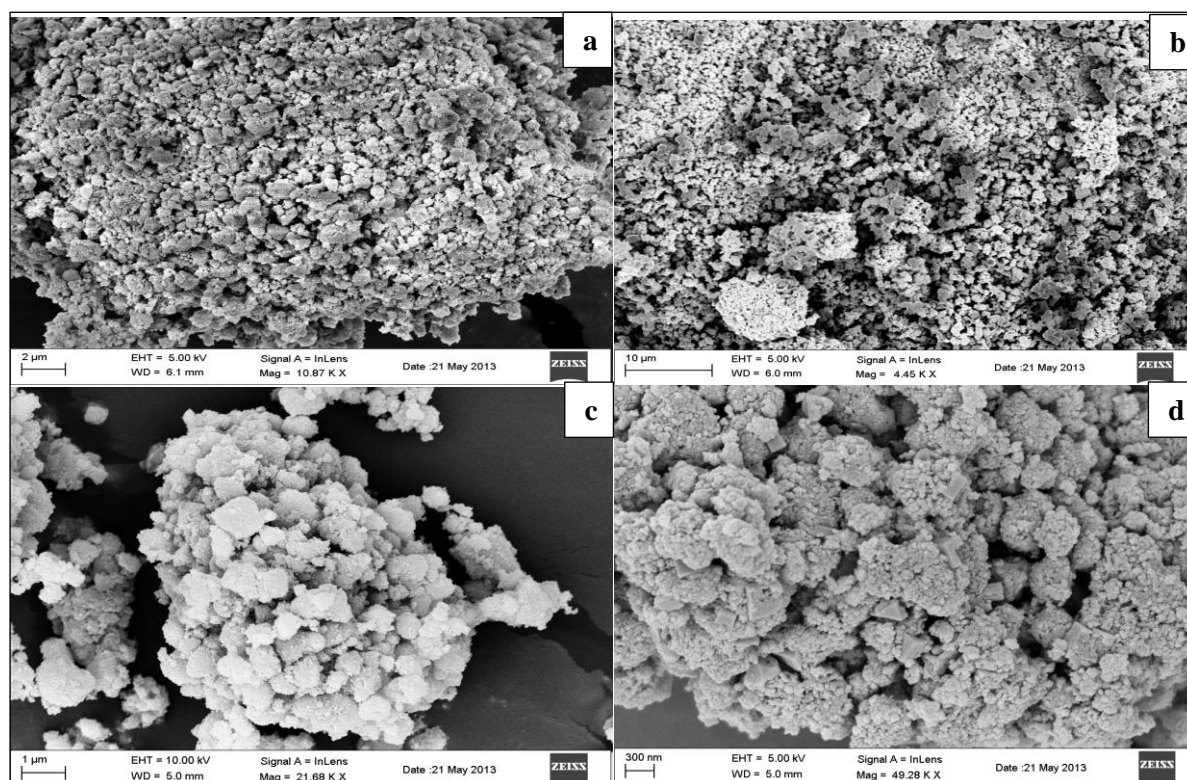
Figure 4.22: SEM micrographs of the spent catalysts: (a) Titania support and the 5 Co/TiO$_2$ catalyst after (b) dehydrogenation, (c) (8C: 4O) ODH reaction and (d) the 10 Co/TiO$_2$ catalyst after the (8C: 4O) ODH reaction.

Several factors may be directly linked to the deformation of the catalyst: repeated reduction and re-oxidation of the surface, products such as water in the product stream, heating effects from the exothermicity of the reactions, as well as 'hotspots' within the catalyst bed.

EDX mapping images of the spent catalysts in Figure 4.23 and Figure 4.24 show the presence of carbon deposits in the encircled regions, which were not observed in the fresh catalysts. This may be from traces of the products from catalytic testing that remained adsorbed on the catalyst. A higher concentration of carbon, appearing in more clumped deposits, was visible on the dehydrogenation reaction catalyst.
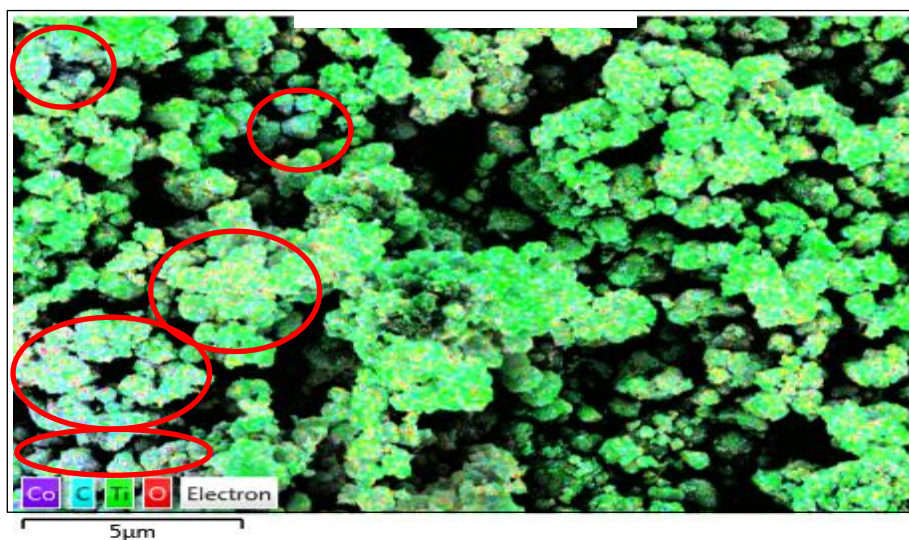
Figure 4.23: SEM-EDX imaging of the 5Co/TiO$_2$ spent catalyst from the dehydrogenation reaction displaying accumulated carbon deposits in the encircled regions

The carbon deposits appear evenly distributed over the surface of the catalyst after the ODH reactions. Carbon deposition has been minimised, since most of the carbon formed carbon oxides in the ODH reactions.
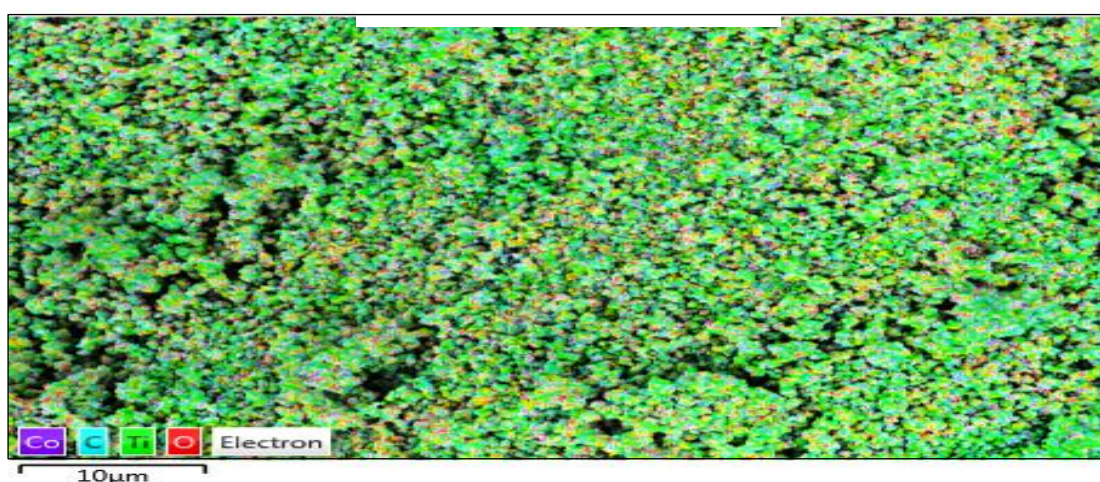
Figure 4.24: SEM-EDX imaging of the 5Co/TiO$_2$ spent catalyst from the ODH reaction with carbon deposits evenly spread throughout the catalyst surface

4.3. Results: Catalytic testing

4.3.1. Introduction

Catalytic testing was carried out as functions of temperature (350-550 ℃) as well as *n*-octane: oxygen (8C:2O and 8C:4O) ratios. A constant 4000 h^{-1} GHSV was maintained. The fuel to air ratio was maintained between 10-11 (v/v) % *n*-octane in air. The catalyst bed was maintained at 1 ml (ca.0.75 g), while pellet size was 600-1000 μm. Single experiments were carried out to assess mass flow and diffusion limitations by firstly decreasing the pellet size to 500 – 600 μm and assessing the impact and secondly increasing the GHSV to 6000 h^{-1} and assessing its impact. The results obtained are outlined in this chapter.

Wherever possible, the structure/activity correlation was sought viz. linking the relationship between catalyst composition/properties (redox, acid-base and electronic) and the catalytic activity.

4.3.2. The role of the anatase phase titania support

Initial catalytic testing commenced on the bare anatase support to evaluate its role in the reaction viz. that of retarding or promoting activity. From the literature on butane activation over vanadia/titania supported and unsupported systems, the support was found to play a retarding role in catalytic acitivity [17]. This is in contrast to other studies, where it was found to play a promoting role [18, 19]. However, on comparative studies with other supports like alumina and silica, it was found that the titania supported vanadia was a less selective oxidative dehydrogenation catalysts [17]. This research effort revealed a highly active support in the anatase phase of titania, as is evident from the results that follow. The high surface area of the support ca. 100 m^2/g is likely a contributing factor in the high activity of the support and the overall activity of the catalysts is a strong function of the support.

Figure 4.25: The product profile for the reaction of *n*-octane over the titania support as a function of temperature at a GHSV of 4000 h^{-1} and a 8C:2O ratio

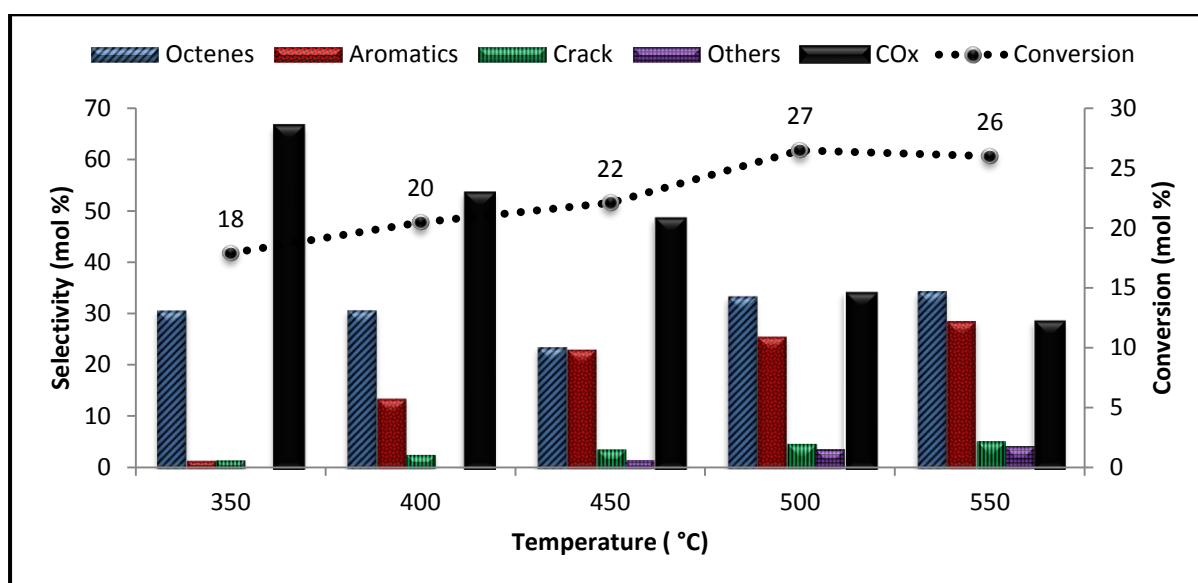The conversion of *n*-octane over the titania showed a steady increase over the temperature range 350 - 550 °C, with the biggest increase of 5 % between 450 to 500 °C being observed, as is evident in Figure 4.25. Generally conversion increases with temperature and this conversion profile follows that trend. Conversion essentially was constant at 500 °C and 550 °C. The levelling off of conversions at the higher temperatures may be related to the consumption of the oxygen by secondary products viz. olefins which are more reactive than the reactant. A competitive reaction pathway possibly exists with the more reactive species preferentially consuming the oxygen species.

Table 4.4: The product distribution arising from catalytic testing of titania at a 4000 h^{-1} GHSV and a 8C:2O aerobic environment

Temperature	350	400	450	500	550
Octenes	31	31	23	33	34
Aromatics	2	14	23	26	29
Crack	2	3	4	5	5
Others	0	0	2	4	4
COx	67	54	49	34	29

The product profile was dominated by COx products at all temperatures except 550 °C, when the octenes dominate and reach their maximum selectivity. The octene selectivity increases marginally across the temperatures investigated, with a decrease of 8 % at 450 °C accompanied by 9 % increase in aromatic formation. Aromatics formation at 350 °C is very low, but a significant increase occurs at both 400 and 450 °C, after which it increases at 3 % increments for 50 °C increases in temperature. Cracked products marginally increase to attain a maximum selectivity of 5 % at 500 and 550 °C. A further minor contribution comes from the unidentified C8 products that occur in trace amounts from 2 % at 450 °C and attain a maximum selectivity of 4 % at 500 and 550 °C. The general trend observed is an increase in selectivity to value added products with temperature. At 500 °C and 550 °C, the product distribution is evenly spread between octenes, aromatics and COx products. This shows the uniformity in the dehydrogenation, dehydrocyclisation and cracking/deep oxidation reaction pathways attained at the higher temperature range.

The general trend observed in Figure 4.26 is the decrease in COx formation with an increase in temperature. The carbon oxides formed more than two thirds of the product profile at 350 °C but declined to one third at 550 °C, indicative of greater cracking and subsequent oxidation at lower temperatures. Overall deep oxidation to carbon dioxide dominated over partial oxidation to carbon monoxide with a $1CO:1.5-2CO_2$ ratio prevailing at all temperatures. A significant drop in the CO_2 selectivity at 400 °C occurred with the take-off in aromatics formation, probably as a result of sufficient activation energy being provided by the system at higher temperatures to promote dehydrocyclisation of the *n*-octane.

The overall oxygen conversion in this system ranged from a minimum of 14 % at 350 °C to a maximum of 47 %, obtained at 550 °C.
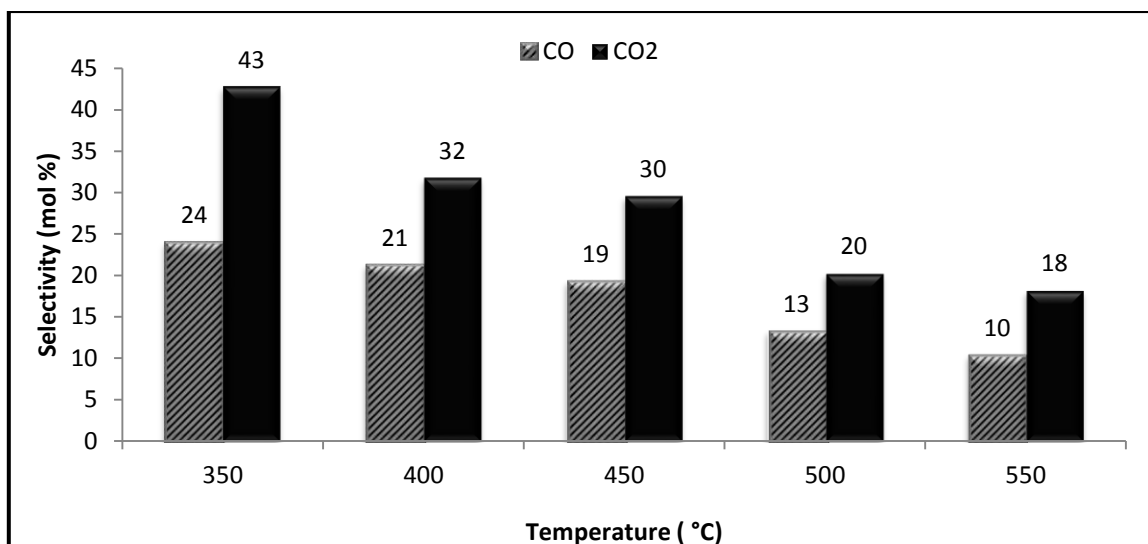
Figure 4.26: The carbon oxides breakdown for the titania support as a function of temperature

Titania is a basic support and its basicity directly influences the product profile. Octenes and aromatics that have electron rich centres, easily desorb off the basic titania support with short contacts times, contributing to the high selectivity (a combined maximum of 63 % at 550 °C) towards these products. Similarly the acidic products would have longer contact times with the basic catalyst surface, which results in cracking and further oxidation to the carbon oxides, enhancing the selectivity to carbon oxides.
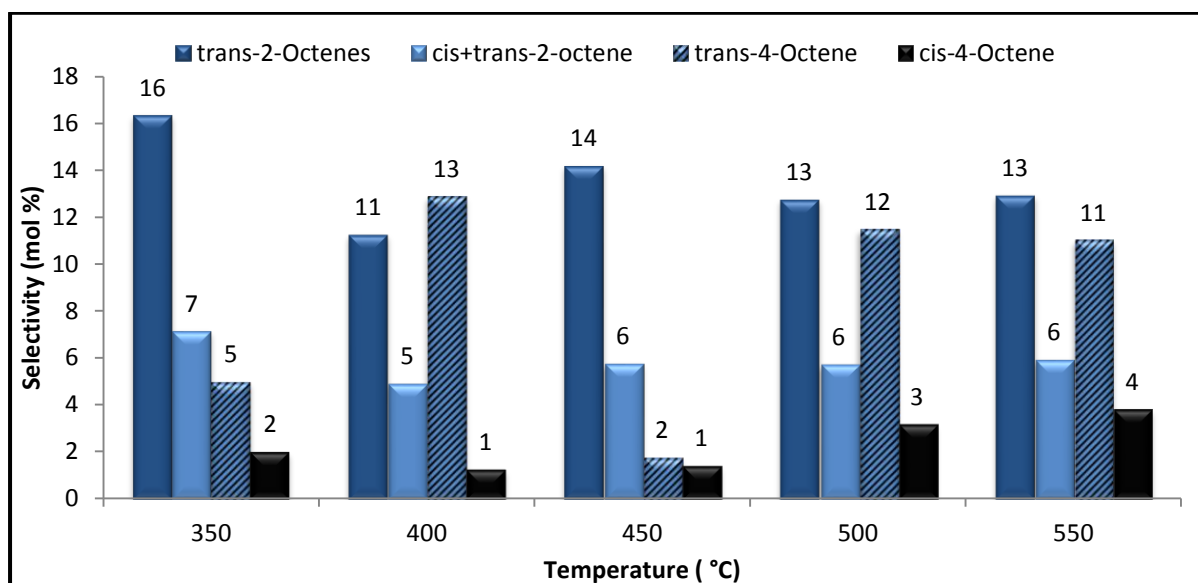
Figure 4.27: The octenes breakdown for the titania support as a function of temperature

A breakdown of the octenes in Figure 4.27 reflects a dominance by the trans isomers of 2-octene and 4-octene. The trans isomer is thermodynamically more stable than the cis isomer and this would account for its higher prevalence in the product stream. This was found to be consistent across all catalytic testing. The selectivity to trans-4-octene at 350 °C and 450 °C is lower than at the other temperatures and cannot be explained at this stage. Trans-2-octene selectivity generally decreased with temperature and the opposite held true for cis-4-octene,

while cis+trans-2-octene selectivity remained fairly stable with an increase in temperature. Collectively the octenes made up approximately one third of the product pool across most temperatures investigated except for 450 °C. Terminal activation of *n*-octane over the titania to form 1-octene was not favoured.
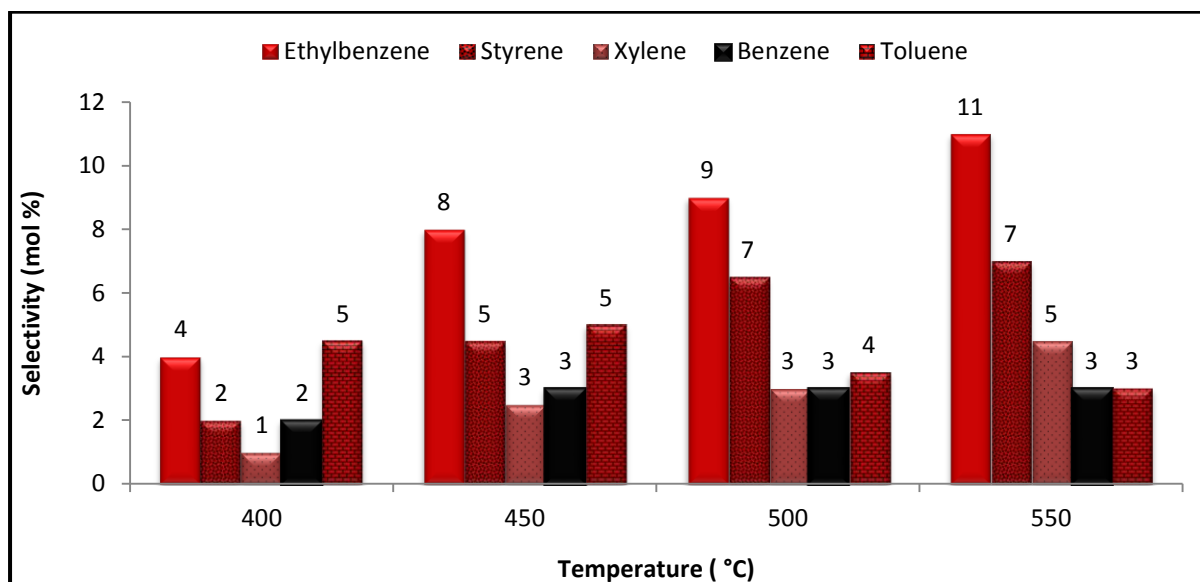
Figure 4.28: The aromatics breakdown for the titania support as a function of temperature

The aromatics pool (Figure 4.28) consisted primarily of C8 aromatics, ethylbenzene, styrene and o-xylene and to a lesser degree the lower aromatics, benzene and toluene. Significant aromatics formation only began at 400 °C onwards with a minor contribution of 2 % from benzene at 350 °C. Ethylbenzene and o-xylene formation results from C1 – C6 and C2 – C7 ring closure, respectively, from dehydrocyclisation of the octene isomer. Styrene is obtained from the dehydrogenation of ethylbenzene. Both ethylbenzene and styrene increase with increasing temperature. The consumption of ethylbenzene in styrene formation may be driving the equilibrium towards higher ethylbenzene formation. The formation of benzene and toluene from ethylbenzene and o-xylene may arise either via hydrogenolysis or as a result of cracking brought about by geometric constraints of the pore channels in the catalyst material [20]. All the aromatics selectivities increase with increasing temperature, except for toluene. Aromatics are the most stable of the hydrocarbons owing to the stable aromatic nucleus and are hence less prone to cracking.

Several different dehydrogenation reactions likely occur in parallel in this catalytic system, holding true for the bare titania as well as the cobalt titania catalysts. The first involves the dehydrogenation of the *n*-octane to yield octenes, with the octenes being the primary product. The octenes are further dehydrogenated and cyclise to form secondary products: aromatics. The secondary product ethylbenzene undergoes further dehydrogenation to form the tertiary product: styrene. The *n*-octane is the least reactive in the series of species exposed to the active sites, with the products being the more reactive species.

4.3.3. The influence of cobalt content on the conversion of *n*-octane and the product profile

Catalytic testing was conducted to probe the activity of the 5Co/TiO$_2$ and 20Co/TiO$_2$ catalysts in the oxidative activation of *n*-octane and to establish the effect of cobalt content on the product distribution. The products obtained were predominantly alkenes, aromatics and carbon oxides, with a minor contribution from cracked products and 'others'. Some unknown products were obtained at GC retention times between 12-20 minutes that still require identification, and these form the major component of the 'others'. The majority of these components were found in trace amounts, but collectively appear to be more significant in the product pool. The cracked products comprised primarily of a mixture of trace amounts of shorter chain (<C8) alkanes, alkenes and alcohols: amongst others methane, ethane, butane, pentane, hexane, 1-pentene, 1-hexene, 2-propanol and ethanol.
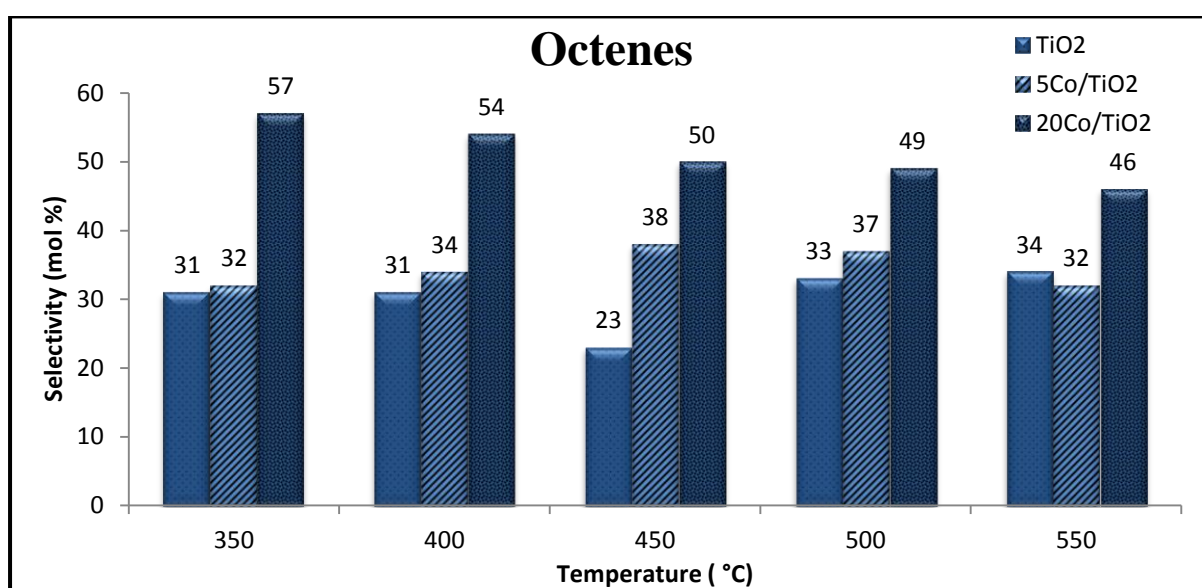
Figure 4.29: The octenes breakdown for different cobalt contents as a function of temperature

Once hydrogen abstraction from *n*-octane occurs, the resulting species can desorb as olefinic products or undergo further reaction with oxygen insertion to produce oxygenated products. The prevalence of octenes in the product stream results from short contact times and quick desorption of these olefinic products, with electron rich centres, off the catalyst surface, which is also basic in nature. The same holds true for aromatic products.

Upon comparison of the data from the runs where 0, 5 and 20 % cobalt were used, the octenes were the dominant product across all temperatures. The breakdown in Figure 4.29 clearly shows the significantly enhanced selectivity as a result of the higher cobalt content in the catalyst. The effects of the 20 % cobalt content is most pronounced at 350 °C and 450 °C, but less so as the temperature reaches higher ranges when the octenes selectivity declines. The octenes form on average more than 50 % of the product pool over the 20Co/TiO$_2$ catalyst. The effect of the lower cobalt loading is less pronounced. The octenes are marginally higher over the 5Co/TiO$_2$ catalyst than the bare support at 350 °C, 400 °C and

500 °C. A slightly lower selectivity was observed at 550 °C than at 500 °C and this may be as a result of the octene cyclisation to aromatics at this temperature. These results are consistent with the behaviour of cobalt in Fischer-Tropsch systems [13, 21-24], where cobalt enhances octenes production as reported by Jalama *et al*. [25].

The overall trend in the higher cobalt loading catalyst was a decrease in octene selectivity with an increase in temperature, converse to what is observed over the bare support and the 5Co/TiO$_2$ catalyst. Upon closer scrutiny of the results in Figures 4.29 and 4.30, it is clear that this trend occurs with the simultaneous increase in aromatics formation with temperature. This is indicative of the octene being consumed in its transformation into aromatics. Interestingly, the formation of aromatics is higher on the lower cobalt loading catalyst but significantly higher than on the support, more obviously so at lower temperatures. As the temperature increases, selectivities almost even out across all loadings, but reach a plateau in the 5Co/TiO$_2$ catalyst from 450 °C onwards. The good dispersion of the cobalt species on the 5Co/TiO$_2$ catalyst may further enhance the aromatics formation, since EDX results showed aggregation of the cobalt species on the higher cobalt loaded catalyst. Good dispersion of the active species leads to easier accessibility of the *n*-octane to the active site and hence activity of the catalyst. A further contributing factor may be the higher surface area of the 5Co/TiO$_2$ catalyst compared to the 20Co/TiO$_2$ catalysts.

Aromatics are the most stable of the hydrocarbons as a result of their stable aromatic nucleus and are less prone to cracking. C1-C6 and C2-C7 ring closure, leads to ethylbenzene and o-xylene formation respectively. For this to occur, the double bond would need to be in the C1 or C2 position. From the product profile, significant amounts of 2-octene are seen and less so the 1-octene isomer. This is consistent with the higher prevalence of ethylbenzene (and styrene), indicative of almost complete transformation of 1-octene and hence its limited prevalence in the product stream.
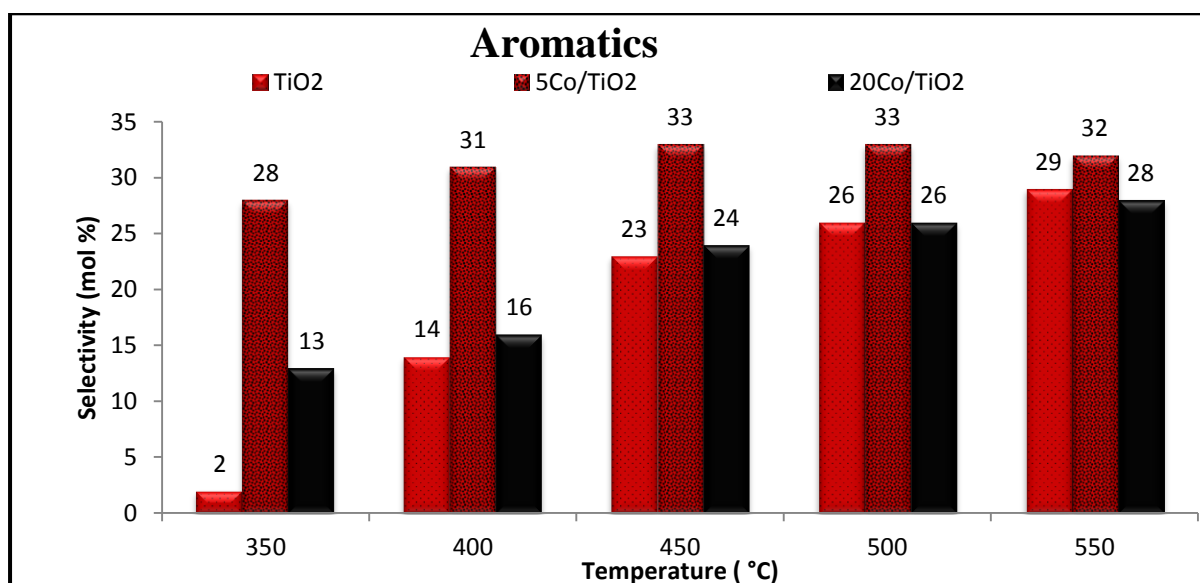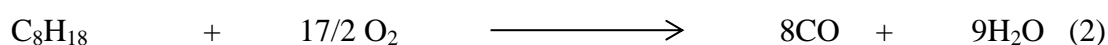

Figure 4.30: The aromatics breakdown for different cobalt content in the catalysts as a function of temperature

This presence of 2-octene isomers also explains the prevalence in the product pool of a significant amount of C8 aromatics viz. ethylbenzene, styrene and o-xylene, together with lower amounts of benzene and toluene. Benzene and toluene formation results from cracking of the C8 aromatics, quite possibly during the dehydrogenation transformation step. Significant formation of aromatics occurred at 350 °C following the impregnation of titania with cobalt, since this did not occur with the bare titania. The increase in the number of active sites and the associated good dispersion may directly be linked to the aromatisation pathway being favoured to a greater extent.

The COx breakdown amongst the different cobalt loaded catalysts reveals the highest selectivities on the bare support. No significant difference exists between the 5 and 20Co/TiO$_2$ catalysts in Figure 4.31, in the higher temperature ranges, from 450 °C to 550 °C. A 10 % and 5 % difference in COx selectivities exist at 350 °C and 400 °C respectively. Overall, higher temperatures favour lower COx formation. Carbon dioxide was the dominant COx product. This trend was observed across all the catalytic testing on these catalysts in this research effort. COx products and water are the thermodynamically favourable products resulting from the combustion reaction of hydrocarbons in oxygen as indicated for *n*-octane in the equations (1) and (2).

$$C_8H_{18} \quad + \quad 25/2\ O_2 \quad \longrightarrow \quad 8CO_2 \quad + \quad 9H_2O \quad (1)$$

$$C_8H_{18} \quad + \quad 17/2\ O_2 \quad \longrightarrow \quad 8CO \quad + \quad 9H_2O \quad (2)$$

The results clearly indicate that COx formation, as the less desired products, can be minimised via temperature manipulation. In general, reaction parameters are manipulated in order to minimise side reactions, like cracking and subsequent COx formation, since the selective oxidation products are preferred over the deep oxidation products.

Following hydrogen abstraction from the *n*-octane molecule, if a high concentration of easily removable oxygen species are in the vicinity of these adsorbed species, then overoxidation will occur to form COx products. Deep oxidation to CO$_2$ is highly favourable in oxygen rich environments, consuming more oxygen in its formation than CO. All the above catalytic testing was carried out at an 8C:2O (1:1) octane to oxygen environment. The oxygen balances revealed an excess of oxygen in the system. The maximum oxygen conversion at 550 °C for the titania, 5 and 20Co/TiO$_2$ catalysts was found to be 47, 69 and 62 % respectively. These results confirm that oxygen exists in excess using this hydrocarbon to oxidant ratio.
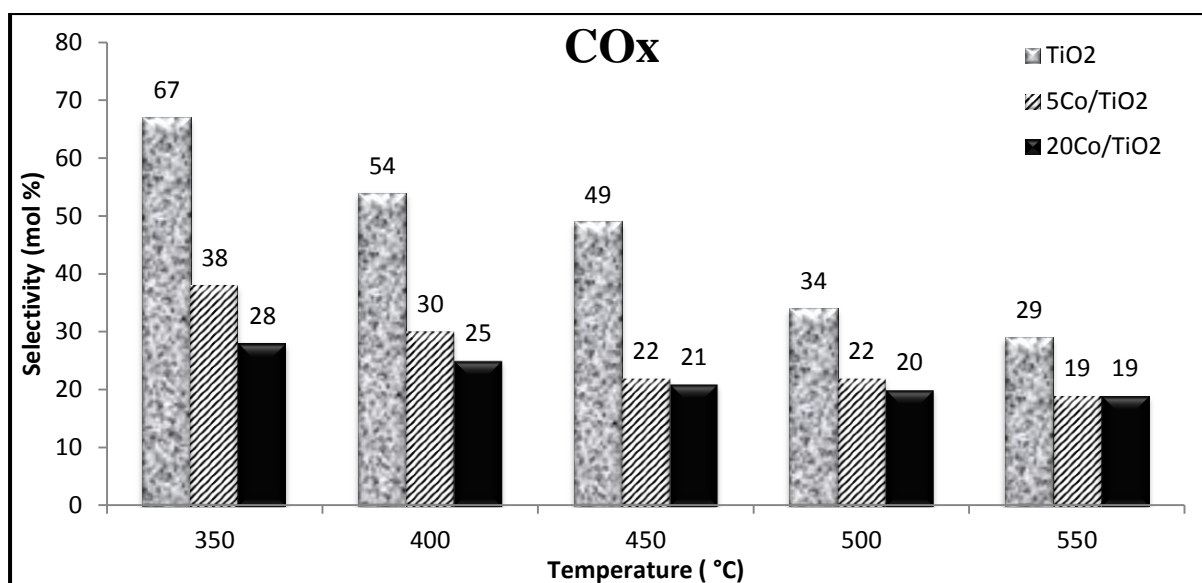
Figure 4.31: The COx breakdown for different cobalt content in the catalysts as a function of temperature

The other interesting observations from the testing of the 20Co/TiO$_2$ catalyst, that was not observed over the support or the 5Co/TiO$_2$ catalyst, was the prevalence of a higher amount of 1-octene in the product stream at all temperatures, as shown in Table 4.5. The 1-octene selectivity decreased with increasing temperature. Terminal activation is energy intensive, producing highly reactive species that become considerably more reactive with higher temperatures, easily transforming to secondary products, which explains the decline in 1-octene selectivity with an increase in temperature. The higher cobalt content appears to be influencing its prevalence, especially at 350 °C. The reason for this is probably the higher reactivity of the surface as a result of the increase in the number of active sites. In comparison, with the 5Co/TiO$_2$ catalyst, 1-octene was observed only at 450 °C, 500°C and 550 °C at low selectivities of 3, 3 and 4 %. Linear alpha olefins are particularly valuable chemicals sought after in the detergent industry.

Table 4.5: Selectivities of octene isomers from the catalytic testing of the 20 Co/TiO$_2$ catalyst

Octene isomer	Temperature (°C)				
	350	400	450	500	550
1-octene	10	8	6	6	5
trans-2-octene	18	18	18	17	16
cis+trans-2-octene	11	10	10	9	8
trans-4-octene	12	13	12	12	12
cis-4-octene	5	5	5	5	5

The selectivities to the 4-octene isomers remains stable across all temperatures, but the selectivities to 2-octene isomers decrease marginally with increasing temperature. Trans-2-octene remains the dominant octene isomer by a significant margin at all temperatures for all the catalysts tested, since it is the most stable thermodynamically.

From Figure 4.32, the general trend observed is an increase in conversion with temperature and cobalt content. Over the 20 % cobalt catalysts, however, the conversions plateau from 450 °C onwards. The plateau may be related to several contributing factors that collectively lead to this observation. The surface is a dynamic one, with multiple reduction/oxidation and adsorption/desorption steps occurring simultaneously. The secondary reactions involve more reactive species than the alkane and, especially with their higher content in the product stream, become more oxygen demanding and preferentially consume the oxygen species, which would otherwise have been consumed in conversion of the alkane. Furthermore, the divalent cobalt species do not easily oxidise [1] and hence the rate at which the reduced cobalt species re-oxidise may be lower than the rate of consumption of the oxygen species, which may inhibit conversions. This ties in with the rate of oxygen migration via the bulk titania lattice, to re-oxidise surface reduced species, based on the typical Mars- and van Krevelen redox cycle.

An additional factor put forward by Schmidt *et al.* [26] in their research into the activation of C5 and C6 alkanes over monolith catalysts, needs to be considered as a significant contributing factor. The size and steric bulk of the C8 linear alkanes, together with their increased concentration in the system, may contribute to significant site blockage and inhibition of conversion of the *n*-octane. Furthermore the steric bulk of alkenes, as well as the aromatic products, have to be taken into consideration in this regard as well, and cannot be dismissed as negligible.
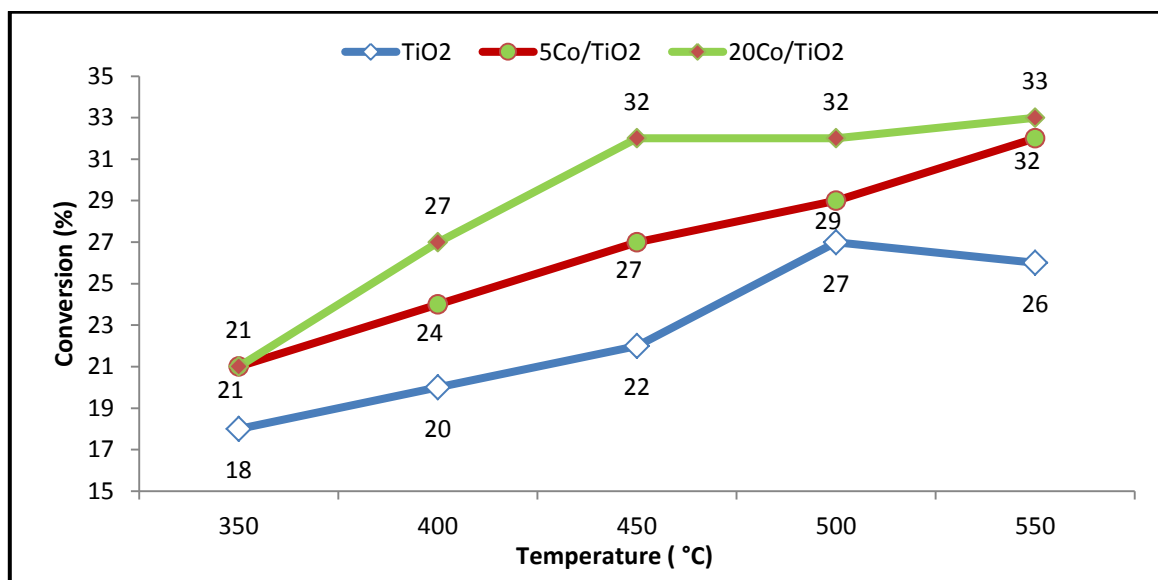

Figure 4.32: The summary of conversion for different cobalt content in the catalysts as a function of temperature

4.3.4. The influence of the oxidative environment on the conversion of *n*-octane and the product profile

Testing was carried out on the 5Co/TiO$_2$ catalyst under varied oxidative environments to investigate the effect on conversions and the product profile. Three different ratios were investigated: 8C:4O, 8C:2O and 8C:0O with the last ratio being non-oxidative (anaerobic) dehydrogenation testing. A further comparison was carried out with the 5Co/TiO$_2$ and 10Co/TiO$_2$ catalysts, to examine the influence of the richer oxidative environment with a doubling of the cobalt content.

4.3.4.1. Testing of the 5Co/TiO$_2$ catalyst in 8C:2O and 8C:4O oxidative environments

From the octenes breakdown in Figure 4.33, it is evident that when the 5Co/TiO$_2$ catalyst was run under two different oxidative environments, the oxygen leaner environment produced significantly higher selectivities to octenes than the oxidatively richer environment, across all temperatures investigated, with the biggest difference (17 %) being observed at 450 °C. The reason for the high octene selectivity is better understood in the context of aromatics and COx breakdowns shown in Figures 4.34 and 4.35 respectively.

Selectivity to octenes for the 5Co/TiO$_2$ catalyst increased with an increase in temperature up to 450 °C and decreased marginally at 500 °C and significantly so at 550 °C. The trend observed for the octenes in the oxidatively richer environment, showed a near plateau from 350 °C to 500 °C, with a slight increase at 550 °C.
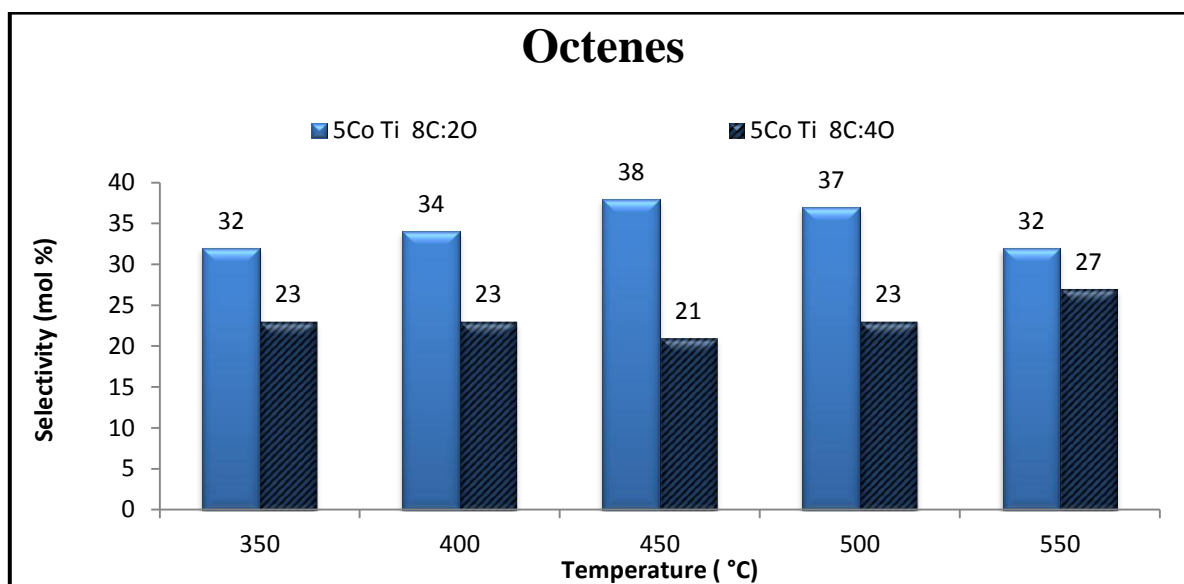
Figure 4.33: The summary of octenes selectivity in relation to oxidative environments as a function of temperature

The higher octenes selectivity is simultaneously accompanied by lower aromatics and COx formation in the oxygen leaner environment. The oxidatively richer environment thus drives enhanced aromatics and COx formation at the expense of octenes. The dehydrocyclisation pathway consumes more oxygen and is better propagated in an environment that is more

abundant in oxygen species. This may be related to the rate at which the reduced catalyst is re-oxidised in the presence of a higher concentration of gaseous oxygen species.
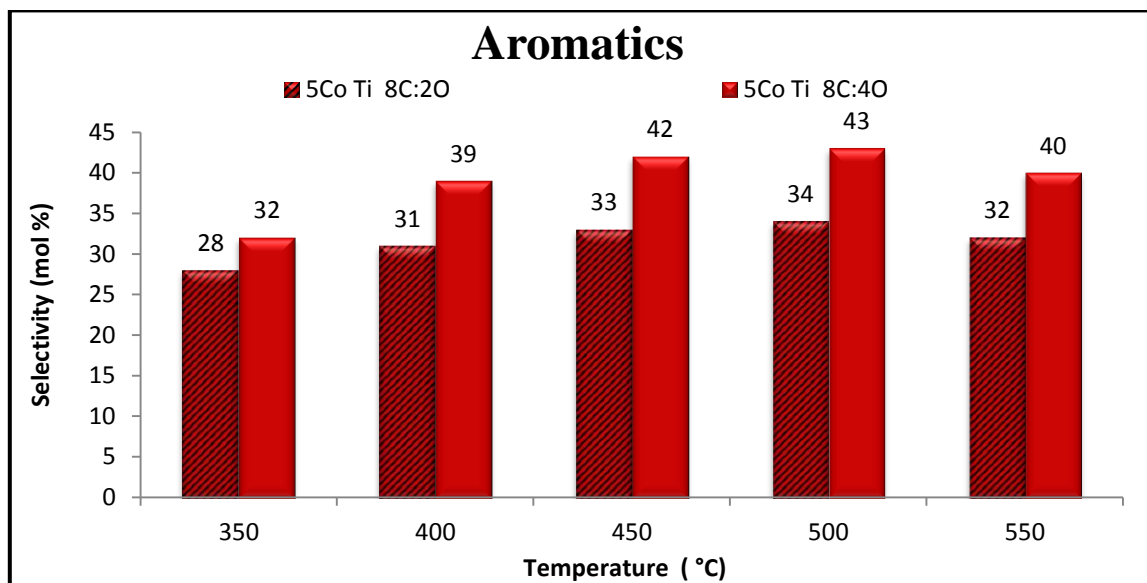
Figure 4.34: The summary of aromatics selectivity in relation to oxidative environments as a function of temperature

The COx breakdown in Figure 4.34 reveals the general trend of decreasing COx formation with an increase in temperature irrespective of cobalt content or the nature of the oxidative environment. The leaner oxidative environment promoted lower COx formation. Carbon dioxide was the dominant COx product. Overall results show a higher CO_2 / CO ratio being promoted by the oxygen richer environment, with this environment favouring deep oxidation over partial oxidation to a much greater extent than in the leaner environment.
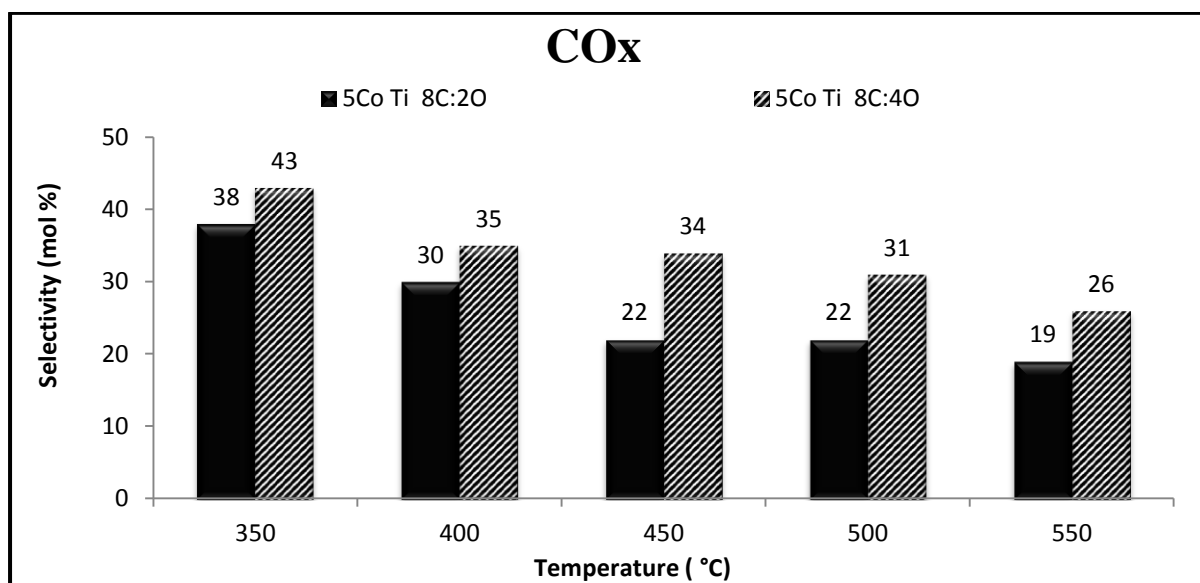
Figure 4.35: The summary of COx selectivity in relation to oxidative environments as a function of temperature

4.3.4.2. The influence of cobalt content on the conversion of *n*-octane and the product profile, in an oxidatively richer environment.

When catalytic testing was carried out in an oxidatively richer environment, with the doubling of the cobalt content from 5 % to 10 %, the results in Figures 4.36 reflect that the octenes selectivities are higher with higher cobalt content in the catalyst, which corresponds with the results from the testing of the $5Co/TiO_2$ and $20Co/TiO_2$ catalysts in the oxygen leaner environment. The selectivities to octenes over the $5Co/TiO_2$ catalysts in this oxidative environment were fairly constant up to 500 °C, with a slight increase at 550 °C. The results for the $10Co/TiO_2$ catalyst, however, showed the highest octene selectivity at 350 °C, but this decreased at 400 °C and remained fairly constant up to 550 °C. No variation in the product profile was observed in the different oxidative environments.

Figure 4.36: The summary of octenes selectivity in relation to cobalt content in a richer oxidative environment as a function of temperature

The aromatics selectivity (Figure 4.37), across all temperatures investigated, was lower over the higher loaded cobalt catalyst. The selectivities to aromatics increased up to 450 °C, remained constant until 500 °C, followed by a decrease at 550 °C for the $10Co/TiO_2$ catalyst. The trend that was observed for aromatics formation over the $5Co/TiO_2$ catalyst, in the richer oxidative environment, was an increase in selectivity from 350 °C to 500 °C, with a slight decrease at 550 °C. The most significant increase (7 %) in selectivity, was observed at 400 °C, over the $5Co/TiO_2$ catalyst.
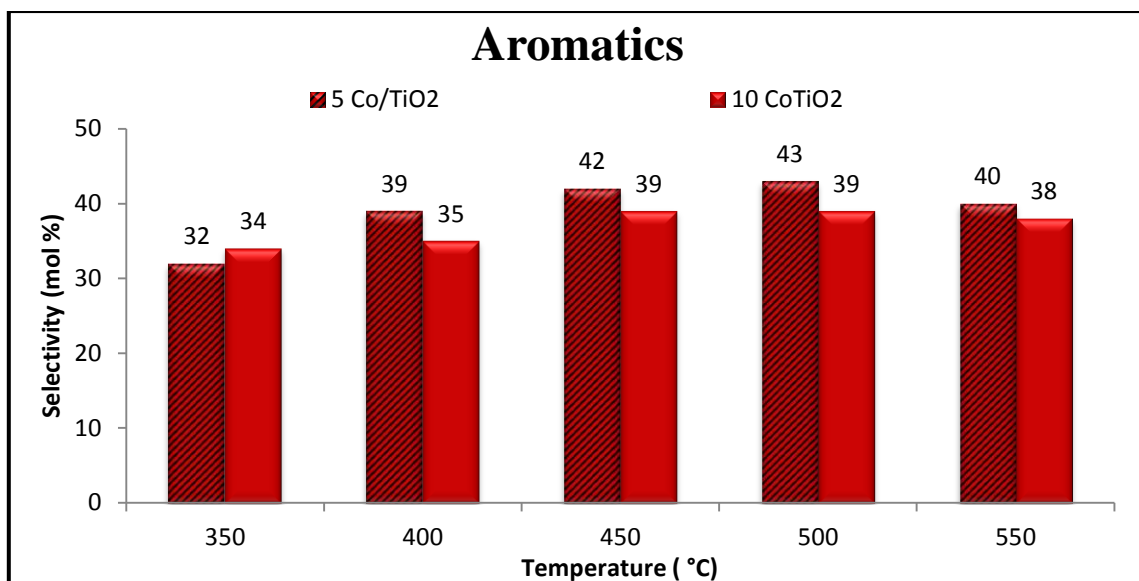
Figure 4.37: The summary of aromatics selectivity in relation to cobalt content in a richer oxidative environment as a function of temperature

The results in Figure 4.38 show that lower COx formation results from the higher cobalt content in the catalyst. This trend was observed across all temperatures investigated. This is again consistent with results from testing in the leaner oxidative environment shown in Figure 4.31. The difference, however, was marginal in the leaner oxidative environment and more significant in the 8C:4O environment.
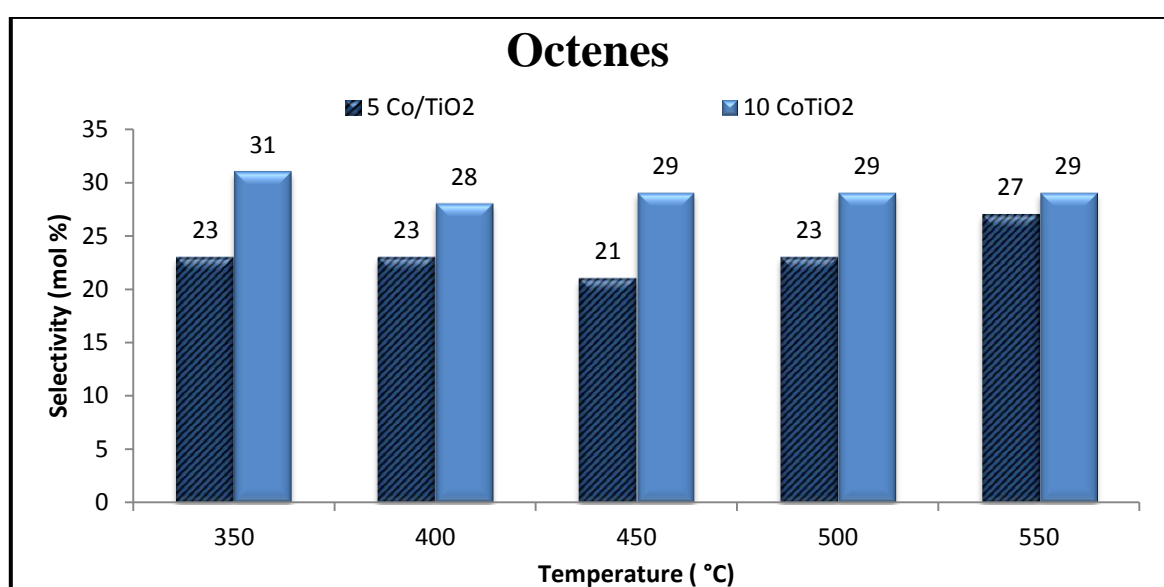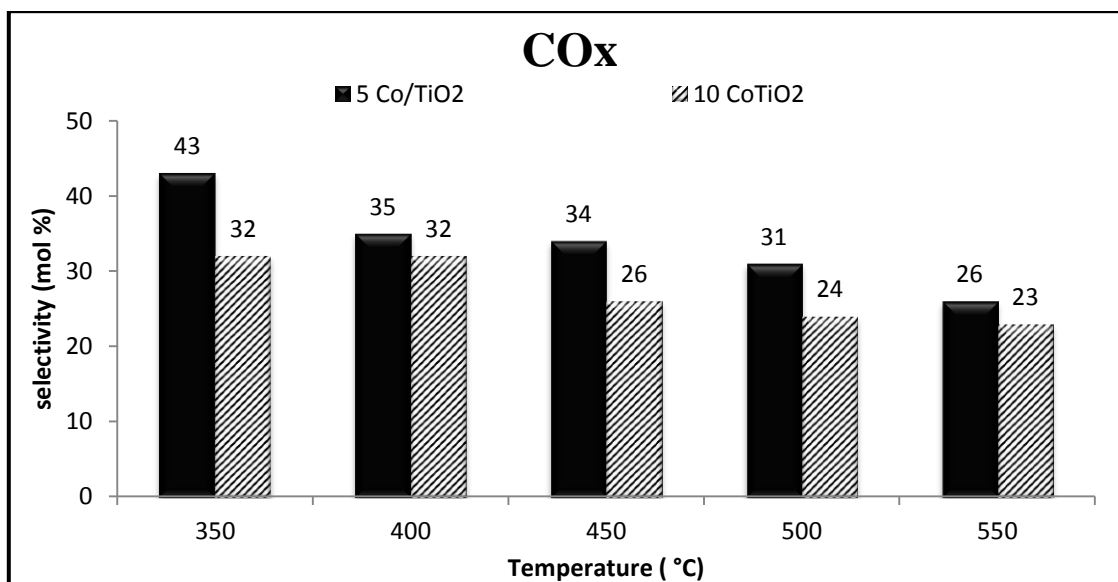

Figure 4.38: The summary of COx selectivity in relation to cobalt content in a richer oxidative environment as a function of temperature

Examination of the results in Figure 4.39, show that the conversion of *n*-octane in an oxygen leaner environment (8C:2O) was significantly lower than in the oxidatively richer environment (8C:4O) when the cobalt content was kept constant (5%). In the oxidatively richer environment, the difference in conversions between the 5 % and 10 % cobalt content catalysts was marginally higher with the doubling in cobalt content. Hence, it is quite apparent that doubling the cobalt content had less of an impact on conversions than doubling of the oxygen to hydrocarbon ratio. These results show that richer oxidative environments promote greater conversion of the *n*-octane.
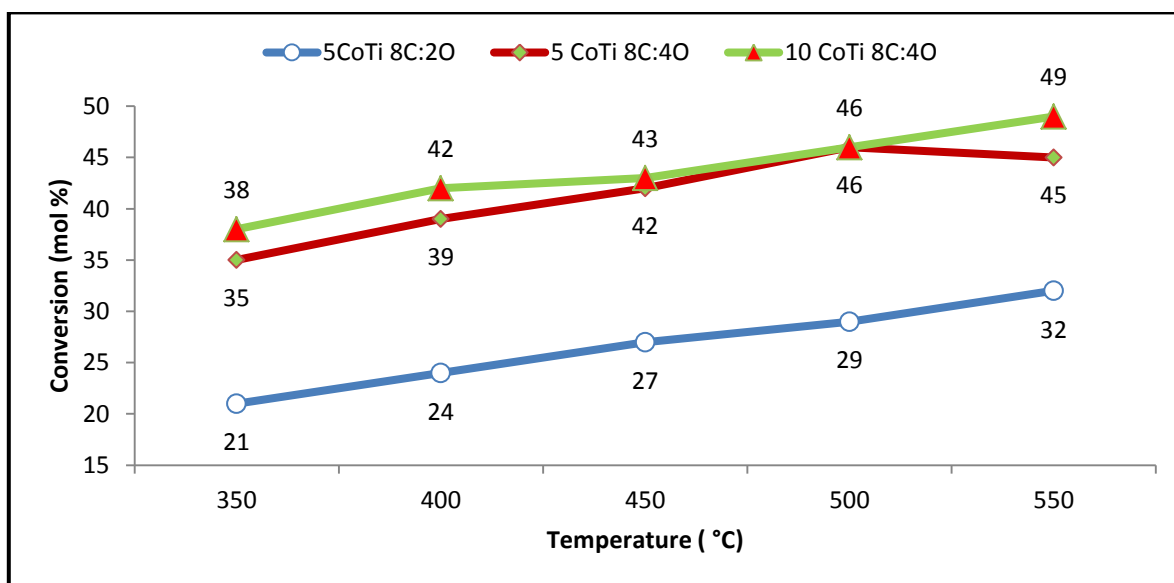
Figure 4.39: The summary of conversion for different cobalt content in the catalysts in varied oxidative environments as a function of temperature

The oxygen conversions, shown in Figure 4.40, steadily increase with temperature from 36 % to 52 % for the $5Co/TiO_2$ catalyst. The $10Co/TiO_2$ catalyst shows a constant oxygen conversion of 35 % from 350-400 °C, but increases thereafter up to 550 °C to reach a maximum of 49 %. The dehydrogenation of *n*-octane proceeds oxidatively, as assumed, under these reaction conditions. Excess (unconverted) oxygen exists in both these cobalt titania systems using the 8C:4O ratio.
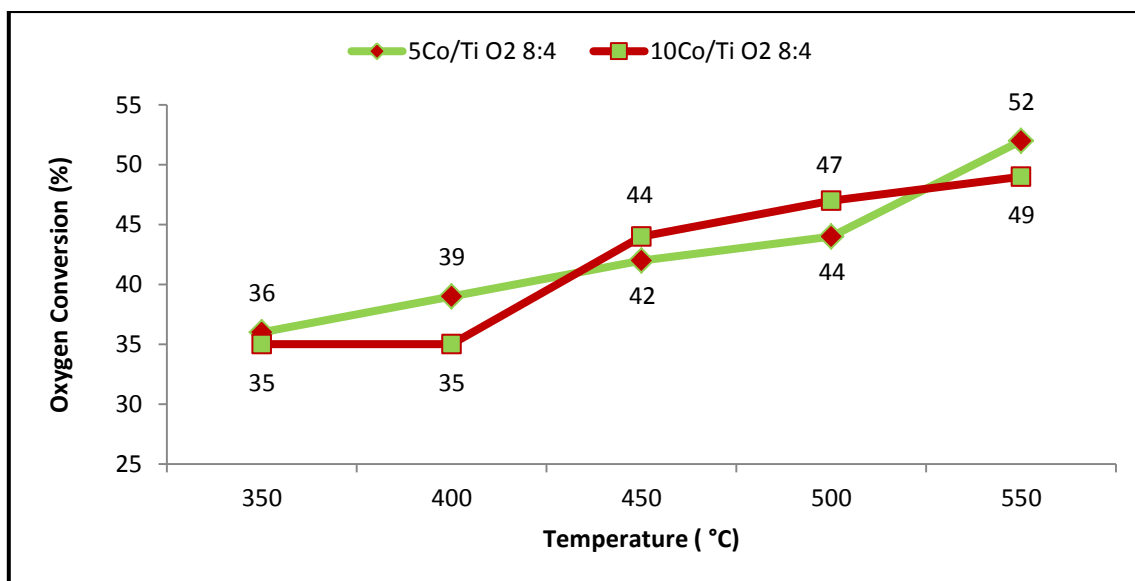
Figure 4.40: The summary of oxygen conversion for different cobalt content in the catalysts in a 8C:4O environment, as a function of temperature

4.3.4.3. Anaerobic testing of the 5CoTiO₂ catalyst

Anaerobic testing carried out in three separate runs did not yield results that were reproducible. In the initial run carried out, as it evident from the data in Table 4.6, conversion of *n*-octane occurred from 400 °C onwards. The trend observed was increased octenes selectivity with an increase in temperature except for 550 °C when the selectivity decreased. The opposite trend was observed for aromatics formation. This may be related to the increased oxygen depletion of the lattice over time. Dehydrogenation of *n*-octane to the octene involves less oxygen consumption than the dehydrocyclisation to the aromatic compounds. Therefore the available oxygen species are preferentially being consumed in octene formation over aromatics formation. o-Xylene was the only aromatic and trans-2-octene the only octene isomer formed at 400 °C.

Table 4.6: The product profile from the initial dehydrogenation catalytic testing of the 5Co/TiO₂ catalyst

Products	Catalytic Run 1			
	Temperature (°C)			
	400	450	500	550
Octenes	46	69	81	75
Aromatics	54	31	18	17
Cracked	0	0	0	1
Others	0	0	1	6
Conversion	5	6	6	8

In repeat runs, catalytic runs 2 and 3, no conversion of *n*-octane occurred at 400 °C and conversion occurred at 450 °C onward, at low conversions, as is evident in Table 4.7. No

reproducibility of results is evident in these two runs at 450 °C. The product profile is, however, dominated by octenes and aromatics, as it was in the first catalytic run, with varying selectivites with an increase in temperature.

Table 4.7: The product profile from the second and third dehydrogenation catalytic testing runs over the 5 Co/TiO$_2$ catalyst

Products	Catalytic Run 2			Catalytic Run 3		
	Temperature (°C)					
	450	500	550	450	500	550
Octenes	77	94	85	0	88	83
Aromatics	23	6	14	100	12	14
Others	0	0	1	0	0	3
Conversion	5	6	8	5	6	7

From the three catalytic runs carried out for the dehydrogenation reactions, the results at 500 °C and 550 °C appear moderately consistent in terms of octenes and aromatics selectivities. Octene selectivity at 550 °C was consistently lower than at 500 °C. 2-octenes (trans-2-octene and cis+trans-2-octene) were the dominant isomers across all temperatures, and a significant amount of 4-octenes (trans and cis-4-octene) were also produced. Ethylbenzene and xylene were the dominant aromatics that were formed. Overall the conversions were consistent from 450 °C–550 °C.

The catalytic testing procedures for the dehydrogenation reactions were kept the same as those adopted for the ODH reactions, but in retrospect, this was not conducive to obtaining reproducible or accurate results. The procedure should have been adapted to suit the anaerobic testing. Within the two hour equilibration time (as outlined in the procedure in Chapter 3) the surface cobalt oxide species would have already been stripped of some of the oxygen species required in the ODH reaction and a fair amount of oxygen depletion would have occurred before any samples were drawn for testing. Thus, this experiment needs to be revisited. Since the dehydrogenation testing was not the primary focus of this Masters research effort, an in-depth study of anaerobic testing, together with isothermal time on stream experiments, will be probed in the PhD study on the same catalytic system, which will follow upon completion of the MSc.

4.3.5. Yield of value added products (VAP) from the catalytic testing

Table 4.8: Summary of the yields for the value added products obtained from the catalytic testing of the titania and Co/TiO$_2$ catalysts

Catalyst	C:O ratio	Temperature (°C)				
		350	400	450	500	550
TiO$_2$	8C:2O	6	9	10	16	16
5Co/TiO$_2$	8C:2O	13	16	19	21	20
20Co/TiO$_2$	8C:2O	15	19	24	24	24
5Co/TiO$_2$	8C:4O	19	26	26	30	30
10Co/TiO$_2$	8C:4O	25	26	29	31	33

In this research effort, octenes and aromatics have formed the bulk of the value added products obtained from the oxidative activation of *n*-octane. The results obtained from the catalytic testing are shown in Table 4.5. It is evident from these results that the oxygen richer environment (8C:4O) with the 10 % cobalt loading, gave the highest yields of VAP, with the 5 % cobalt loading in the same environment yielding marginally lower results. Despite the significantly higher cobalt loading (20 %) in the oxidatively leaner environment, yields to the VAP were substantially lower (5-9 %) than the 10 % cobalt loaded catalyst in the oxygen richer environment.

4.3.6. An investigation into diffusion and mass transfer in the titania supported cobalt catalytic system

Two separate experiments were carried out to consider diffusion and mass transfer limitations. The 5Co/TiO$_2$ catalyst was firstly tested by holding all parameters the same as for all the other testing (GHSV of 4000 h^{-1}, flow rate of octane at 0.05 ml/min, catalyst bed of 1 ml) except for decreasing the pellet size from 600-1000 μm to 500-600 μm and secondly all parameters were held constant (600-1000 μm pellet size and a catalyst bed of 1 ml) while the GHSV was increased to 6000 h^{-1} by increasing the air, nitrogen and *n*-octane flow rates (outlined in detail in Chapter 3)

The two sets of results obtained in the catalytic testing of the 5Co/TiO$_2$ catalyst, with increased GHSV while maintaining the catalyst pellet size at 600-1000 μm and maintaining the GHSV at 4000 h^{-1} with the smaller pellet size, yielded very similar product profiles with minor variations in selectivity, comparable with the results obtained at a GHSV of 4000 h^{-1} and 600-1000 μm pellets. COx selectivities and conversions, however, were not comparable.
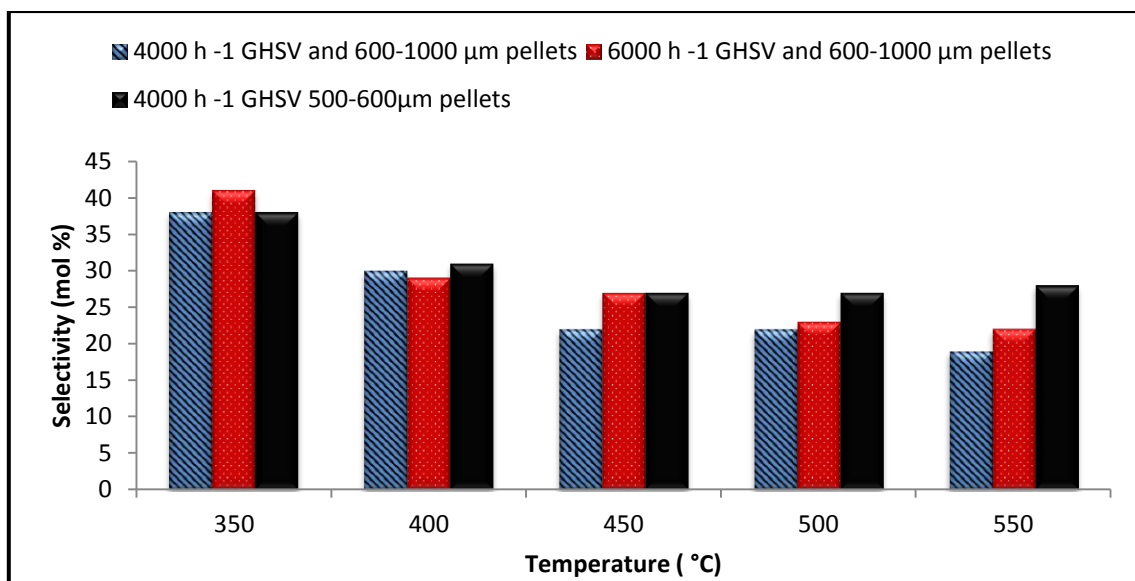
Figure 4.41: The summary of COx selectivity for the 5Co/TiO$_2$ catalyst at different GHSV and pellet size as a function of temperature

Some differences were observed when the data for COx formation was reviewed (Figure 4.41). The overall trend for COx formation showed decreased COx selectivity with an increase in temperature. With the smaller pellets, however, the COx formation plateaued from 450 °C onwards. Smaller pellet sizes will result in smaller interparticle voids, which may contribute to enhanced cracking, especially so at higher temperatures with the increased kinetic element, and hence the higher selectivity to COx products. At all temperatures, except 400 °C, the COx selectivities are marginally higher than with the lower GHSV. The reason may relate to higher GHSV's leading to shorter contact times of the reactant with the active site and thus a greater probability of reaction with radical oxygen species in the gas phase. These radical species are more reactive and promote enhanced COx formation [27].

The conversion results, however, show some differences (Figure 4.42). Uniformity (± 1 %) in conversion is only observed at 450 °C, independent of pellet size or GHSV variations. At 450 °C, factors other than pellet size and GHSV govern the dynamics around conversion. This temperature is the reduction temperature for the cobalt species from trivalency to divalency. At 350 °C and 400 °C, the conversions are ± 5 % lower when smaller sized pellets are used but at higher temperatures the conversions are only marginally lower. At 450 °C isothermal iso-conversions are observed for the catalysts with different pellet size as well as different GHSV. At 500 °C and 550 °C, however, variation in conversions becomes more pronounced with temperature, with the higher GHSV yielding increasingly lower conversions. Generally higher GHSV leads to lower conversions as a result of shorter contact times with higher flowrates. The difference in conversions based on pellet size is most pronounced at temperatures other than 450 °C, when smaller pellet size effects significantly lower conversions, implying that diffusion limitations exist.
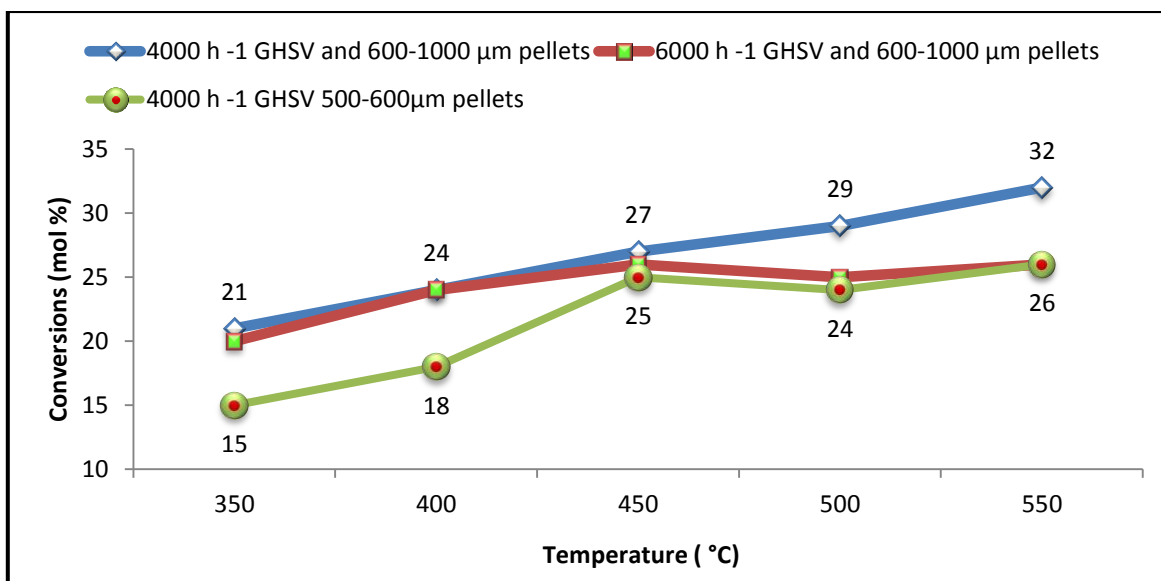
Figure 4.42: The summary of conversion for the $5Co/TiO_2$ catalyst at different GHSV and pellet size as a function of temperature

These results are indicative of diffusion limitations existing, that cannot entirely be neglected in this system. This suggests that the titania supported cobalt catalyst system, does not function exclusively under the kinetic domain.

Furthermore, these results also indicate that the 600-1000 µm pellet size and a GHSV of 4000 h^{-1} result in the best conversion with uniformity in the product profile. The bulk of the testing was carried out in this manner and these results confirm the suitability of that choice of parameters for catalytic testing.

4.3.7. Summary of the oxygen conversion using the leaner oxidative environment

The overall results for the oxygen conversion in Figure 4.43, under oxygen leaner conditions (8C:2O), show that they range between 30-70 % from 350 °C to 550 °C. These results support the assumption that the dehydrogenation of *n*-octane occurs oxidatively over the cobalt titania catalysts.

The conversions for the supported catalysts displayed a very similar trend up to 500 °C. At 550 °C, however, the differences in conversion were more significant. Significantly lower results for the oxygen conversion over the titania support were obtained, especially at 350 °C (14 %), but increased considerably from 450 °C onwards. The low conversions for the support may be indicative of a homogeneously assisted transformation of *n*-octane to carbon oxides and octenes, especially at lower temperatures, which becomes less significant with an increase in temperature.
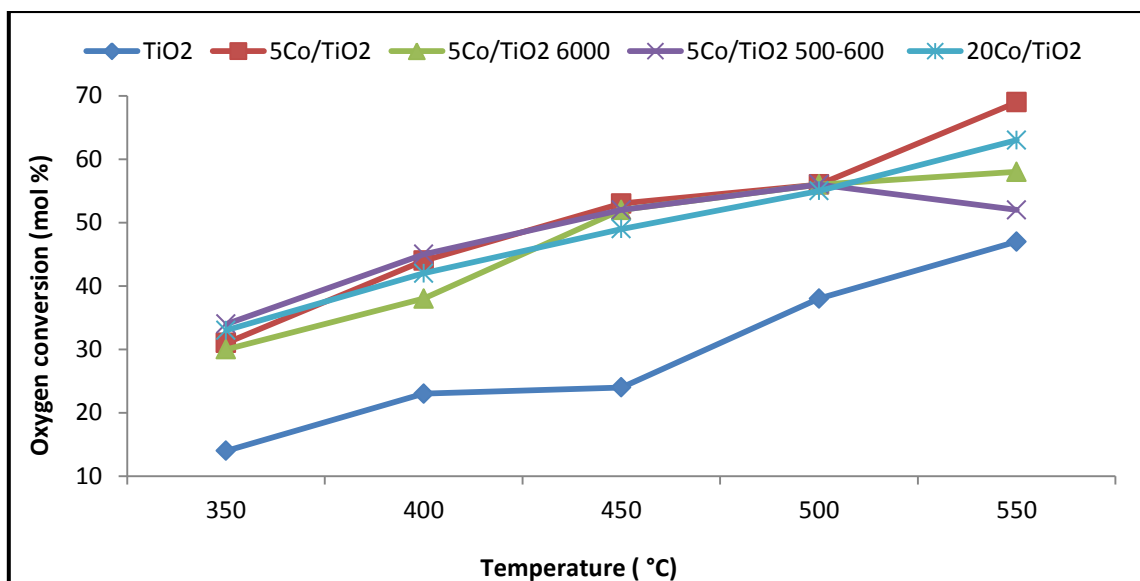
Figure 4.43: The summary of oxygen conversion over the support and Co/TiO$_2$ catalysts at a 8C:2O ratio

4.3.8. Summary of the oxidative transformation of *n*-octane

In summarising the ODH function of the titania supported cobalt catalysts, Figure 4.44 provides an overview of the proposed stepwise transformation of *n*-octane to value added products and COx products, within the temperature range of 350–550 °C, employing the reaction conditions outlined in this thesis.
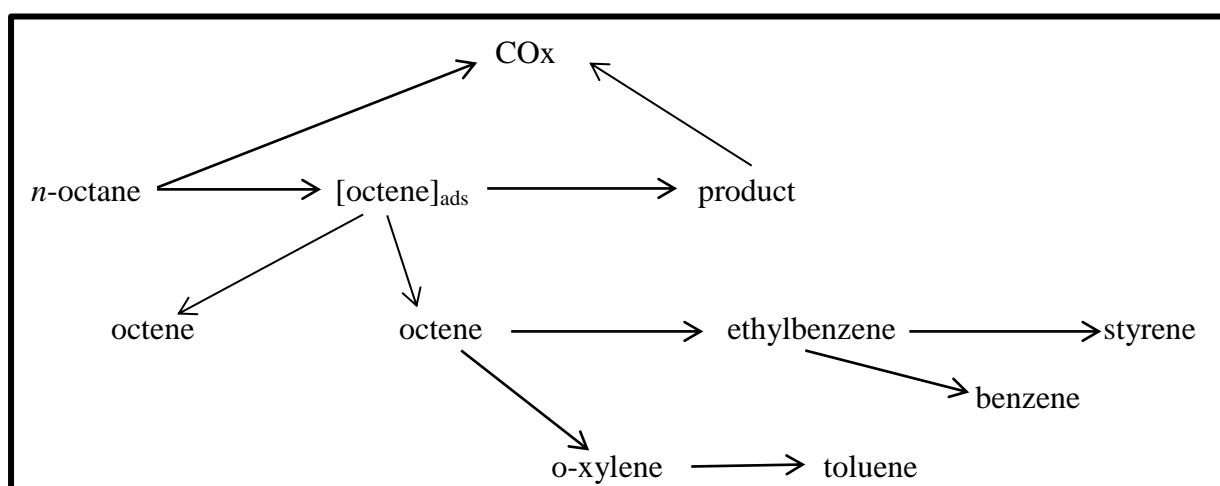
Figure 4.44: The overview of the transformation of *n*-octane to products over the titania supported cobalt catalysts

References

[1]   Y. Brik, M. Kacimi, M. Ziyad, F. Bozon-Verdura, Journal of Catalysis. 202 (2001) 118-128.

[2]   J.M. Lopez Nieto, A. Corma, N. Paredes, M. Perez, Y. Shen, H. Cao, S.L. Suib, Studies in Surface Science and Catalysis. 72 (1992) 213-220.

[3]   M.M. Yung, E.M. Holmgreen, U.S. Ozkan, Journal of Catalysis. 247 (2007) 356-367.

[4]   J.W. Niemantsverdriet, Spectroscopy in Catalysis: An Introduction, Wiley-VCH, Weinheim, 2007.

[5]   B. Gates, Catalytic Chemistry, Wiley, New York, 1992.

[6]   M. Rayner, PhD Thesis, University of Witswatersrand, 2011.

[7]   M. Che, J.C. Vedrine (Eds.), Characterisation of Solid Materials and Heterogeneous Catalysts, Wiley VCH, Weinheim, 2012.

[8]   M. Vob, D. Borgmann, G. Wedler, Journal of Catalysis. 212 (2002) 10-21.

[9]   B. Pillay, M.R. Mathebula, H.B. Friedrich, Catalysis Letters. 141 (2011) 1297-1304.

[10]   P.M. Shreekanth, D.A. Pena, P.G. Smirniotis, Industrial and Engineering Chemistry Research. 45 (2006) 6444-6449.

[11]   T. Xiao, S. Ji, H. Wang, K.S. Coleman, M.L.H. Green, Journal of Molecular Catalysis A: Chemical. 175 (2001) 111-123.

[12]   L. Backman, PhD Thesis, Helsinki University of Technology, 2009.

[13]   J. Li, G. Jacobs, T. Das, B.H. Davis, Applied Catalysis A : General. 233 (2002) 255-262.

[14]   S.L. Soled, E. Iglesia, R.A. Fiato, G.B. Ansell, European Patent 0 542 527 A1, 1992.

[15]   B. Jongsomjit, C. Sakdamnuson, J.G. Goodwin, P. Praserthdama, Catalysis Letters. 94 (2004) 209-215.

[16]   K. Takanabe, K. Nagaoka, K. Nariai, K. Aika, Journal of Catalysis. 232 (2005) 268-275.

[17]   E.A. Mamedov, V. Cortes Corberan, Applied Catalysis A : General. 127 (1995) 1-40.

[18]   Y. Brik, M. Kacimi, F. Bozon-Verdura, M. Ziyad, Journal of Catalysis. 211 (2002) 470-481.

[19]   L. Luciani, N. Ballarini, F. Cavani, C. Cortelli, Catalysis Today. 142 (2000) 132-137.

[20]   S. Jongpatiwut, P. Sackamduang, T. Rirksomboon, S. Osuwan, D. Resasco, Journal of Catalysis. 218 (2003) 1-11.

[21]   K. Jalama, N.J. Coville, D. Hildebrandt, D. Glasser, L.L. Jewell, J.A. Anderson, S. Taylor, D.I. Enache, G.J. Hutchings, Topics in Catalysis. 44 (2007) 129.

[22]   K. Jalama, J. Kabuba, H. Xiong, L.L. Jewell, Catalysis Communications. 17 (2012) 154-159.

[23]   A.Y. Khodakov, Catalysis Today. 144 (2009) 251-257.

[24]   J. Li, N.J. Coville, Applied Catalysis A: General. 181 (1999) 201-208.

[25]   K. Jalama, PhD Thesis, University of Witwatersrand, 2007.

[26]   A.G. Dietz, A.F. Carlsson, L.D. Schmidt, Journal of Catalysis. 176 (1996) 459.

[27]   M.J. Tiernan, E.A. Fesenko, P.A. Barnes, M. Ronane, G.M.B. Parkes, Thermochimica Acta. 379 (2001) 163-175.

Chapter Five

Summary & Conclusions

The Co/TiO$_2$ catalysts are suitable catalysts for the oxidative activation of *n*-octane in the temperature range of 350-550 ℃ under the oxidative environments and reaction conditions employed. This catalyst system is a strong candidate in oxidative dehydrogenation, favouring the dehydrogenation and dehydrocyclisation reaction pathways since the dominant valorised products observed in variable amounts were the octenes and aromatics. The maximum yield of value added products (octenes and aromatics), was obtained on the 10 Co/TiO2 catalyst at 550 ℃, using an 8C:4O ratio at a 4000 h^{-1} GHSV and 600-1000 µm pellet size.

The surface of the catalyst allows for the efficient redox cycle to propagate, increasingly so with an increase in temperature, with strong ODH characteristics. The bare titania support was not an inert support but displayed high activity in the ODH of *n*-octane. Activity is a strong function of the support.

The higher linear alkane, *n*-octane, upon dehydrogenation, does maintain the chain length without cracking, and proceeds to aromatise over this catalytic system under the reaction conditions employed. The TiO$_2$ support and the well dispersed Co$_3$O$_4$ may have a synergistic effect which leads to the high activity of the system in the oxidative dehydrogenation of *n*-octane.

The *n*-octane to oxygen molar ratios have a greater impact on catalyst performance than cobalt content or GHSV's tested. This catalytic system, probing the oxidative activation of *n*-octane, does not favour partial oxidation, as oxygen insertion, as it shows poor tendency to form oxygenated valorised products such as alcohols and ketones. The titania supported cobalt catalyst system either does not furnish the oxygen species that insert into the reactant molecule, to produce valorised oxygenated products or they are formed and are further oxidised rapidly to carbon oxides. The higher selectivity of carbon oxides at lower temperatures are suggestive of acidic products forming, having longer contact times with the basic catalyst surface and subsequently leading to cracking, with further oxidation to carbon oxides. This is suggested or inferred from analysis of the product distribution, but cannot be conclusively proven since it was not directly observed.

Carbon oxides are the undesirable products in this research effort, but in an industrial context, however, the COx products have a role to play. Amongst others CO makes a contribution in the Fischer-Tropsch process and water-gas shift reaction while CO$_2$ is used in ethane and ethylbenzene ODH as a mild oxidant in oxidation catalysis.

Two key challenges were identified that warrant further investigation. Firstly, the non-oxidative dehydrogenation testing parameters require optimisation and secondly, stopping the

reactions at the intermediate stage to inhibit COx formation or to minimise selectivities to the carbon oxides requires further investigation.

The formation of the aromatics through the dehydrocyclisation mechanism may have been facilitated by the interaction of the large *n*-octane molecule and simultaneous hydrogen abstractions over the large clustered Co_3O_4 molecule.

Titania has been found to be in the anatase phase and the cobalt exists as a crystalline Co_3O_4 phase supported on the titania. The material has high thermal stability with minimal decomposition up to 1000 °C and is mesoporous with medium surface area. The surface is enriched in Co_3O_4 species. The cobalt species are fairly well dispersed on the surface, but some aggregation occurs in the higher cobalt loaded catalysts. The onset of reduction of the cobalt oxide trivalent species to the divalent species, occurs around 350 °C to maximise around 450 °C. The surface of the catalysts have strong basic character that promotes the desorption of alkenes and aromatics.

Appendix A

PXRD diffractogram

(a)Titania support and (b) 5 Co/TiO2
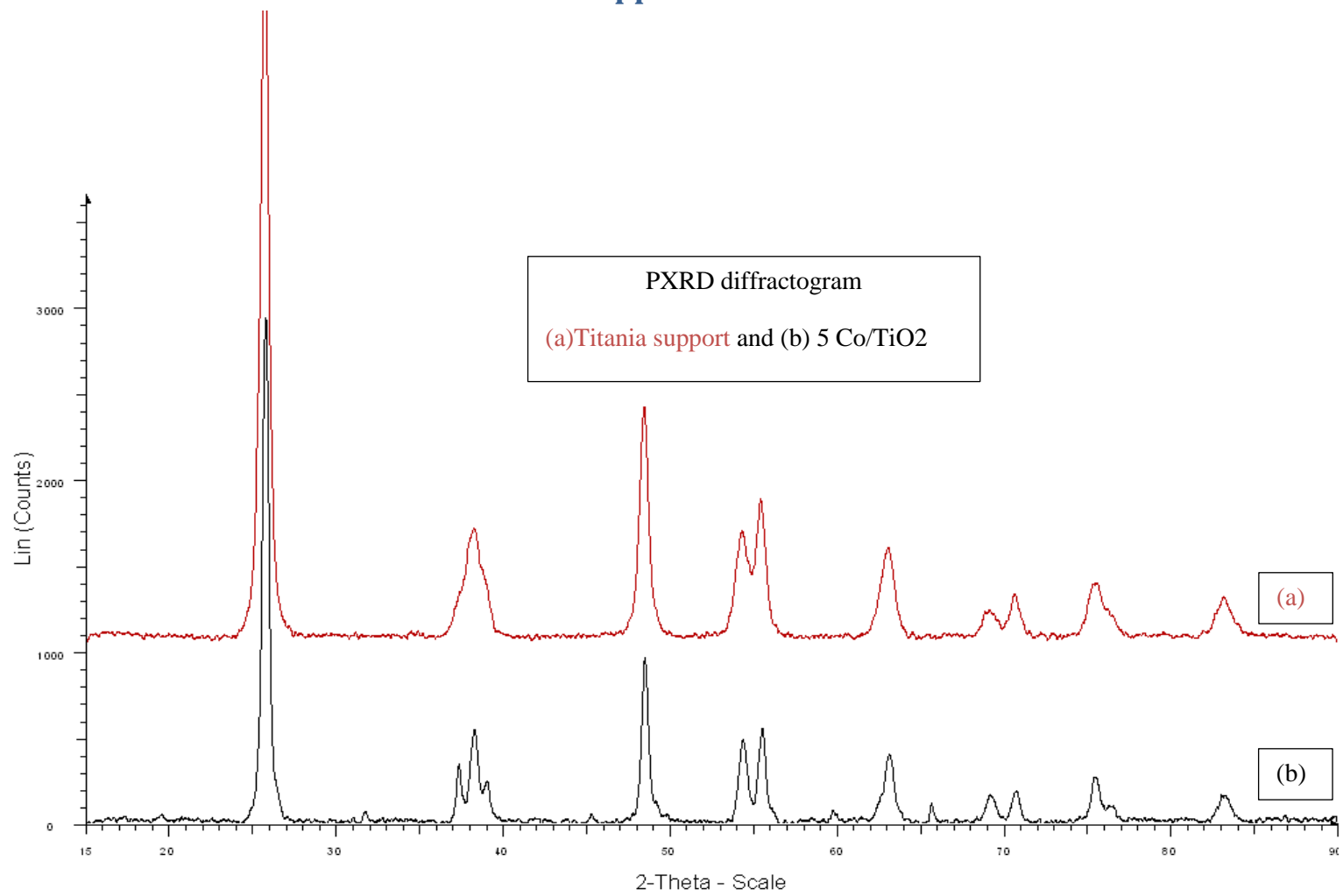
PXRD diffractogram

20 Co/TiO$_2$
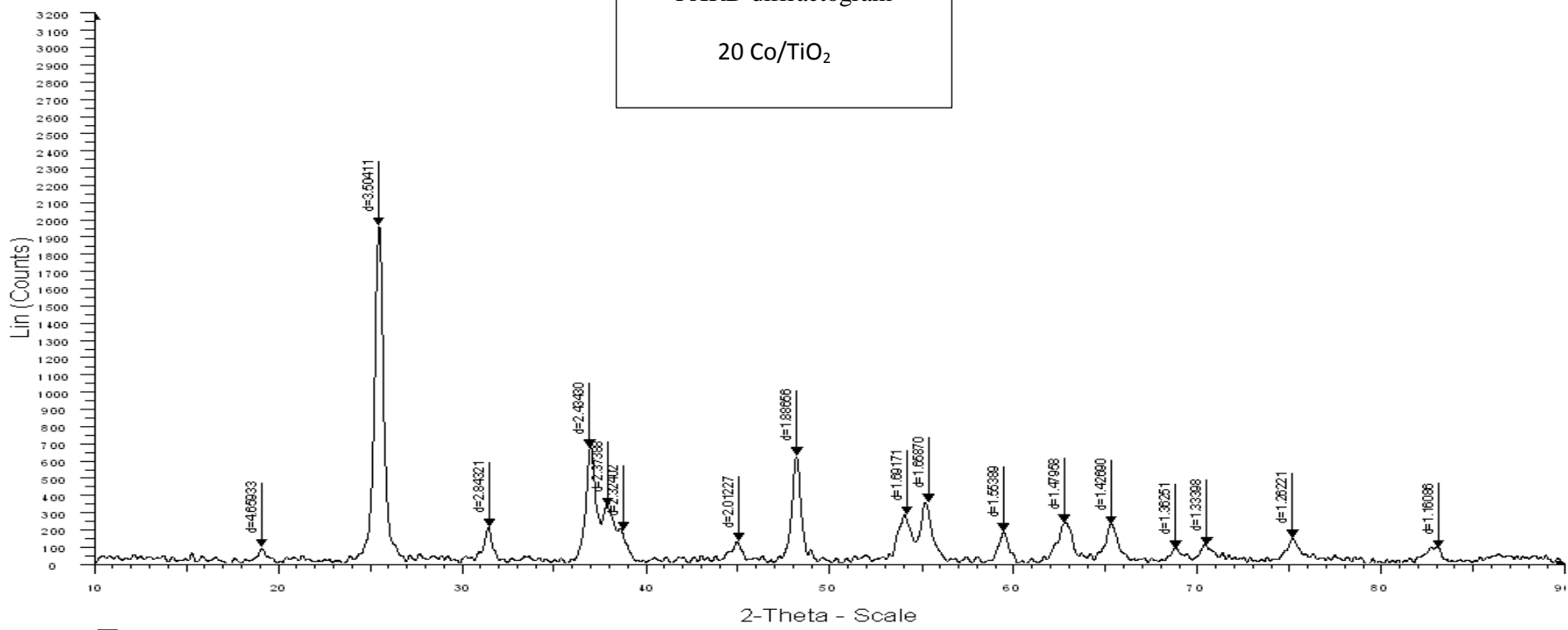
TGA 10Co/TiO$_2$ spent 1:2

70.86°C

1.084%
(0.1041mg)

578.82°C

0.09721%
(0.009336mg)

205.18°C

521.26°C
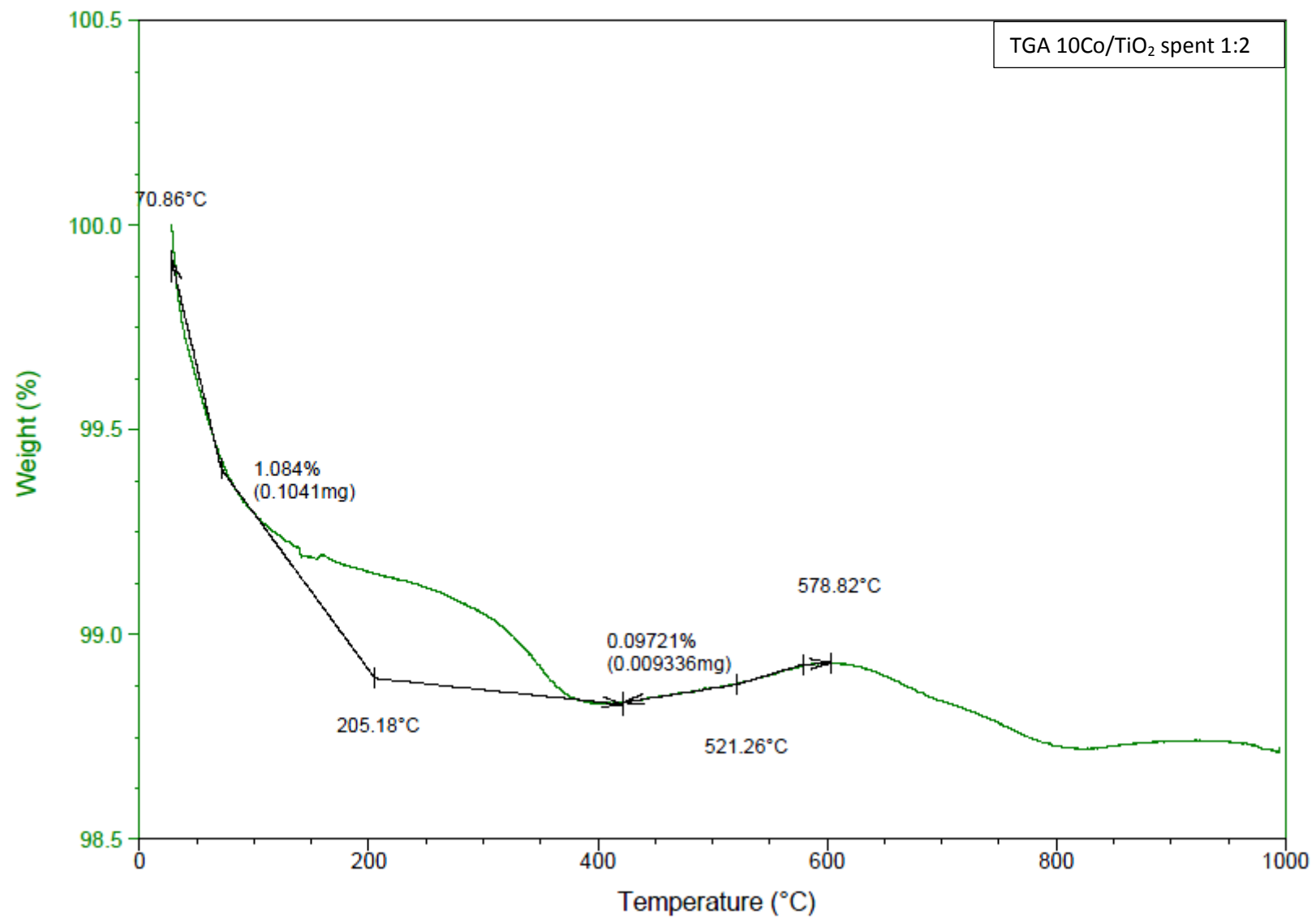
Rotameters (early stages of reactor building)

Bronkhorst Mass Flow controllers for Nitrogen & Air

n-octane feed on OHAUS balance

LabAlliance Series II HPLC pump

Heating block

Reactor tube & Carborundum

Wet Gas Flowmeter

Gas Chromatograph

Copy of Spreadsheet

5CoTiO2

8C: 2O

GHSV 6000

Date 16/05/2013

GHSV	**6000**	**6000**	**6000**	**6000**	**6000**
Time(hour)	**1**	**1**	**1**	**1**	**1**
Temperature(bed)	350	400	450	500	550
Mass of octane(initial)	2.44	2.43	2.44	2.41	2.37
Mass of octane (final)	0	0	0	0	0
Mass of Octane in	2.44	2.43	2.44	2.41	2.37
Moles of Octane in	0.02136041	0.021272871	0.021360413	0.021097785	0.020747614
Moles of carbon in	0.17088331	0.170182964	0.170883306	0.168782281	0.165980916
Out gas (initial)	24820.31	24827.6	24835.27	24846	24853.13
Out gas (final)	24826.48	24833.75	24841.55	24852.22	24859.25
Out gas flow(L)	6.17	6.15	6.28	6.22	6.12
out gas flow(ml)	6170	6150	6280	6220	6120
Total mass of liquid	2.2953	2.345	2.3081	2.2891	2.2487
Mass of Organic layer	2.0277	1.9302	1.9351	1.9447	1.8999
Mass of Aqueous layer	0.2676	0.4148	0.373	0.3444	0.3488
% of water in Organic	0	0	0	0	0
% of water in Aqeous	0	0	0	0	0
Actual mass of organic	2.0277	1.9302	1.9351	1.9447	1.8999
Actual mass of aqeous	0.2676	0.4148	0.373	0.3444	0.3488
moles of water	0.01486667	0.023044444	0.020722222	0.019133333	0.019377778
Conversion :					
Moles of Octane in	0.02136041	0.021272871	0.021360413	0.021097785	0.020747614
Moles of Octane out	0.0172542	0.0162008	0.0159771	0.0159150	0.0154767
Conversion (%)	19.2236739	23.84278283	25.20212302	24.56566579	25.4049004
Norm Conv (%)	20.0396939	24.29812076	26.09512667	25.33417923	26.21991306
Carbon balance:					
Moles of Carbon in	0.17088331	0.170182964	0.170883306	0.168782281	0.165980916
Moles of Carbon out	0.16392491	0.166993797	0.165035493	0.163662263	0.16082161
Carbon balance	95.9279817	98.12603645	96.57789113	96.96649563	96.89162713
Temperature	350	400	450	500	550
O2 conversion	30.01	38.32	52.37	56.51	58.37

Selectivity of Product	350	400	450	500	550
Ethylene	0.00	0.00	0.00	0.00	0.00
Ethane	0.00	0.00	0.00	0.00	0.00
Butane	0.00	0.00	0.00	0.00	0.00
Propene/propylene	0.00	0.00	0.00	0.00	0.00
Propane	0.00	0.00	0.00	0.00	0.00
Methane	0.00	0.00	0.00	0.00	0.00
n-octane	1930.40	1552.04	1150.52	1042.85	984.20
Benzene	3.01	3.69	3.37	2.77	2.63
Toluene	0.00	0.00	0.00	0.00	0.00
1-octene	0.00	0.00	2.49	3.46	3.72
trans-2-octene	13.95	14.23	13.03	14.13	13.86
2-octene, cis + trans	6.53	6.57	6.36	6.88	7.03
trans-3-octene	0.00	0.00	0.00	0.00	0.00
trans-4-octene	10.20	10.49	9.48	10.30	10.22
cis-4-octene	4.22	4.41	3.92	4.19	4.16
Ethylbenzene	6.18	11.12	12.63	13.09	13.97
Styrene	12.37	17.10	17.63	16.86	15.47
o-xylene	2.05	3.05	3.57	3.70	4.61
Cracked (RT >10)	0.00	0.01	0.02	0.38	1.03
Others(RT = 12-22)	0.00	0.00	0.90	0.83	1.01
Oxygenates(RT=20-27)	0.00	0.00	0.00	0.00	0.00
heavys(RT > 27)	0.00	0.00	0.00	0.00	0.00
impurites	0.00	0.00	0.00	0.00	0.00
CO	9.68	7.15	6.35	5.56	4.80
CO2	31.81	22.19	20.26	17.85	17.48
Total	100.00	100.00	100.00	100.00	100.00

Calibration factors

Product	Carbon Number	Molar mass	Density	RRF
n-octane	8	114.23	0.703	1
Benzene	6	78.11	0.87	0.8525
Toluene	7	92.14	0.87	0.8514
1-octene	8	112.22	0.715	0.78694
trans-2-octene	8	112.22	0.715	1.05192
2-octene, cis+ trans	8	112.22	0.715	0.91459
trans-3-octene	8	112.22	0.716	1.08287
trans-4-octene	8	112.22	0.714	0.58158
cis-4-octene	8	112.22		0.57439
2-octanone	8	128.23	0.8202	0.62071
3-octanone	8	128.23	0.821	1.05209
ethylbenzene	8	106.16	0.8665	0.95481
styrene	8	104.19	0.909	0.62581
o-xylene	8	106.16		0.86337
1-heptanol	7	116.2	0.8187	1.17325
Cracked (RT >10)	8	75		1
Others(RT = 12-22)	8	110		1
Oxygenates(RT 20-27	8	128		0.9
heavys(RT > 27)	8	140		0.8
impurites	8	114		1

Calibration factors GAS

Product	Carbon No	Gradient from Calibration curve
Ethylene	2	1.79E+15
Ethane	2	4.31E+13
Butane	4	2.07E+15
Propene/propylene	3	2.16E+14
Propane	3	1.92E+14
Methane	1	4.73E+14
Benzene	6	5.63E+14
Toluene	7	4.96E+14
n-octane	8	4.93E+14
1-octene	8	6.22E+14
trans-2-octene	8	4.77E+14
2-octene, cis+ trans	8	5.29E+14
trans-3-octene	8	6.22E+14
trans-4-octene	8	8.54E+14
cis-4-octene	8	8.57E+14
2-octanone	8	8.28E+14
3-octanone	8	7.23E+14
ethylbenzene	8	6.11E+14
styrene	8	1.01E+15
o-xylene	8	6.70E+14
1-heptanol	7	4.49E+14
Cracked (RT >10)	8	4.93E+14
Others(RT = 12-22)	8	4.93E+14
Oxygenates(RT 20-27)	8	4.93E+14
heavys(RT > 27)	8	4.93E+14
impurites	8	4.93E+14
CO	1	2.90E+11
CO_2	1	3.36E+11

GHSV

Flow rate of octane	0.06
Density of octane (g / ml)	0.703
Molar mass of octane g.mol^{-1}	112.224
Universal gas Constant R	0.08206
Temperature(k)	298
Pressure (Atm)	1
Mass of Octane	0.04218
Moles of Octane	0.00038
Volume of Octane (mls/min)	9.19112
hydrocarbon :oxygen	1
Moles of oxygen	0.00038
volume of oxygen(mls/min)	9.19112
Moles of air	0.00179
volume of air (mls/min)	43.7673
GHSV(hr^{-1})	**6046.14**
volume of Catalyst (mls)	1
Total gaseous feed (ml/min)	100.769
Volume of Nitrogen (from air) (mls/min)	34.5761
Volume of Nitrogen (individually)	57
Total Volume of Nitrogen (mls/min)	91.5761
Fuel : Total feed ratio	9.12098
fuel : air ratio	21

Oxygen Balances

Moles of oxygen/min	0.00038	0.00038	0.00038	0.00038	0.00038
Moles of oxygen(O2)/hr	0.0228	0.0228	0.0228	0.0228	0.0228
Moles of oxygen(O)/hr (in)	0.0456	0.0456	0.0456	0.0456	0.0456
Temp	**350**	**400**	**450**	**500**	**550**
Ethylene	0	0	0	0	0
Ethane	0	0	0	0	0
Butane	9.5097E-08	1.8552E-07	3.769E-07	5.3616E-07	6.549E-07
Propene/propylene	0	0	0	0	0
Propane	0	0	0	0	0
Methane	0	0	0	0	0
n-octane	0.41409977	0.38881983	0.38345125	0.38195937	0.3714409
Benzene	0.00064464	0.00092381	0.00112403	0.0010151	0.0009921
Toluene	0	0	0	0	0
1-octene	0	0	0.00027616	0.00042273	0.0004676
trans-2-octene	0.00099732	0.00118792	0.00144704	0.00172494	0.0017442
2-octene, cis+ trans	0.00046691	0.0005483	0.00070609	0.00084038	0.0008846
trans-3-octene	0	0	0	0	0
trans-4-octene	0.00072955	0.0008757	0.00105311	0.00125788	0.0012858
cis-4-octene	0.00030161	0.00036837	0.00043538	0.00051154	0.0005238
ethylbenzene	0.00132498	0.00278619	0.00420779	0.004794	0.0052717
styrene	0.00353938	0.00571357	0.00783406	0.0082325	0.0077862
o-xylene	0.0004393	0.00076345	0.00119141	0.00135466	0.0017403
Cracked (RT >10)	5.6974E-07	2.1261E-06	6.8568E-06	0.00013937	0.0003885
Others(RT = 12-22)	0	0	0.00030073	0.00030285	0.0003806
Oxygenates(RT= 20-27)	0	0	0	0	0
heavys(RT > 27)	0	0	0	0	0
impurites	0	0	0	0	0
CO	0.00069247	0.00059679	0.00070506	0.00067836	0.0006044
CO2	0.00454922	0.00370671	0.00450215	0.0043587	0.0043971
Total	0.01368605	0.01747312	0.02379024	0.02563353	0.0264675
Moles of oxygen (out)	0.03191395	0.02812688	0.02180976	0.01996647	0.0191325
Oxygen Conversion	**30.013263**	**38.318254**	**52.17157**	**56.21389**	**58.04271**
Temperature	350	400	450	500	550